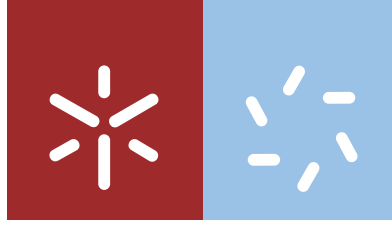


**Universidade do Minho**  
Escola de Ciências

Ruben Carpinteiro Pastilha

## **Chromatic filters for color vision deficiencies**



**Universidade do Minho**  
Escola de Ciências

Ruben Carpinteiro Pastilha

## **Chromatic filters for color vision deficiencies**

Dissertação de Mestrado  
Mestrado em Optometria Avançada

Trabalho realizado sob orientação do  
**Professor Doutor Sérgio Miguel Cardoso Nascimento**  
e do  
**Professor Doutor João Manuel Maciel Linhares**

junho de 2018

## **Declaração**

**Nome:** Ruben Carpinteiro Pastilha

**Endereço eletrónico:** [rubenpastilha@gmail.com](mailto:rubenpastilha@gmail.com)

**Telefone:** 917621898

**Número do Cartão de Cidadão:** 14366568 5 ZY8

### **Título da Dissertação de Mestrado:**

Chromatic filters for color vision deficiencies

### **Orientadores:**

Professor Doutor Sérgio Miguel Cardoso Nascimento

Professor Doutor João Manuel Maciel Linhares

**Ano de conclusão:** 2018

**Designação do Mestrado:** Mestrado em Optometria Avançada

DE ACORDO COM A LEGISLAÇÃO EM VIGOR, NÃO É PERMITIDA A REPRODUÇÃO DE QUALQUER PARTE DESTA DISSERTAÇÃO.

Universidade do Minho, \_\_\_/\_\_\_/\_\_\_\_\_

Assinatura: \_\_\_\_\_

## **Acknowledgments**

I would like to express my outmost gratitude to my advisors, Professor J Sérgio Miguel Cardoso Nascimento and Professor João Manuel Maciel Linhares, for all their support, guidance, knowledge and companionship.

I would like to thank my parents, brothers, girlfriend, and friends for all their help and support.

I would also like to thank my friends and colleagues from the Color Science Lab and the dermatology service of the Coimbra Hospital and University Centre for all their collaboration and contribution to this work.

And I would like to thank all color vision defectives and control participants, for their kindness and availability, and all those who somehow contributed to the completion of this work.



## **Abstract**

About 10% of the population have some form of color vision deficiency. One of the most severe deficiencies is dichromacy. Dichromacy impairs color vision and impoverishes the discrimination of surface colors in natural scenes. Computational estimates based on hyperspectral imaging data from natural scenes suggest that dichromats can discriminate only about 7% of the number of colors discriminated by normal observers on natural scenes. These estimates, however, assume that the colors are equally frequent. Yet, pairs of color confused by dichromats may be rare and thus have small impact on the overall perceived chromatic diversity. By using an experimental setup that allows visual comparison between different spectra selected from hyperspectral images of natural scenes, it was estimated that the number of pairs that dichromats could discriminate was almost 70% of those discriminated by normal observers, a fraction much higher than anticipated from estimates of the number of discernible colors on natural scenes. Therefore, it may be rare for a dichromat to encounter two objects of different colors that he confounds. Thus, chromatic filters for color vision deficiencies intended to improve all colors in general may constitute low practical value. On this work it is proposed a method to compute filters specialized for a specific color-detection task, by taking into account the user's color vision type, the local illuminant, and the reflectance spectra of the objects intended to be distinguished during that task. This method was applied on a case of a medical practitioner with protanopia to idealize a filter to improve detection of erythema on the skin of its patients. The filter improved the mean color difference between erythema and normal skin by 44%.



## Resumo

Cerca de 10% da população possui alguma forma de deficiência de visão de cor. Uma das deficiências mais severas é a dicromacia. Dicromacia prejudica a visão das cores e empobrece a discriminação de superfícies coloridas em cenas naturais. Estimativas computacionais baseadas em dados de imagens hiperespectrais de cenas naturais sugerem que dicromatas só pode discriminar cerca de 7% do número de cores discriminadas por observadores normais em cenas naturais. Estas estimativas, no entanto, assumem que todas as cores são igualmente frequentes. Contudo, pares de cores confundidos por dicromatas podem ser raros e, portanto, têm pequeno impacto na diversidade cromática global percebida. Ao usar uma montagem experimental que permite comparação visual entre espectros diferentes selecionados a partir de imagens hiperespectrais de cenas naturais, estimou-se que o número de pares que dicromatas poderiam discriminar era quase 70% dos discriminados por observadores normais, uma fração muito maior do que o antecipado a partir de estimativas do número de cores percebidas em cenas naturais. Portanto, pode ser raro para um dicromata encontrar dois objetos cujas cores ele confunde. Assim, filtros cromáticos para deficiências de visão das cores pretendidos para melhorar todas as cores em geral podem constituir baixo valor prático. Neste trabalho é proposto um método para calcular filtros especializados para uma tarefa específica de detecção de cor, tendo em conta o tipo de visão de cor do utilizador, o iluminante local, e os espectros de reflectância dos objetos pretendidos a serem distinguidos durante essa tarefa. Este método foi aplicado em um caso de um médico com Protanopia para idealizar um filtro para melhorar a detecção de eritema na pele de seus pacientes. O filtro melhorou a diferença média de cor entre o eritema e a pele normal por 44%.



# Index

ACKNOWLEDGMENTS .....	III
ABSTRACT .....	V
RESUMO .....	VII
INDEX.....	IX
ABBREVIATIONS AND ACRONYMS .....	XII
INDEX OF FIGURES.....	XIII
INDEX OF TABLES.....	XVII
INTRODUCTION AND RESEARCH RATIONALE .....	19
CHAPTER 1. LITERATURE REVIEW .....	23
1.1. The visual process.....	24
1.1.1. The retina .....	24
1.1.2. In the lateral geniculate nucleus .....	25
1.1.3. In the cortex.....	26
1.2. Color Vision .....	27
1.1.4. The evolution of color vision.....	27
1.1.5. Color perception.....	28
1.1.6. Color vision deficiencies .....	28
1.1.7. Solutions for color vision deficiencies .....	32
1.3. Colorimetry.....	33
1.1.8. Tristimulus XYZ .....	34
1.1.9. CIELAB .....	35
1.1.10. Color ordered systems.....	36
CHAPTER 2. COMPARISON BETWEEN NATURAL COLORS OF THE MINHO REGION AND ARTIFICIAL COLORS OF COLOR ORDERED SYSTEMS – MUNSELL AND NCS.....	37

2.1. Introduction.....	38
2.2. Methods.....	39
2.3. Results.....	42
2.4. Discussion.....	47
CHAPTER 3. THE COLORS OF NATURAL SCENES BENEFIT DICHROMATS .....	49
3.1. Introduction.....	50
3.2. Methods.....	51
3.2.1. Experimental setup.....	51
3.2.2. Stimuli .....	52
3.2.3. Procedure .....	54
3.2.4. Observers.....	55
3.3. Results.....	56
3.4. Discussion.....	57
CHAPTER 4. DATA BASE OF SPECTRAL DATA FROM NORMAL AND ABNORMAL SKIN OF HOSPITAL PATIENTS. ....	59
4.1. Introduction.....	60
4.2. Methods.....	60
4.2.1. Participants.....	61
4.2.2. Skin measuring .....	61
4.3. Results.....	63
4.4. Discussion.....	66
CHAPTER 5. COMPUTATION OF A COLORED FILTER TO IMPROVE ERYTHEMA DETECTION ON THE SKIN OF PATIENTS FOR A MEDICAL PRACTITIONER WITH PROTANOPIA – A CASE REPORT.....	67
5.1. Introduction.....	68
5.2. Methods.....	69
5.2.1. Appointed illuminant.....	69
5.2.2. Filter computation .....	70
5.3. Results.....	72

5.3.1. Filter optimization .....	72
5.3.2. Filter assessment .....	73
5.4. Discussion.....	76
CHAPTER 6. CONCLUSION AND FUTURE WORK .....	79
6.1. Main conclusions.....	80
6.2. Future work.....	80
REFERENCES.....	81
APPENDICES .....	97
Appendix I.           Model of informed consent for the experiment of Chapter 3 .....	99
Appendix II.           Research protocol submitted to the SECVS ethics committee of the University of Minho..	101
Appendix III.           Copy of the approval given by the SECVS ethics committee of the University of Minho..	117
Appendix IV.           Acquisition record sheet.....	119
Appendix V.           Model of informed consent for the experiment of Chapter 4 .....	121

## **Abbreviations and acronyms**

CAD: Color Assessment & Diagnosis test

CCT: Cambridge Color Test

CHUC: *Centro Hospitalar e Universitário de Coimbra* (Coimbra Hospital and University Centre)

CIE: *Commission Internationale de l'Eclairage* (International Commission on Illumination)

CVD: Color vision deficiency

HRR: Hardy-Rand-Rittler test

L: relative to the cone type sensitive to long visible wavelengths.

LGN: Lateral Geniculate Nucleus

M: relative to the cone type sensitive to middle visible wavelengths.

MCS: Munsell Color System

MBC: Munsell Book of Color

NCS: Natural Color System

pRGC: Photosensitive Retinal Ganglion Cells

S: relative to the cone type sensitive to short visible wavelengths.

SC: Superior Colliculus

SD: Standard Deviation

SECVS: *Subcomissão de ética para as ciências da vida e da saúde* (Subcommission of Ethics for Life and Health Sciences)

V1: Primary visual cortex

## Index of figures

Figure 1.1. Schematic representation of a vertical section of the eye highlighting the retinal layers (adapted from [20]).	24
Figure 1.2. Relative spectral sensitivity of the cone types, In linear units of energy and assuming a visual field of 2° (adapted from [29]). The S, M and L cones are represented respectively by the blue, green and red lines.	25
Figure 1.3. Schematic representation of the optic pathway (viewed from above), showing how the optical fibers are organized in the optical chiasm (adapted from [31]).	26
Figure 1.4. Orientations of the confusion lines of the three types of dichromats, protanope (left panel), deuteranope (middle panel), and tritanope (right panel), plotted on the Judd revised chromaticity diagram (adapted from [69]).	29
Figure 1.5. Limits of the object-color solid in CIELAB color space under illuminant D65 for normal observers and color vision defectives (adapted from [12]).	30
Figure 1.6. Color matching functions $x(\lambda)$ , $y(\lambda)$ , and $z(\lambda)$ of the CIE 1931 standard colorimetric observer (solid lines) and $x_{10}(\lambda)$ , $y_{10}(\lambda)$ , and $z_{10}(\lambda)$ of the CIE 1964 standard colorimetric observer (dashed lines) (adapted from [8,11]).	34
Figure 1.7. Schematic representation of the coordinate system that make the tree-dimensional CIE 1976 ( $L^*a^*b^*$ ) color space (adapted form [115]).	35
Figure 2.1. Representation of the natural colors obtained from spectral imaging (a), Munsell Color System (b) and Natural Color System (c) in CIELAB color space. Colors were computed assuming D65 illuminant. For illustration purposes only a fourth of the data points of (a) are represented.	41
Figure 2.2. Color distributions of the three data sets. Colored solid lines represent mean frequency of colors across 60 illuminants and the corresponding range for the illuminant set (colored shaded area).	42
Figure 2.3. Results of the convex hull and point analysis. (a) The CIELAB diagram represents for the CIE standard illuminant D65 the convex hulls of the natural colors (grey solid line), MCS (blue solid line), and NCS (red solid line). (b) Fraction of the volume and areas of natural colors occupied by the color systems. (c) Fraction of the natural colors inside each color system. (b) and (c) represent mean data across the illuminants set.	43

Figure 2.4. Results of the color difference analysis. (a) and (c) Represent the relative frequency and cumulative frequency, respectively, of color differences expressed in CIELAB between each natural color from the set of natural scenes (NS) and the corresponding one in the MCS or NCS. (b) and (d) Represent similar data but for the subset (NS') of the natural colors which includes only data points within the volume of each color system. Data represent mean across illuminants for MCS (blue solid line) and NCS (red solid line) and corresponding range across illuminants for MCS (blue shaded area) and NCS (red shaded area)..... 44

Figure 2.5. Variations of  $\Delta E$  color differences between the COS and natural colors across the color space. Voronoi diagrams map  $\Delta E$  values for  $a^*b^*$ ,  $L^*a^*$ , and  $L^*b^*$  between each natural color and the corresponding color of MCS (a) and NCS (b). Data corresponds to the colors of Figure 2.1 assuming D65 illuminant. .... 46

Figure 3.1. Front view of the test setup (A), close view of the test scene (B), and the radiance spectrum of the discharge lamp (OSRAM HQI 150W RX7s) reflected by the white Styrofoam mask that served as the adapting illuminant for the experiment (C). The white Styrofoam mask illuminated by the adapting illuminant provided an adapting field. A rectangular aperture on this mask allowed the scene to be seen by the observer. .... 51

Figure 3.2. Images of the four natural scenes tested. Scenes A and B are from rural environments. Scenes C and D are from urban environments. The scenes represented in A and B are from the Minho region, C is from Braga and D is from Porto, all in Portugal. They belong to an existing database [130,131]. The colors of the scenes were simulated as illuminated by the adapting illuminant. In each trial of the experiment two pixels were selected randomly and their radiance spectra were used to illuminate successively the objects inside the booth. Each scene was tested in different experimental sessions. .... 53

Figure 3.3. Color volume of each natural scene represented in Figure 3.2. The illumination was the adapting illuminant with a CCT of 5200 K and the colors are represented in the CIELAB color space for the CIE 1964 standard observer. .... 54

Figure 3.4. Stimuli sequence of each trial. The experiment was a 1AFC single alternative same-different test. The adapting illuminant was kept on for the first 1.5 s of the trial. The two test spectra and the three dark ISI lasted 0.5 s each. The adapting illuminant was the same in all trials but spectrum 1 and spectrum 2 varied between trials. .... 55

Figure 3.5. Results from the experiment for normal observers (N) and dichromats, protanopes (P) and deuteranopes (D). (A) Average pairs of colors identified as different. (B) Average discrimination index  $d'$  computed for an 1AFC, same-different task by the differencing mode [150]. (C) Average pairs of colors identified as different derived by the discrimination index  $d'$  assuming that all observers have the same criterion. Data based on 2640 trials for each observer. Error bars represent standard error across observers. .... 56

Figure 4.1. Age distribution of the participants recruit at the hospital. .... 61

Figure 4.2. Contact spectrophotometer (CM-2600D, Konica Minolta, Japan) used for measuring dermatological patients. For biological protection it was repacked with a new plastic protector for every new patient. The transparent plastic covered the measure sensor ate the bottom of the instrument and therefore its calibration had to be made having g the plastic in account. .... 62

Figure 4.3. The 7 body locations of the normal skin measures (forehead, right cheek, left cheek, back of right hand, back of left hand, right inner forearm, and left inner forearm)..... 63

Figure 4.4. Mean reflectance spectra of the normal skin on forehead, cheeks, back of hands, and inner forearms. The data of the 83 Caucasian are presented on (a) and (b) shows the same data for the only African participant. .... 64

Figure 4.5. Pictures and mean reflectance spectra of examples of abnormal skin cases. .... 65

Figure 5.1. Mean radiance spectrum of the work place illuminant indicated by the protanope medical practitioner to be used in the filter computations. .... 69

Figure 5.2. Representation in projections of the CIELAB color space planes of the colors perceived by a protanope, for the data sets of normal skin (a) and erythema (b). Similar data is also shown for the CIE 1931 standard observer in (c) and (d), respectively. It is assumed the appointed illuminant. .... 71

Figure 5.3. Filter transmittance spectrum optimized for erythema detection, for protanope (red line) and for normal CIE 1931 standard observer (blue line)..... 72

Figure 5.4. Spectral effect of the computed filters on the radiance spectra of normal skin (blue lines) and erythema (red lines). Comparison between the radiance spectra of skin seen through the filters (solid lines) and the original spectra (dashed lines), for the protanope filter (a) and the filter computed for the CIE 1931 standard observer (b). .... 73

Figure 5.5. Chromatic effect of the computed filters. Representation of skin colors (normal skin and erythema) by its 2-D projections on planes of the CIELAB color space, as seen by the protanope observer, without filter (a) and with filter (b). Similar data is also shown for the CIE 1931 standard observer in (c) and (d), respectively. It is assumed the illuminant of Figure 5.1. .... 74

Figure 5.6. Comparison of color difference results for skin observation without filter (dashed lines) and with filter (solid lines). (a) and (b) Represent the relative frequency and cumulative frequency, respectively, of the color differences expressed in CIELAB between the data sets of normal skin and erythema when viewed by a protanope. (c) and (d) Represent similar data but assuming the normal CIE 1931 standard observer. .... 75

## **Index of tables**

Table 1.1. Incidence of hereditary CVD (adapted from [9,69]).....	31
Table 4.1. Data base of Caucasian skin samples organized by type of clinical sign.....	64



## Introduction and research rationale

Normal human color vision is trichromatic, based on three type of cone photoreceptors with photopigments absorbing light in the short-, medium- and long-wavelength regions of the visible spectrum [1]. It evolved from the Old World primates who developed trichromatic vision about 40 million years ago [2], probably as an adaptation for foraging [3,4]. It allows discrimination of several million surface colors [5,6]. With the possible exception of tetrachromatic women [7] the genetic anomalies underlying color deficiencies imply limitations in color discrimination either because photopigments are spectrally closer, like in anomalous trichromats, or missing, like in dichromats or monochromats [8].

Dichromacy is most frequent in the red-green range of the spectrum because the photopigments are X-linked and individuals lack either the long-wavelength-sensitive (L) cones (protanopes) or the middle-wavelength-sensitive (M) cones (deuteranopes). It affects a small number of females, about 0.02%, but a larger number of males, about 2% [9]. Dichromats confound colors that are discriminated by normal trichromats. Estimates based on Brettel's dichromatic perceptual model [10] and on how much the object color volume [11] is compressed in dichromacy predict that dichromats see less than 1% percent of the object colors that normal trichromats can see [12]. These estimates, however, assume that the all colors are possible and equally frequent. Yet, pairs of colors confused by dichromats may be rare and thus have small impact on overall perceived chromatic diversity.

Chromatic filters have the potential to improve the chromatic diversity [13–18] and may be useful as a compensation for dichromacy.

To explore some of these aspects, the present dissertation was developed covering the following main issues:

- 1) Performance of Dichromats' dealing with the colors of the possible to encounter in rural and urban environments.
- 2) Computation of chromatic filters specialized to improve a dichromat's color discrimination on a specific color-related task.

The common line of reasoning linking the whole work is expressed in the following summary of showing the organization of chapters and how they relate to each other:

### **Chapter 1. Literature Review**

The Chapter 1 is a literature review that address the fundamentals of the visual process, color vision and colorimetry that are the intellectual foundation for the following chapters.

### **Chapter 2. Comparison between natural colors of the Minho region and artificial colors of color ordered systems – Munsell and NCS**

This chapter corresponds to a study, done recently by the candidate, that compares natural colors of the world to the sets of artificial color samples of two color ordered systems. This study is not directly related to color vision deficiencies, but provides as secondary result a statistics analysis on the colors of an existing hyperspectral images data base that was used on Chapter 3 and therefore, it was thought to be a useful inclusion on the dissertation.

### **Chapter 3. The colors of natural scenes benefit dichromats**

This study estimated, empirically, how much dichromats are impaired in discriminating surface colors drawn from natural scenes. The stimulus for the experiment was a scene made of real three-dimensional objects painted with matte white paint and illuminated by a spectrally tunable light source. In each trial the observers saw the scene illuminated by two spectra in two successive time intervals and had to indicate whether the colors perceived in the two intervals were the same or different. The spectra were drawn randomly from hyperspectral data of natural scenes and therefore represented natural spectral statistics. Four normal trichromats and four dichromats carried out the experiment. It was found that the number of pairs that could be discriminated by dichromats was almost 70% of those discriminated by normal trichromats, a fraction much higher than anticipated from estimates of discernible colors.

#### **Chapter 4. Data base of spectral data from normal and abnormal skin of hospital patients.**

The purpose of this work was to construct a data base of spectral reflectance of normal and abnormal skin of hospital patients to be implemented on the computations at Chapter 5 of a colored filter for a medical practitioner with protanopia. Several skin disorders were measured along with normal skin samples. But the data set of erythema was the only data set of abnormal skin with satisfactory sample size to use on Chapter 5.

#### **Chapter 5. Computation of a colored filter to improve erythema detection on the skin of patients for a medical practitioner with protanopia – a case report.**

The findings of Chapter 3 suggest that dichromats can distinguishing colors of general environments almost as well as normal trichromats. Therefore, they may not need CVD filters to discriminate all colors in general, and could benefit more from filters optimized for specific objects and situations. On Chapter 5 it is proposed a method to compute CVD filters specialized for the user, by considering the dichromacy type, work place illumination, and the spectra of the objects desired to detect. This method was applied to idealize a filter to help a medical practitioner with protanopia to detect skin abnormalities like erythema. It was used the erythema data and normal skin data acquired on Chapter 4

#### **Chapter 6. Conclusion and future work**

This final chapter summarizes the main conclusions of the previous chapters highlighting the main outcomes of the work and indications for future work in the research lines addressed.



## **Chapter 1. Literature Review**

## 1.1. The visual process

The visual system consists of a set of organs that cooperate with each other to produce an interpretation of the environment using a specific portion of the electromagnetic spectrum. The visual process begins in the eye whose anatomy and physiology allow the capture of light. Figure 1.1 shows the optics of the eye focusing the light rays and projecting an optical image onto the retina. Light travels through the retinal layers and reach the photoreceptors layer hitting photosensitive pigments that trigger the process of light transduction converting light into electric energy, thus coding the light signal [19,20]. The nerve electrical signal is then sent throughout the optic nerve way for visual processing.

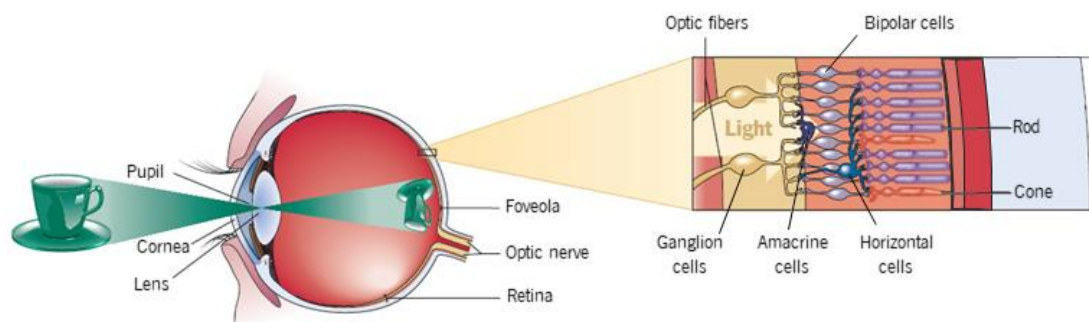


Figure 1.1. Schematic representation of a vertical section of the eye highlighting the retinal layers (adapted from [20]).

### 1.1.1. The retina

The human retina has an average of about 92 millions of rods, mostly distributed in the peripheral retina and absent in the foveola [21]. The average number of cones in the retina is approximately 4.6 millions of cones and its maximum density is found on the foveola with an average value of 199 000 cones per  $\text{mm}^2$  [21]. It is possible to distinguish three types of cones (S, M and L) that contain pigments with different sensitivities to the wavelengths of the visible spectrum. The relative sensitivity spectra of each cone type are represented in Figure 1.2.

The electric signal generated at the cones and rods is transmitted as a nervous impulse across the remaining nerve cells of the retina: bipolar, horizontal, amacrine, and the ganglion cells whose fibers group together to form the optic nerve. The retinal signals transported by the optic nerve carries with it a preliminary level of organization and modulation indicating that the processing of the visual signal begins in the retina [20].

The cones and rods are not the only photosensitive cells in the mammalian retina. Some ganglion cells were identified as having their own photosensitive molecule, the melanopsin [22]. These photosensitive retinal ganglion cells (pRGC) were traditionally associated with physiological responses to light, like regulation of circadian rhythms and pupilar response [23]. But recently has been suggested that pRGC may also contribute to visual perception, specifically in the perception of brightness [24,25] and color [26–28].

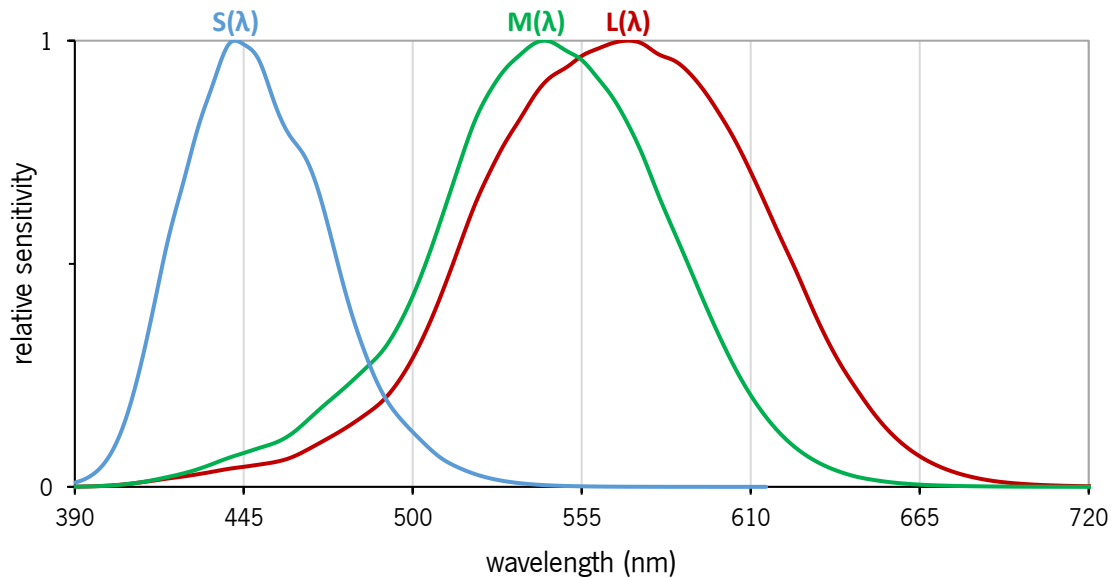


Figure 1.2. Relative spectral sensitivity of the cone types, In linear units of energy and assuming a visual field of 2° (adapted from [29]). The S, M and L cones are represented respectively by the blue, green and red lines.

### 1.1.2. In the lateral geniculate nucleus

Figure 1.3 shows how the optic nerve of each eye branches in the optic chiasm sending the ganglion fibers of the nasal retina to the contralateral hemisphere. Thus, information of the left visual field will be processed by the right side of the brain and vice versa. About 90% of these fibers connect to the lateral geniculate nucleus (LGN) located at the thalamus [30]. The remaining fibers connect to the superior colliculus (SC) in the midbrain and assumes a role on the control of eye movements and other visual behaviors [30].

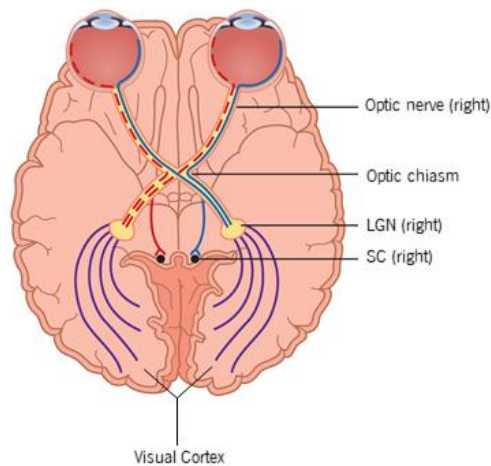


Figure 1.3. Schematic representation of the optic pathway (viewed from above), showing how the optical fibers are organized in the optical chiasm (adapted from [31]).

The LGN presents a laminated structure of 6 main layers. The main function of the LGN is to organize and regulate the flow of neural information coming from the retina before being sent to the visual cortex [32,33]. The retinal signals that reach the LGN are organized in three parallel neurological pathways: magno-, parvo-, and koniocellular pathways. These pathways correspond to distinct sets of LGN cells that connect different types of ganglion cells to specific areas of the primary visual cortex. The neurons of each LGN layer are distributed in a spatial organization concordant with the spatial organization of the correspondent receptive fields in the retina [32,33].

The two ventral layers of the LGN correspond to the magnocellular pathway which is believed to be involved in the perception of movement and contrast sensitivity [34,35]. The four dorsal layers belong to the parvocellular pathway which presents smaller receptive field cells involved in the visual acuity process and possibly also in the color vision [34–37]. In between these 6 layers lays the cells of the Koniocellular pathway. These cells receive the signal of the S cones and therefore contribute to color vision [36,38].

### 1.1.3. In the cortex

The information from the LGN is transmitted to the visual areas of the cortex where the most complex visual processing occurs and the perceived image is generated. The primary visual cortex (V1) receives the LGN fibers and delivers information to other areas of the occipital lobe. The V1 is

the most studied area and seems to be mostly involved with visual awareness [39]. The scientific consensus on the function of other areas devoted to vision are not so significant [34], but studies based on cases of brain lesions seem to relate color vision mainly to two areas known as V4 and V8 [40–43]. The occipital lobe is considered the cortical center of vision, but the visual signals do not stay limited to only this portion of the cortex. Other cortical regions also contribute to the visual process by establishing reciprocal connections with the occipital lobe. More than 80% of the cortex reacts when a light stimulus reaches the retina [31].

## 1.2. Color Vision

### 1.1.4. The evolution of color vision

Trichromatic vision evolved about 40 million years ago from Old-World primates that had two cone types coded by the X and Y chromosomes [2]. Mutations on the X chromosome led to the split of the ancestral long-wavelength cone type into the contemporary L and M cone types found in modern humans [44].

This new phenotype may have granted Old-World primates an advantage in frugivory allowing a better detection of ripe fruits among foliage [3,4,45], and for this reason was kept throughout their descendants. This idea is supported by studies revealing that the spectral sensitivities of the red-green mechanism seems tuned for the spectral differences between leaves and fruit [4,45]. Thus, co-evolution with yellow and orange tropical fruits could have driven the development of trichromacy [45], but other factors influencing the evolution of trichromacy may be involved [46]. The gap between the sensitivity peaks of the L and M cones is also described as optimized for discriminating blood-related skin color changes [47], and it was demonstrated that the large network of blood vessels of the face is used to communicate emotions through reddening of the skin [48]. This and the fact that trichromat primates, unlike dichromat species, tend to have hairless faces, supports a relation between the development of skin color communication and trichromacy [47]. But phylogenetic analyses show that trichromacy evolved before red skin communication [49]. Therefore, it seems that the evolution of fruits drove the development of trichromacy which consequently also allowed for better discrimination in color changes like skin reddening and opened the possibility for developing emotion communication through face color

changes that co-evolved with hairless faces. This idea is supported by reports of dichromats having difficulties in tasks related with fruit [3,4,50] and skin [50–55].

### 1.1.5. Color perception

Color vision is a perceptual modality with the purpose of distinguishing different spectral compositions. For the standard human vision, the main components of the mechanism essential for color perception are: three classes of cones sensitive to different wavelengths (trichromacy), a color-opponent system in the LGN for comparing the signals of the cones, and the complex processing that occurs at the cortical level [1].

According to the color-opponent theory of Hering, the perception of color works based on a luminance mechanism and two channels of opponent hues: green *versus* red and blue *versus* yellow [56]. All the perceived hues will correspond to the combined perception of the signals produced by the two parallel channels [57]. This theory allows to explain why it is not possible to perceive colors that would be described as reddish-green or yellowish-blue. These characteristics of the color perception mechanism relate to the neurological organization that occurs at the level of the ganglion cells and the LGN [35].

The color appearance can be influenced by memory, ambient lighting and visual context, which are all aspects taken into consideration by the cortical processing [58]. The total volume of object colors, i.e. colors arising only by reflection and transmission, allowed by human trichromacy corresponds to about 2 million of discernible colors [6,59].

### 1.1.6. Color vision deficiencies

With the possible exception of tetrachromatic women [60,61], any changes in the anatomy or physiology of the standard color vision system will result in an impaired chromatic discrimination [58].

The most frequent color vision deficiencies (CVD) are hereditary conditions that occurs due to mutation of the genes that encode the retinal cones. Non-hereditary factors such as systemic pathologies (e.g. multiple sclerosis and diabetes) [62,63], eye pathologies (e.g. Cataracts, glaucoma, degeneration of cones, Macular degeneration, choroid pathologies and optic nerve lesions) [62,63] and brain diseases [62–64] can also cause color vision defects. This work is

focused on hereditary deficiencies and does not cover acquired deficiencies. The forms of hereditary CVD are monochromacy, dichromacy and anomalous trichromacy.

Monochromacy corresponds to the absence of functional cones of two or all three cone types [65]. Its typical form (all cone types absent) is only present in about 0.001% of the population [58] and besides total loss of color vision it also produces photophobia, nystagmus, central scotoma, and sever loss of visual acuity [65].

Dichromacy occurs when an individual is born with only two types of functional cones and the absence of the signal of the third cone results in an image with only two hues [10]. Dichromacy can be classified in tritanopia, deuteranopia, and protanopia, if the missing cone type corresponds to the S, M, or the L cones, respectively. The missing M or L photopigment may be replaced by the other [61] but in some cases the photoreceptor is missing completely [66] and there is disruption of the cone mosaic [67,68]. The other red-green photopigment that remains, M or L, may also vary [64]. For each dichromacy type there is a set of colors discriminated by normal observers that are confounded by a dichromat. In a chromaticity diagram these colors lie on series of lines called confusion lines [69] whose orientations are represented by the lines of Figure 1.4. All colors that lie on a confusion line will be perceived as the same color, therefore the chromatic volume of a given dichromat will be shaped as an almost plane perpendicular to the confusion lines.

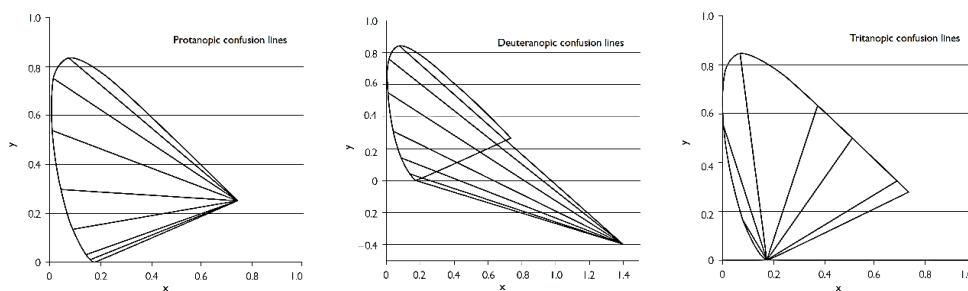


Figure 1.4. Orientations of the confusion lines of the three types of dichromats, protanope (left panel), deuteranope (middle panel), and tritanope (right panel), plotted on the Judd revised chromaticity diagram (adapted from [69]).

Using models of dichromatic vision [10,70] based on unilateral inherited color vision deficiencies [71–73] is possible to outline the dichromatic volume of all object colors that a given dichromat type can perceive, as demonstrated by Perales *et al.* [12]. The volume of all object colors of the dichromatic types are represented in Figure 1.5 in comparison to the same volume of all

object colors perceived by a normal trichromat. These theoretical gamuts indicate that dichromats perceive about 0.5% to 1% of the total number of object colors that a normal trichromat can perceive [12].

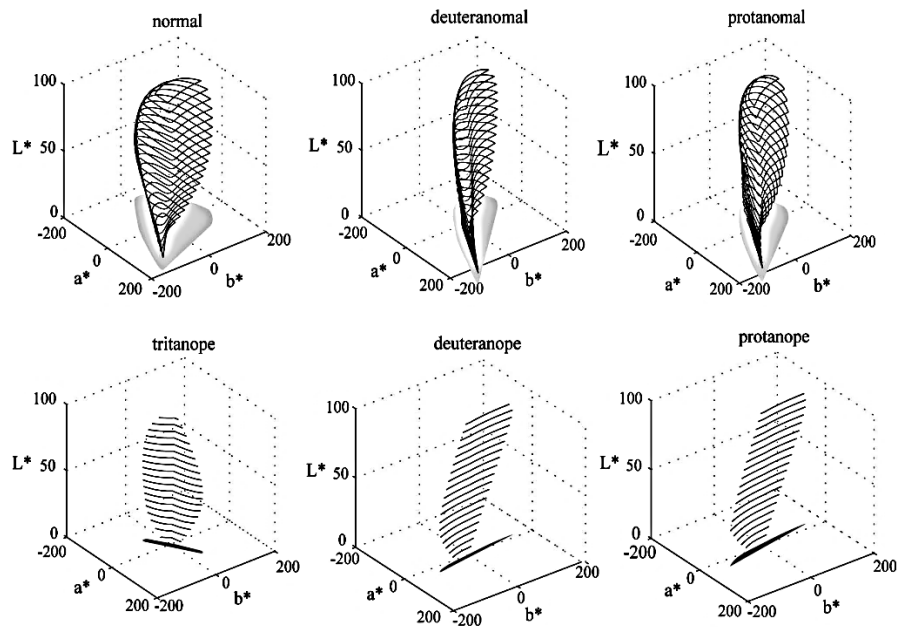


Figure 1.5. Limits of the object-color solid in CIELAB color space under illuminant D65 for normal observers and color vision defectives (adapted from [12]).

In reported cases of anomalous trichromacy there is an abnormality in the M cones (deuteranomaly) or in the L cones (protanomaly) which causes a relative approximation between the peaks of the sensitivity curves of these two cone types. Cases of anomalous trichromacy due to affection of S cones are not well documented in the literature and therefore there is no conclusive evidence that tritanomaly occurs. According to estimates based on the theoretical limits of the object-color solid, the anomalous trichromats perceive about 50%–70% of the object colors by normal trichromats [12].

In the literature is possible to find some attempts to model the color perception of the different types of hereditary CVD [10,12,74,75]. The only model used in the simulations of this work corresponds to the computational algorithm from Brettel *et al.* [10] that is based on visual comparison between the two eyes of people with unilateral CVD [10]. It is intended to simulate the colors of dichromats and of anomalous trichromats, but model for anomalous trichromacy may not be sufficiently accurate [76]. No simulations of anomalous trichromacy were used on this work, which focused only on dichromacy.

Screening for the presence of CVD can be made by using simple color vision tests like pseudoisochromatic plates (e.g. Ishihara test, Hardy-Rand-Rittler (HRR) test, etc.) and arrangement tests (e.g. Farnsworth Munsell 100 hue test, Panel D-15 (D15), etc.) [77]. But for the quantification of deficiency severity more complex tests like the Color Assessment & Diagnosis (CAD) test and Cambridge Color Test (CCT) are recommended. The gold standard for diagnosing hereditary CVD is the anomaloscopy because it allows to perfectly distinguish between dichromacy and severe anomalous trichromacy [77]. Anomaloscopy consists on a color matching test of monochromatic lights that lie on CVD confusion lines. Unlike normal and anomalous trichromats that have unique match, the dichromats present a fully extended matching range. In addition, there are also matching differences within the types of trichromats and within the types of dichromats, which makes the different types of trichromacy and dichromacy easily distinguishable by anomaloscopy.

While the defects related to the S cone (tritanopia) present prevalence values in the order of 0.002%–0.007%, the defects related to the M and L cones are more frequent presenting prevalence values of about 8%–10% in men and less than 1% in women [69]. This difference between values, in both gender and defect type, is related to M and L cones being coded by the sex chromosome X. From those 8%–10% of men, 1% are deuteranopes and 1% are protanopes [69]. Among the different types mentioned the most frequent is deuteranomaly and is estimated to be present in 5% of the male population [69]. The incidence values of hereditary CVD are organized in Table 1.1 by type and gender.

Table 1.1. Incidence of hereditary CVD (adapted from [9,69]).

<b>Type</b>	<b>Incidence (%)</b>	
	<b>Males</b>	<b>Females</b>
Tritanopia	From 0.002 to 0.007% [69] *	
Protanopia	1.01	0.02
Deuteranopia	1.27	0.01
Protanomaly	1.08	0.03
Deuteranomaly	4.63	0.36

\* Data not available in separate for males and females.

### 1.1.7. Solutions for color vision deficiencies

The most promising technique for treatment is perhaps gene therapy which has been tested on monkeys [78]. At this moment all available solutions for human CVD can only provide some specific aid and does not allow to perceive the same colors that a normal trichromat would experience. These solutions can provide two different types of help, to name colors correctly or to visually differentiate colors that otherwise would be confounded. The first type is typically made through words, symbols, or patterns that evidence the presence of a specific color, and can come in the form of printing work on real objects [79–81] or augmented-reality [82]. The second type of help consists on enhancing color differences by manipulating the visual elements observed, and it can be achieved by designing objects without the colors that color vision defectives could confound [83,84], color correction of digital displays [85,86], augmented-reality [87–92], specialized light sources [93,94], and colored filters or lenses [14,95–102].

This work will focus on colored filters that increase the chromatic discrimination by filtering certain wavelengths of the spectrum that reaches the eye. Provided that two objects have in fact some significant spectral difference, this difference can be exploited by selective filtering using a colored lens to enhance very small or even undetected differences to the naked eye of the observer. Therefore, colored lenses have the potential to improve the chromatic diversity by increasing the chromatic volume of a scene [13–18] but always within the overall volume of colors that the observer can perceived without the lenses. There is no scientific evidence that colored lenses can provide normal color vision to a color vision defective and therefore it does not cure color vision deficiencies [14,98,103,104]. When a CVD observer uses colored lenses the color appearance of the observed objects will be disturbed [14] but will not include colors out of the limits of the object-color solid of that CVD observer.

The color filtering induced by color filters or light sources can be managed in order to optimize the observed chromatic volume [105–107] and maybe improve discriminability between different spectra, allowing to better distinguish certain objects from others using chromatic information.

This method of visual enhancing is especially useful for tasks that require detection of a specific object on a specific background, but not for color naming tasks. Similar techniques had already been applied in sports to improve chromatic contrast of normal observers [108–111].

### 1.3. Colorimetry

Colorimetry consists on numerical specification of a spectral distribution within the visible spectrum (between about 400 nm to about 700 nm [112]). The numerical specification is made according to a certain color specification system, in such a way that spectra with the same specification must produce the same color appearance. The elements of a colorimetric numerical specification represent continuous functions of physical parameters of the stimulus that can define the quantity of each primary color directly, like the real tristimulus (RGB) and imaginary tristimulus (XYZ), or indirectly, like systems based on the three perceptual dimensions of color (luminance, hue and saturation) [113]. The most used color specification systems come in the form of tristimulus (e.g. RGB, XYZ), uniform color spaces (e.g. CIELAB, CIELUV), or color ordered systems (e.g. Munsell Color System, Natural Color System).

For matters of consistency all the colorimetric analysis presented in this work were done using the same colorimetric system, the CIELAB color space. This is an almost uniform color space recommended by the CIE [113] to be used in the absence of an improved uniformly-spaced system. The CIELAB is a well-established international standard for color specification and commonly used by color measurement instrumentation [114].

The correspondent CIE technical report [113] states that CIELAB is intended for comparing “object color stimuli of the same size and shape, viewed in identical white to middle grey surroundings, by an observer photopically adapted to a field of chromaticity not too different from that of average daylight”. Most of the analysis done in this work deal with color samples measured in real environments. Therefore, the conditions mentioned previously are not completely ensured and it may occur some unavoidable impairments on the estimated values of CIELAB chromaticities and CIELAB color differences. Nevertheless, it is a well-established method to perform such estimations.

The process to represent a color object on the CIELAB color space begins with the estimation of the XYZ tristimulus from the reflectance spectrum of the object considering a given illuminant, and later conversion of the XYZ values to the CIELAB coordinates [113].

### 1.1.8. Tristimulus XYZ

Tristimulus are colorimetric parameters that represent the magnitudes of the three primaries required to produce a specific color in additive mixing. The XYZ tristimulus are based on color matching functions  $\bar{x}(\lambda)$ ,  $\bar{y}(\lambda)$ ,  $\bar{z}(\lambda)$  defined to produce imaginary tristimulus that reproduce all colors always assuming only positive values. The CIE recommends two sets of color matching functions [113],  $\bar{x}(\lambda)$ ,  $\bar{y}(\lambda)$ ,  $\bar{z}(\lambda)$  and  $\bar{x}_{10}(\lambda)$ ,  $\bar{y}_{10}(\lambda)$ ,  $z_{10}(\lambda)$  (see Figure 1.6). These functions correspond to the CIE 1931 standard colorimetric observer and the CIE 1964 standard colorimetric observer. The data of the CIE 1931 standard colorimetric observer is intended for color stimuli subtending between about  $1^\circ$  and about  $4^\circ$  at the eye of the observer. The data of the CIE 1964 standard colorimetric observer should be used for visual angles larger than  $4^\circ$ .

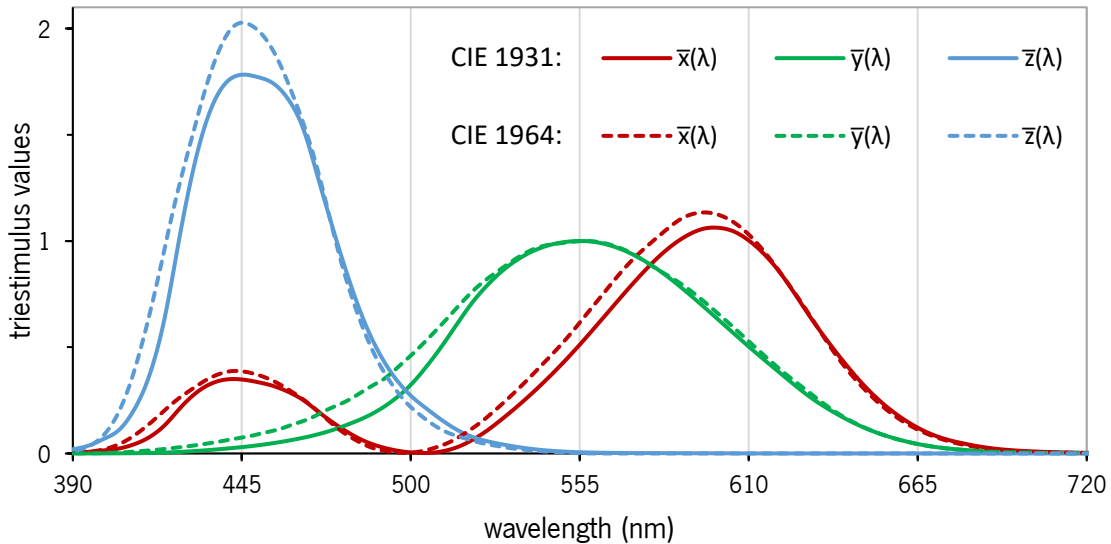


Figure 1.6. Color matching functions  $\bar{x}(\lambda)$ ,  $\bar{y}(\lambda)$ , and  $\bar{z}(\lambda)$  of the CIE 1931 standard colorimetric observer (solid lines) and  $\bar{x}_{10}(\lambda)$ ,  $\bar{y}_{10}(\lambda)$ , and  $z_{10}(\lambda)$  of the CIE 1964 standard colorimetric observer (dashed lines) (adapted from [8,11]).

The CIE 1931 XYZ tristimulus can be estimated using the following equations [113]:

$$X = k \sum_{\lambda} \phi(\lambda) \cdot \bar{x}(\lambda) \Delta\lambda \quad (1.1)$$

$$Y = k \sum_{\lambda} \phi(\lambda) \cdot \bar{y}(\lambda) \Delta\lambda \quad (1.2)$$

$$Z = k \sum_{\lambda} \phi(\lambda) \cdot \bar{z}(\lambda) \Delta\lambda \quad (1.3)$$

Where  $\phi(\lambda)$  corresponds to the relative spectral radiance of the color stimulus for a given wavelength ( $\lambda$ ). When necessary, radiance spectra of objects can be estimated from the multiplication between the relative spectral reflectance of the object  $R(\lambda)$  and the spectral radiance of the illuminating  $S(\lambda)$ :  $\phi(\lambda) = R(\lambda) \cdot S(\lambda)$ .

The constant  $k$  is defined in a way that the tristimulus  $Y$  value of a Lambertian object ( $R(\lambda) = 1$ ) is equal to 100. It can be obtained by the following equation:

$$k = 100 / \int_{\lambda} S(\lambda) \cdot \bar{y}(\lambda) \Delta\lambda \quad (1.4)$$

### 1.1.9. CIELAB

CIELAB is a color specification system designed to match human visual perception. This space is fairly uniform, i.e. the colors tend to be distributed according to human perception and the approximated value of the difference between two colors can be obtained directly from the Euclidean distance between the points of space corresponding to those colors [113,114]. Figure 1.7 shows that the CIELAB system maps colors either by using three cartesian coordinates ( $L^*$ ,  $a^*$ ,  $b^*$ ) or by using cylindrical coordinates that are approximate correlates of the three perceived attributes of color: lightness ( $L^*$ ), chroma ( $C^*_{ab}$ ), and hue ( $h_{ab}$ ) [113,114]. The  $L^*$  values are set between 0 and 100, and all the space is defined so that the color of the illuminant is placed at the top of that scale.

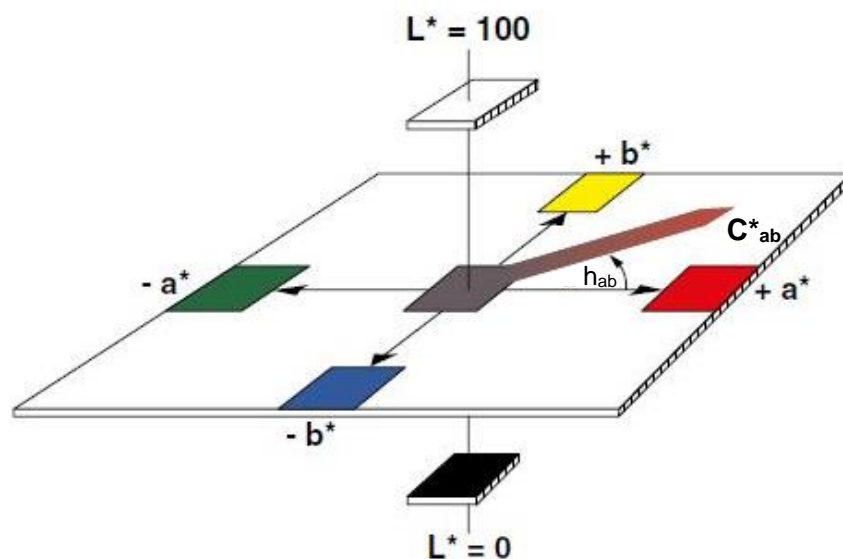


Figure 1.7. Schematic representation of the coordinate system that make the tree-dimensional CIE 1976 ( $L^*a^*b^*$ ) color space (adapted form [115]).

The CIE 1976 (L\*a\*b\*) color space coordinates can be obtained from the CIE 1931 XYZ tristimulus by using the following equations [113]:

$$L^* = 116 f\left(\frac{Y}{Y_n}\right) - 16 \quad (1.5)$$

$$a^* = 500 \left[ \left(\frac{X}{X_n}\right) - f\left(\frac{Y}{Y_n}\right) \right] \quad (1.6)$$

$$b^* = 200 \left[ f\left(\frac{Y}{Y_n}\right) - f\left(\frac{Z}{Z_n}\right) \right] \quad (1.7)$$

$$C^*_{ab} = (a^{*2} + b^{*2})^{1/2} \quad (1.8)$$

$$h_{ab} = \arctan(b^*/a^*) \quad (1.9)$$

Where:

$$f\left(\frac{X}{X_n}\right) = \begin{cases} \left(\frac{X}{X_n}\right)^{\frac{1}{3}} & \text{if } \left(\frac{X}{X_n}\right) > \left(\frac{24}{116}\right)^3 \\ \left(\frac{841}{108}\right)\left(\frac{X}{X_n}\right) + \frac{16}{116} & \text{if } \left(\frac{X}{X_n}\right) \leq \left(\frac{24}{116}\right)^3 \end{cases} \quad (1.10)$$

$$f\left(\frac{Y}{Y_n}\right) = \begin{cases} \left(\frac{Y}{Y_n}\right)^{\frac{1}{3}} & \text{if } \left(\frac{Y}{Y_n}\right) > \left(\frac{24}{116}\right)^3 \\ \left(\frac{841}{108}\right)\left(\frac{Y}{Y_n}\right) + \frac{16}{116} & \text{if } \left(\frac{Y}{Y_n}\right) \leq \left(\frac{24}{116}\right)^3 \end{cases} \quad (1.11)$$

$$f\left(\frac{Z}{Z_n}\right) = \begin{cases} \left(\frac{Z}{Z_n}\right)^{\frac{1}{3}} & \text{if } \left(\frac{Z}{Z_n}\right) > \left(\frac{24}{116}\right)^3 \\ \left(\frac{841}{108}\right)\left(\frac{Z}{Z_n}\right) + \frac{16}{116} & \text{if } \left(\frac{Z}{Z_n}\right) \leq \left(\frac{24}{116}\right)^3 \end{cases} \quad (1.12)$$

Where X, Y, Z are the tristimulus values of the colored object in test.  $X_n$ ,  $Y_n$ ,  $Z_n$  are the tristimulus values of a Lambertian surface exposed to the same illuminant as the test object.

### 1.1.10. Color ordered systems

A color ordered system is a color appearance system based on a collection of printed colored samples, arranged and labeled according to perceptual attributes of color to enable intuitive search and visual interpolation between samples [67,114,116–118]. These systems are typically used for identification of colors of objects without instrumentation by using only visual comparison. The Munsell Color System (MCS) and the Natural Color System (NCS) are two examples of such systems [114,119] (for more details on these systems see Chapter 2).

## **Chapter 2. Comparison between natural colors of the Minho region and artificial colors of color ordered systems – Munsell and NCS**

## 2.1. Introduction

The chromatic gamut of printed color ordered systems is constrained by the limitations of the printing process [120]. Therefore, not all colors that may be important are in the printed catalogs. The Munsell Color System (MCS) and the Natural Color System (NCS) are two examples of such systems [114,119].

The Munsell system was devised by the artist A.H. Munsell in 1905 for color recording and color teaching [121,122]. It achieved an unmatched popularity by his contemporaries by successfully implementing three dimensions of color on a printed representation with uniform color scaling [123]. These three dimensions are expressed by the Munsell notation as Munsell value, Munsell hue, and Munsell chroma, and correspond respectively to the perceptual attributes of lightness, hue, and saturation [114,124]. The Munsell value of 0 is the ideal black and 10 the ideal white. On the Munsell Book of Color (MBC) the Munsell value is represented on a scale from 1 to 9 in steps of 1. This dimension is the axis around which the Munsell hue is established. The perceptual scaling of hue is done in circular steps between 10 major hues represented as 40 pages on the MBC. The major hues are referred as: Red (R), Yellow–Red (YR), Yellow (Y), Green–Yellow (GY), Green (G), Blue–Green (BG), Blue (B), Purple–Blue (PB), Purple (P), and Red–Purple (RP). The Munsell chroma is scaled from 0 to a maximum value that varies with the values of the two other dimensions. The system underwent several improvements over the years but the most notable one corresponds to adjustments on the correspondence between Munsell notation and printed samples [125]. This renotation was based on a study of over 3 million visual observations conducted by an OSA Subcommittee between 1937 and 1940 [126,127].

The NCS is a Swedish standard for color notation which was developed in 1964 by the Swedish Color Center Foundation [128]. The purpose was to make a practical model of the opponent-color theory conceived by the German physiologist Ewald Hering. Therefore, it consists on judging the appearance of a color by using two perceptual attributes of hue (chromaticness) and one of lightness (blackness). These are defined as the relative amount of red or green, the relative amount of blue or yellow, and the relative amount of black or white, respectively. Researchers involved reported that more than 60 thousand observations were made in psychophysical experiments based on the visualization of samples of colored papers [128]. These experiments served as guidance to produce a color atlas founded on the ideas of Hering. It was intended to represent every chromaticity at steps of 10% for blackness and for chromaticness for

40 different hues. This would result in 2000 samples but due to the pigments limitations this version (SIS Color Atlas NCS) was left with only 1412. Later more samples were added and the NCS ALBUM 1950 ORIGINAL with 1950 samples was achieved.

The colors of the natural world are produced by a range of physical and chemical phenomena that go behind the absorption of light by pigments, e.g. interference, diffusion and diffraction [129]. The colors that can be produced by pigments are represented by the object color solid, which is delimited by the optimal colors [34], but the real natural gamut is much smaller than this theoretical limit [5]. If the color ordered systems are designed to sample in a useful way the colors of the natural environment their colors should match as close as possible the structure of natural colors. The ideal color ordered system would have a chromatic gamut comparable to that of natural colors and their samples would be spaced to match the visual chromatic threshold.

The goal of this work was to assess how well the MCS and NCS represent the colors of nature. We used spectral imaging of natural scenes (NS) and spectral data of these systems to render its colors under a range of different illuminants. The ability of the color ordered systems to represent natural colors was quantified in terms of chromatic volume and color difference between their colors and the natural colors.

## 2.2. Methods

The NS data set corresponds to about  $68 \times 106$  pixels from 50 hyperspectral images of natural scenes of rural and urban outdoor environments from the Minho region of Portugal [130,131] obtained in the form of effective spectral reflectance from 400 nm to 720 nm, in steps of 10 nm. As effective spectral reflectances are obtained from a grey reference surface in the scene they need to be normalized to compute the corresponding colors in CIELAB. The reflectance array of each scene was normalized by dividing by a constant equal to the maximum effective spectral reflectance evaluated over all pixels and wavelengths in each scene (for technical details see [130]). This procedure guarantees that the reference white, a unitary spectral reflectance, is always the brightest surface in each scene.

The MCS data set corresponds to the 1269 color chips from the Munsell Book of Color - Matte Finish Collection (Munsell Color, Baltimore, Md., 1976) obtained from the online database of the University of Joensuu Color Group (Finland) [132]. Reflectance data was acquired from 380 nm to 800 nm in 1 nm steps.

The NCS data set corresponds to 1943 of the 1950 NCS standard color samples of the NCS ALBUM 1950 ORIGINAL (NCS - NATURAL COLOR SYSTEM, Scandinavian Color Institute AB, Stockholm, Sweden 2004). Each sample was measured using a portable spectrophotometer (CM-2600D, Konica Minolta, Japan) to obtain reflectance data from 400 nm to 700 nm in 10 nm steps with specular component excluded.

The illuminants used were 60 representing natural and artificial lighting: 55 CIE illuminants [113] and 5 white LEDs (Luxeon, Philips Lumileds Lighting Company, USA.). CIE Incandescent light: the CIE standard illuminant A correspondent to a tungsten filament at a temperature of 2856 K. CIE daylight illuminants: D50, D55, D65, D75 and other 19 D illuminants estimated from the correspondent CIE equations [113] (for a x coordinate value within the range of 0.3775 to 0.25 in steps of 0.0075 on the CIE (x,y)-chromaticity system). CIE fluorescent illuminants: FL1, FL2, FL3, FL4, FL5, and FL6 are traditional fluorescent lamps, FL7, FL8, and FL9 are broad-band, FL10, FL11, and FL12 are narrow band, FL3.1, FL3.2, and FL3.3, are standard halophosphate, FL3.4, FL3.5, and FL3.6 are DeLuxe, FL3.7, FL3.8, FL3.9, FL3.10, and FL3.11 are three band, FL3.12, FL3.13, and FL3.14 are multi band, and FL3.15 is a D65 simulator. CIE High-pressure illuminants: HP1 correspondent to a standard high-pressure sodium lamp, HP2 correspondent to a color enhanced high-pressure sodium lamp, HP3, HP4 and HP5 are typical high-pressure metal halide lamps. White LED illuminants: LXHL-BW02, LXHL-BW03, LXML-PWC1-0100, LXML-PWN1-0100, and LXML-PWW1-0060.

For the computations the NS and NCS reflectance data sets were interpolated to 5 nm to fit the spectral profile of some of the illuminants which present important peaks that would be overlooked if using a larger step. All computations were carried out between 400 nm and 700 nm in steps of 5 nm. Radiance spectra were estimated from the reflectance data by multiplying the spectral radiance of each illuminant spectrum. Assuming the CIE 1931 standard observer, the radiance data was converted into tristimulus values and then converted into the CIELAB color space. The reference white was assumed to be a sample with unitary spectral reflectance. The data points of NS, MCS, and NCS expressed in CIELAB assuming the illuminant D65 are represented in Figure 2.1.

To assess the extent to which the color ordered systems can represent natural colors we compared MCS and NCS data sets against the NS set in terms of chromatic volume and color differences. The volume and areas occupied by the NS set in CIELAB were estimated by convex

hull using the “convhull” function available in MatLab (MathWorks, Inc., Natick, MA, United States of America) based on the quickhull algorithm [133].

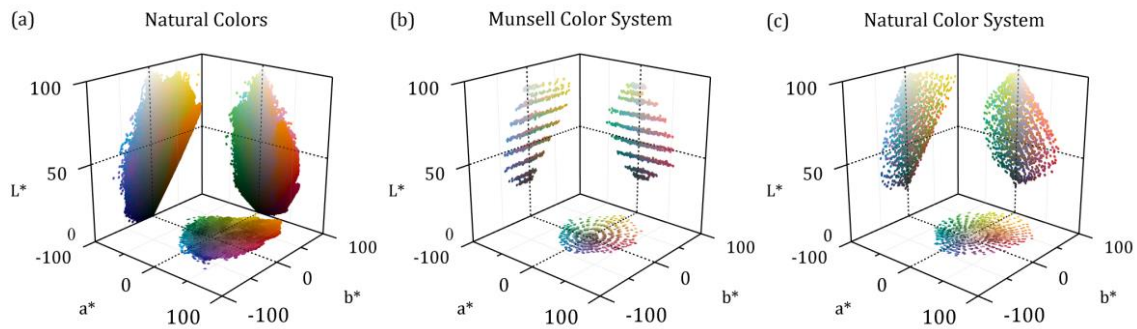


Figure 2.1. Representation of the natural colors obtained from spectral imaging (a), Munsell Color System (b) and Natural Color System (c) in CIELAB color space. Colors were computed assuming D65 illuminant. For illustration purposes only a fourth of the data points of (a) are represented.

The color difference  $\Delta E_{L^*a^*b^*}$  between the colors of NS and each of the systems was estimated by calculating the Euclidean distance between each natural color and the closest color in the color systems. Nearest neighbor calculations were implemented through the “nearestNeighbor” function available in MatLab (MathWorks, Inc., Natick, MA, United States of America) which resorts on Delaunay Triangulation. Because the color volume of the natural colors outgrows some portions of the volume of MCS or NCS, two subsets of natural colors were considered each including only the colors within the volume of MCS or NCS.

Figure 2.1 compares the color distributions of the three data sets. The MCS scatter is chromatically less dense, has 35% less data points than NCS. The MCS shows a more regular pattern than NCS and have distinct sub-sets of colors grouped at defined regions of the color space. In  $L^*a^*$  and  $L^*b^*$  planes MCS shows a well-defined pattern of 9 distinct clusters parallel to each other and to the  $a^*$  and  $b^*$  axes. Colors in the same cluster have similar  $L^*$  and different saturations. These concentrated clusters are located on 9 different lightness levels set apart, on average, by  $7.5 (\pm 2.3)$  CIELAB units. This value was computed from the mean  $L^*$  values estimated for the 9 clusters (26.2, 30.2, 39.3, 48.7, 57.8, 67.2, 76.6, 81.1, and 86.2 CIELAB units) through clustering analysis based on the Lloyd’s algorithm [134] and k-means++ algorithm [135] by using the “kmeans” function available in MatLab (MathWorks, Inc., Natick, MA, United States of America). These levels correspond to the 9 levels of grey on the notation scale of Munsell value. On the hue plane  $a^*b^*$  MCS presents a pattern of well-defined concentric circles indicating that MCS has larger sampling steps on saturation than on hue. These data are generally consistent

other studies involving the chromatic structure of the 1269 Munsell Samples [136]. The NCS scatter on  $L^*b^*$  has a more homogeneous appearance with a less perceptible structure pattern.

## 2.3. Results

Figure 2.2 shows that both color systems offer more color samples of low saturation matching the saturation distribution of the natural colors. The  $L^*$  distributions of the three data sets, however, are distinct. Figure 2.2 (a) shows that natural colors have higher frequency in the lower half of the  $L^*$  axis. The bin of  $L^*$  from 0 to 1, corresponding to points of extreme shadow, has the highest frequency and presents a protruding peak. These points correspond to regions of almost complete darkness that are mostly found in distant areas under shadow, cracks of surfaces, and empty space between agglomerates of objects (e.g. plant leaves) where the illuminant light cannot penetrate and be reflected.

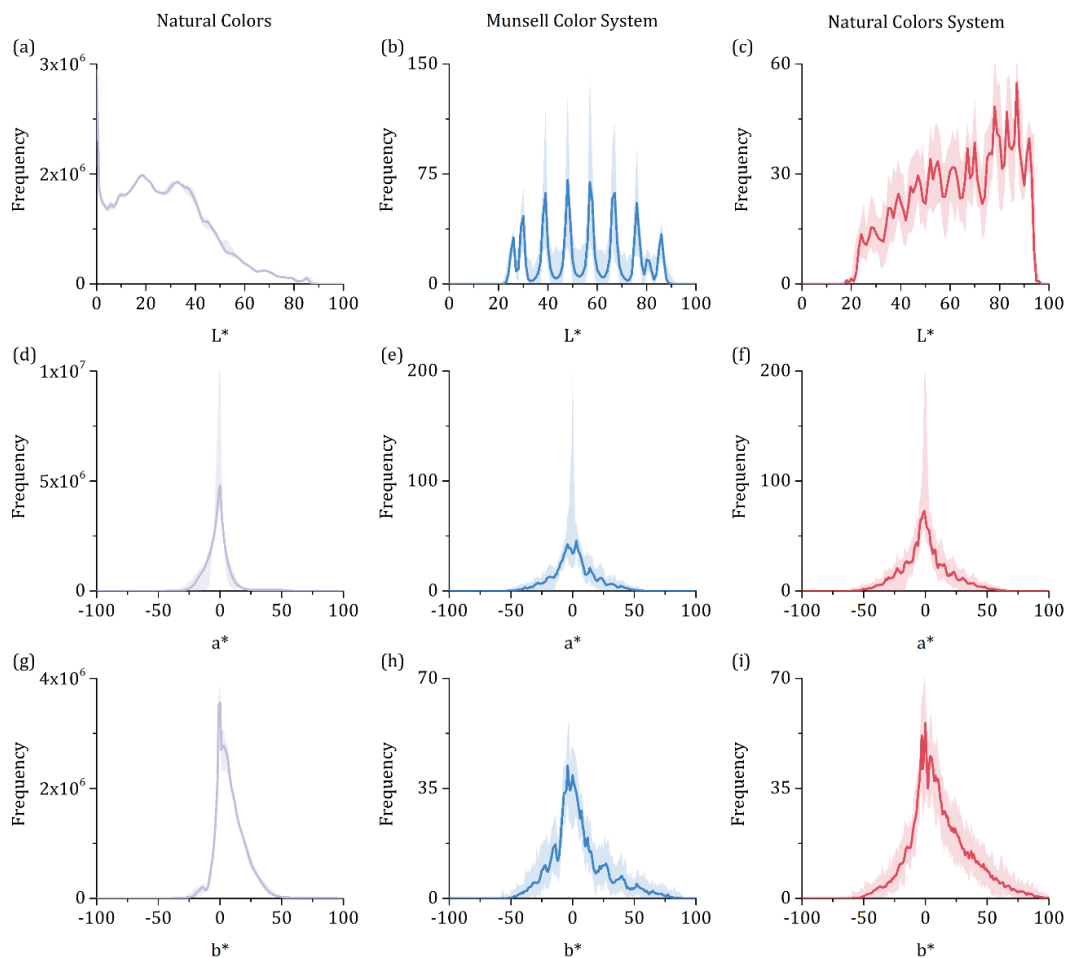


Figure 2.2. Color distributions of the three data sets. Colored solid lines represent mean frequency of colors across 60 illuminants and the corresponding range for the illuminant set (colored shaded area).

Figure 2.2 (b) and (c) show that the MCS system has more data points on median levels of  $L^*$  whereas the NCS shows a preference for higher levels of  $L^*$ . For MCS and NCS the lightness levels for the mean illuminant range from 22 to 91 and from 18 to 96, respectively (Figure 2.2 (b) and (c), colored solid lines). These intervals do not cover the full extent of the natural colors, particularly for  $L^*$  lower than around 20 CIELAB units. Natural colors are more frequent on this low lightness region than on the high lightness one. Thus, the color systems cover the ranges of  $L^*$ ,  $a^*$ , and  $b^*$  on natural colors distribution with higher frequency, but for  $L^*$  some portions are underrepresented. Figure 2.2 shows the colored shading areas corresponding to the range of illuminants tested. The variability is modest. The mean and the D65 data are similar in all cases, and most of the variability on  $a^*$  is caused by the illuminant HP1.

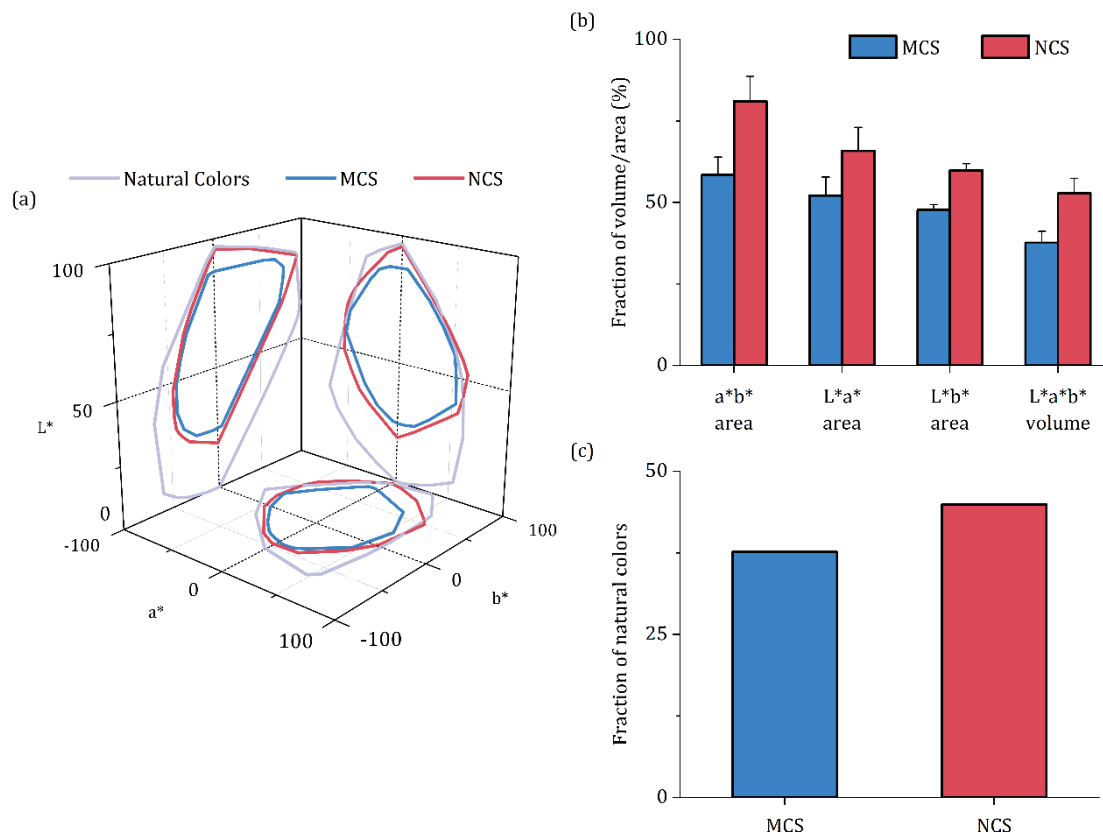


Figure 2.3. Results of the convex hull and point analysis. (a) The CIELAB diagram represents for the CIE standard illuminant D65 the convex hulls of the natural colors (grey solid line), MCS (blue solid line), and NCS (red solid line). (b) Fraction of the volume and areas of natural colors occupied by the color systems. (c) Fraction of the natural colors inside each color system. (b) and (c) represent mean data across the illuminants set.

Figure 2.3 shows the results of the convex hull and point analysis. Figure 2.3 (a) compares the convex hulls between the data sets for D65. The volume of natural colors outgrows the volume of both color systems. The MCS has smaller volume than NCS, covering 71,5% of the NCS volume.

2.5% of NCS colors are outside the volume of natural colors. Figure 2.3 (b) shows the mean volume and mean area of the color systems relatively to natural colors. The MCS and NCS relative volumes are 37.7% ( $\pm 3.4$ ) and 52.7% ( $\pm 4.6$ ), respectively. Figure 2.3 (c) shows the fraction of natural colors inside MCS and NCS color volumes, about 37.6% ( $\pm 0.1$ ) and 44.9% ( $\pm 5.8$ ), respectively.

Figure 2.4 (a) and (c) show the results of the color difference analysis. The MCS and NCS mean distributions present peaks at  $\Delta E_{L^*a^*b^*}$  25.0 and 18.6 CIELAB units, respectively, as a result of the dense agglomeration of natural colors near the origin of the CIELAB color space (see Figure 2.2 (a), (d) and (g)). Figure 2.4 (c) shows that a visual perfect match for all natural colors requires an observer with chromatic threshold of 25.0 and 19.2 CIELAB units for MCS and NCS, respectively.

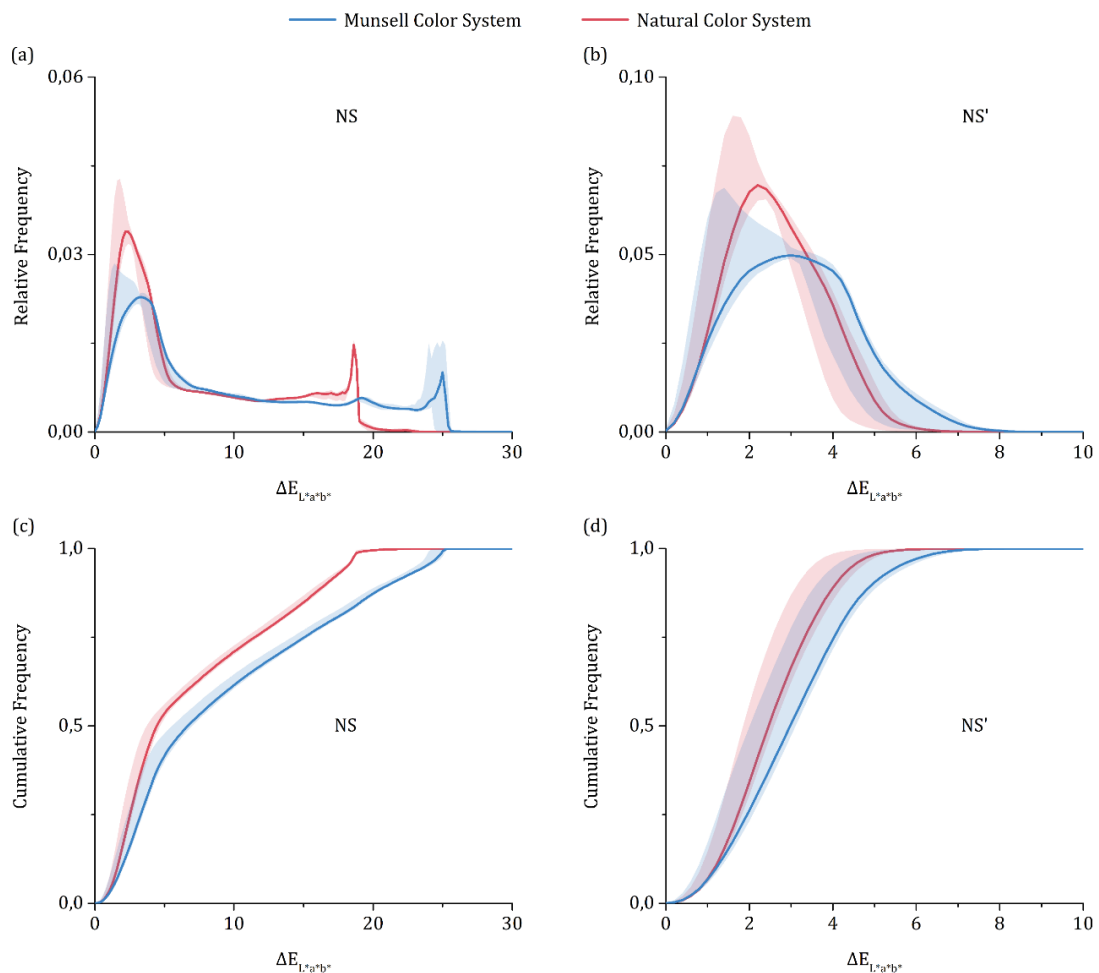


Figure 2.4. Results of the color difference analysis. (a) and (c) Represent the relative frequency and cumulative frequency, respectively, of color differences expressed in CIELAB between each natural color from the set of natural scenes (NS) and the corresponding one in the MCS or NCS. (b) and (d) Represent similar data but for the subset (NS') of the natural colors which includes only data points within the volume of each color system. Data represent mean across illuminants for MCS (blue solid line) and NCS (red solid line) and corresponding range across illuminants for MCS (blue shaded area) and NCS (red shaded area).

Figure 2.4 (b) and (d) present similar data but for the NS' set that corresponds to the natural colors within the volumes of each color system. Figure 2.4 (b) shows that the most frequent  $\Delta E_{L^*a^*b^*}$  value across illuminants is on average 3.0 and 2.2 CIELAB units for MCS and NCS, respectively. Figure 2.4 (d) shows the corresponding cumulative frequency. For an observer with a chromatic threshold of 1 CIELAB unit 6.7% and 6.9% of the NS' colors will look the same as the correspondent MCS and NCS samples. For a chromatic threshold of 2 CIELAB units 26.3% and 34.2% of the NS' colors will look the same as the correspondent MCS and NCS samples, respectively. Figure 2.4 (d) also shows that the threshold needed to achieve color match on NS' colors would be on average 6.8 and 5.4 for MCS and NCS, respectively.

The distributions are similar across illuminants, except for HP1 which has its most frequent  $\Delta E_{L^*a^*b^*}$  value significantly lower than the most frequent value for the mean distribution. For HP1, the most frequent  $\Delta E_{L^*a^*b^*}$  value is only 1.4 and 1.6 for MCS and NCS, respectively. Match for all NS' colors is achieved with thresholds of 4.8 and 4.2 for MCS and NCS, respectively. The chromatic volume produced by this illuminant is contracted across the  $a^*$  axis resulting in small values of relative volume (33.1% and 47.9% for MCS and NCS, respectively) while covering a reasonable portion of NS points (37.7% and 46.0% for MCS and NCS, respectively). This indicates that for HP1 a stronger concentration of natural colors occurs inside the zones of the color space occupied by the color systems, decreasing the distance between the NS data points and the correspondent color systems data points.

The analysis was complemented with Voronoi diagrams to study how  $\Delta E$  varies across color space. Voronoi decomposition of MCS and NCS for each CIELAB plane ( $a^*b^*$ ,  $L^*a^*$ , and  $L^*b^*$ ) was carried out by using "voronoin" function available in MatLab (MathWorks, Inc., Natick, MA, United States of America) which is based on the quickhull algorithm [133]. The Voronoi decomposition defines for each color system data point the boundaries of a polygonal area that only includes the points of space closer to that data point than to any other data point. Thus, each polygonal area represents the chromatic territory of a color system sample and is color coded for the mean value of color difference ( $\Delta E_{a^*b^*}$  or  $\Delta E_{L^*a^*}$  or  $\Delta E_{L^*b^*}$ ) between the COS data point and each NS data point enclosed by that area.

Figure 2.5 shows how color difference vary across the CIELAB planes by using Voronoi diagrams mapping  $\Delta E$  values computed for  $a^*b^*$ ,  $L^*a^*$ , and  $L^*b^*$  color spaces. What is represented

is the color difference between each natural color and the corresponding color of MCS (a) and NCS (b). Data corresponds to the chromaticity coordinates of Figure 2.1, i.e. assuming D65 as the illuminant. For the majority of the Voronoi cells the mean  $\Delta E$  values seem to range from around 0 to 3, which agrees with the greatness of values of  $\Delta E_{L^*a^*b^*}$  in Figure 2.4. Voronoi diagrams for NCS are overall more uniform and present lower mean  $\Delta E$ , in particular for data points close to the achromatic locus. The  $a^*b^*$  diagram of MCS shows larger color differences for positive values of  $b^*$  than for negative values and the diagrams  $L^*a^*$  and  $L^*b^*$  of MCS show irregularities across the color space that are consistent with the scatter pattern of MCS shown in Figure 2.1. In both color systems  $\Delta E_{a^*b^*}$  tends to be larger for more saturated colors.

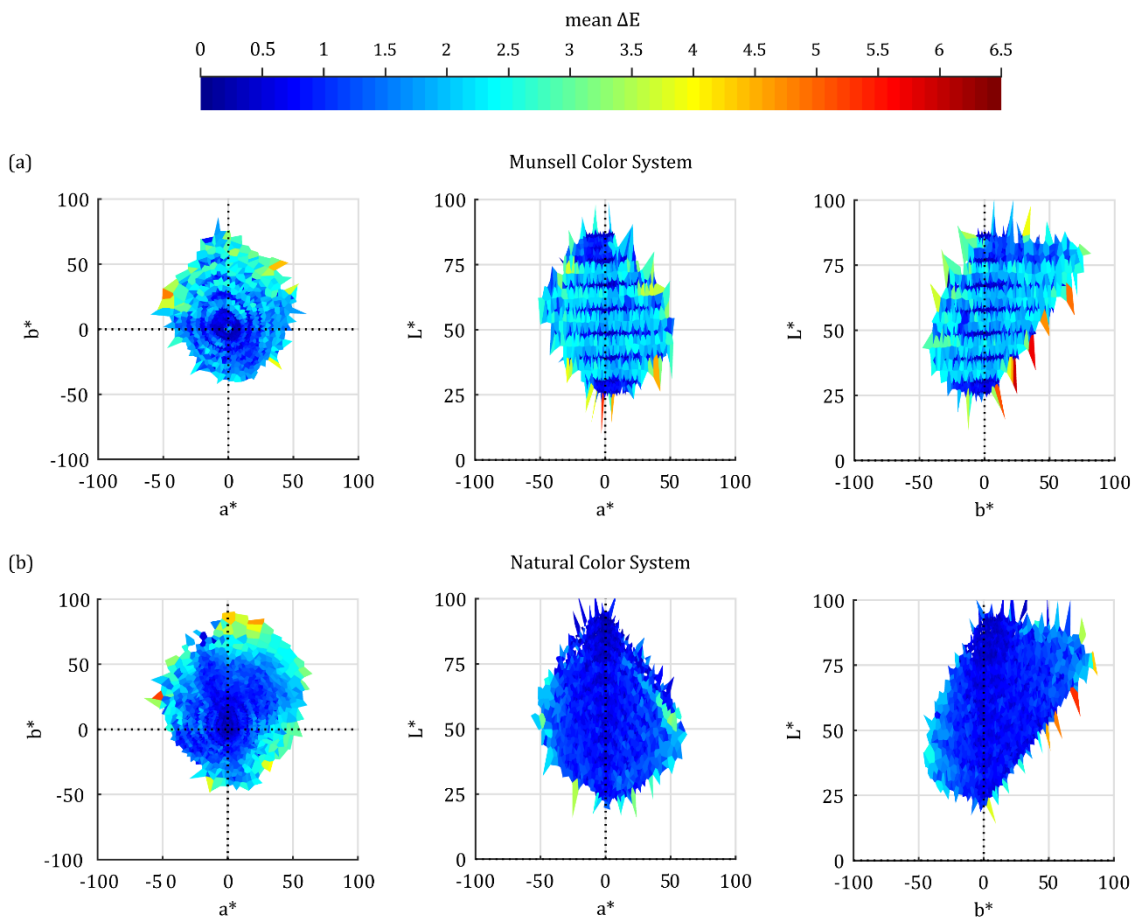


Figure 2.5. Variations of  $\Delta E$  color differences between the COS and natural colors across the color space. Voronoi diagrams map  $\Delta E$  values for  $a^*b^*$ ,  $L^*a^*$ , and  $L^*b^*$  between each natural color and the corresponding color of MCS (a) and NCS (b). Data corresponds to the colors of Figure 2.1 assuming D65 illuminant.

## 2.4. Discussion

The portion of the volume of the natural colors accounted by MCS and NCS was about 38% and 53%, respectively. The color ordered systems do not include mainly colors with low lightness, which are frequent in natural scenes. Apart from the dark colors both color systems are a good match to the natural colors, especially for non-saturated colors.

The NCS has a lower average color difference in relation to the natural colors than MCS, i.e., on average for each natural color there is a color in the NCS system that is visually closer than a color in the MCS. For an observer with a color threshold of 1 CIELAB unit only about 7% of the natural colors have a corresponding color (perceived as the same) both in MCS and NCS. For a threshold of 2 CIELAB units the percentage is 25% and 19% for MCS and NCS, respectively. To obtain a complete match to all natural colors contained by the color systems volumes thresholds of 7 and 5 CIELAB units would be required for MCS and NCS, respectively. For the complete set of natural colors thresholds of about 25 and 20 for MCS and NCS, respectively, would be required. The NCS has some very saturated colors that are outside the volume of natural colors and therefore represent colors that are not frequent in nature.

The computation of natural colors in CIELAB color space were carried out assuming that the reference white is the brightest color in each scene. Although this is a reasonable assumption it may not hold for all viewing conditions. In practice, however, it will work well in most conditions. The computations also do not take into account the variation of the illumination across scenes which can be considerable [137]. The computations for different illuminants, however, suggest that these variations have a small effect in the conclusions.

The results presented here suggest that both color systems are limited at representing the natural colors with low lightness levels. They are, however, quite good otherwise. The ideal color ordered system for describing natural colors would need a chromatic gamut covering the saturation levels, for  $a^*$  and  $b^*$ , between about -100 to 100 CIELAB units and include all levels of lightness. Its samples would need to be evenly distributed in a step corresponding to the discrimination threshold of the observer in a way that all natural colors would have a perfect color match on the correspondent sample.

Using the Munsell system or the NCS as models of the colors of the natural world may be insufficient in some cases and more complete spectral data may be necessary.

In regard only to the analysis on Minho's natural scenes, the results show that natural colors can assume very saturated colors but that these are very rare. In the natural scenes is possible to find colors of almost any possible level of  $L^*$ , but below lightness level of 50 CIELAB units is contained about 90% of the natural colors.

## **Chapter 3. The colors of natural scenes benefit dichromats**

### 3.1. Introduction

Dichromats confound colors that are discriminated by normal trichromats. These confused colors lie along the confusion lines and can only be discriminated by luminance differences [11]. Given that many natural colors are close to these confusion lines dichromats may be in disadvantage in discriminating natural objects only using chromatic cues [138]. Dichromats, however, do not seem impaired in other visual aspects, e.g. in color constancy with natural stimuli [5,139–142]. In some tasks, they seem to be even better than normal trichromats, e.g. cone-isolating stimuli at high temporal frequencies [143] or camouflage detection [144,145]. They can also use color names almost like normal trichromats [74,146,147], can discriminate most of the objects in everyday life and show only rarely evidences of their disability, e.g. selecting colors of clothes, working with man-made color codes, judging ripeness and cooking state of food [52], in the medical profession [51,148] or in artistic activities [149].

Estimates based on Brettel's dichromatic perceptual model [10] and on how much the object color volume [11] is compressed in dichromacy predict that dichromats see less than 1% percent of the object colors that normal trichromats can see [12]. These estimates assume that lightness is a chromatic dimension that is used for discrimination. They also assume that all colors of the theoretical object color volume occur in nature. More realistic estimates based on spectral imaging data from natural scenes suggest numbers of about 7% [14]. These estimates suggest a larger impairment than observed in dichromats' practical everyday life. One hypothesis is that pairs of colors confused by dichromats are rare and thus have small impact on the overall perceived chromatic diversity.

The goal of the present work was to empirically quantify how much dichromats are impaired in discriminating the colors of natural objects if those colors are viewed with the same frequency distributions as they occur in nature. Thus, it was prepared a discrimination test based on spectral data from hyperspectral imaging of natural scenes. These data were used for the illumination of a real scene assembled in the laboratory with three-dimensional objects of flat reflectance spectrum that reflected light as if they were surfaces sampled from natural scenes. The setup was built in such a way that the objects of the scene look as having a tunable intrinsic color. The spectrally tunable light source reproduces the spectra with high accuracy and therefore the methodology avoids the usual assumptions about dichromat's photoreceptor spectral sensitivities that have to be made when doing display monitor experiments. The experiment was carried out by color normal

observers and dichromats. It was found that dichromats discriminate almost 70% of the colors normal observers discriminate when comparing in pairs and therefore the impairment is, in practice, relatively small. The discrimination data can be predicted using Brettel's models of dichromats color perception together with the actual distributions of colors in natural scenes and confirms the hypothesis that the frequency of occurrence of natural colors benefits dichromats.

## 3.2. Methods

### 3.2.1. Experimental setup

Figure 3.1 shows the experimental setup with the test scene assembled inside an illumination booth with a size of 66 cm (width) × 48 cm (length) × 46 cm (height). The objects were three geometric objects: a sphere, a cylinder, and a parallelepiped. They were fixed to an acrylate plate, supported by a Styrofoam support which was slightly tilted towards the observer. The objects and the acrylate plate were uniformly sprayed with a white matte powder (Spray-Rotrivel U, CGM Cigiemme s.r.l) which gave an approximately lambertian finish with a reflectance spectrum flat in the visible spectral region.

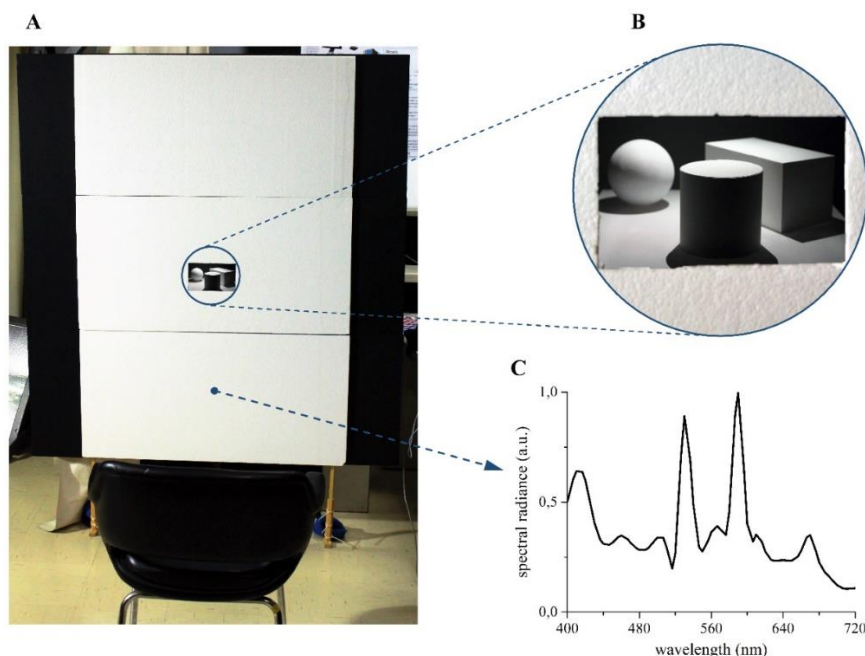


Figure 3.1. Front view of the test setup (A), close view of the test scene (B), and the radiance spectrum of the discharge lamp (OSRAM HQI 150W RX7s) reflected by the white Styrofoam mask that served as the adapting illuminant for the experiment (C). The white Styrofoam mask illuminated by the adapting illuminant provided an adapting field. A rectangular aperture on this mask allowed the scene to be seen by the observer.

The visible booth's wall was painted with a Munsell N7 matt emulsion paint (VeriVide Ltd, Leicester, UK). The test scene inside of the booth was illuminated by a spectrally tunable light source (OL 490 Agile Light Source, Gooch & Housego), based on the Digital Light Processor (DLP) technology. With such setup it is possible to tune the color of the test scene to any arbitrary spectral composition without having to resort to metameric systems of color reproduction, e.g. monitor displays, which always need assumptions about the visual system of dichromats. The spectrally tunable light source was calibrated with a spectral resolution of 20 nm and its light was delivered to the scene from above by an optical diffuser (10DKIT-C2 25°, Newport) placed at the end of the flexible optical fiber light guide. This guaranteed a level of uniformity of about 90% over the visible part of the scene.

Between the observers and the booth there was a Styrofoam mask with a flat white surface with an aperture that allowed the observers to see the test scene. The size of the white surface was 99.5 cm (width) × 149 cm (height) corresponding to a visual angle of 57 ° × 79 ° at the distance of 93 cm. Relatively to the test scene position, the white surface was at 54 cm and the observer was at a viewing distance of 147 cm. With this configuration the visual angle of the aperture width (17 cm) and scene width (26 cm) was 10 °. The white surface was illuminated by a discharge lamp (OSRAM HQI 150W RX7s) located at 240 cm from the experimental setup and at an angle of approximately 45° such that no light contaminated the test scene. This illuminant was considered the adapting illuminant and its spectrum as reflected by the white surface is represented in Figure 3.1 C. The spectrum had a correlated color temperature (CCT) of 5200 K, a luminance of 30 cd/m<sup>2</sup> and was uniform across the white surface.

### 3.2.2. Stimuli

The stimulus for the experiment was the three-dimensional scene inside the booth which simulated objects reflecting as in natural scenes. This was accomplished by selecting spectra from natural scenes obtained by hyperspectral imaging from 400 nm to 720 nm. These data were obtained from single pixels from four natural scenes of an existing database [130,131]. The four scenes are shown in Figure 3.2 and their color volume expressed in CIELAB are represented in

Figure 3.3. The scenes were selected to represent rural and urban environments and their colors span a considerable volume of the color space of natural colors.

The scenes were assumed illuminated by the illuminant from the discharge lamp, thus with a CCT of 5200 K. This illuminant was selected to be the same as the adapting illuminant which spectrum is presented on Figure 3.1 C.

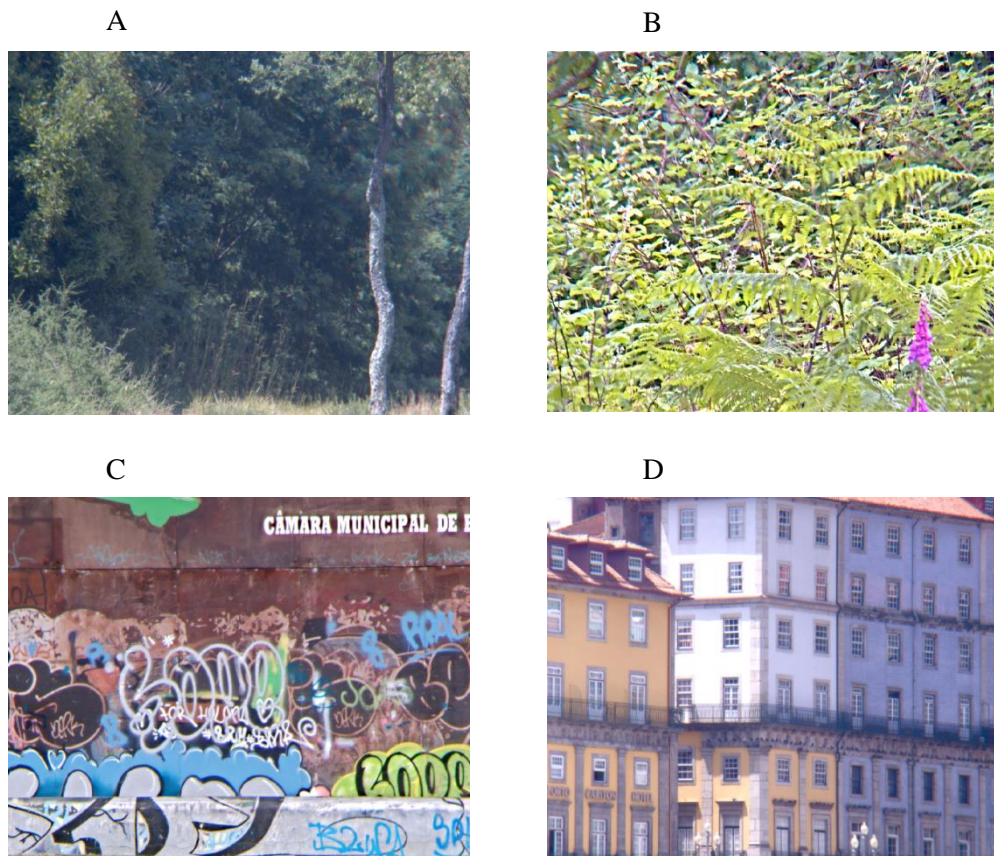


Figure 3.2. Images of the four natural scenes tested. Scenes A and B are from rural environments. Scenes C and D are from urban environments. The scenes represented in A and B are from the Minho region, C is from Braga and D is from Porto, all in Portugal. They belong to an existing database [130,131]. The colors of the scenes were simulated as illuminated by the adapting illuminant. In each trial of the experiment two pixels were selected randomly and their radiance spectra were used to illuminate successively the objects inside the booth. Each scene was tested in different experimental sessions.

The testing scene was viewed monocularly to avoid diplopia resulting from viewing the scene binocularly through the aperture of the Styrofoam mask located at a different plane. Because the observers were viewing the scene through this aperture the test scene looked as a group of objects of an intrinsic color illuminated by the illuminant from the discharge lamp, rather than white objects illuminated by a colored illuminant.

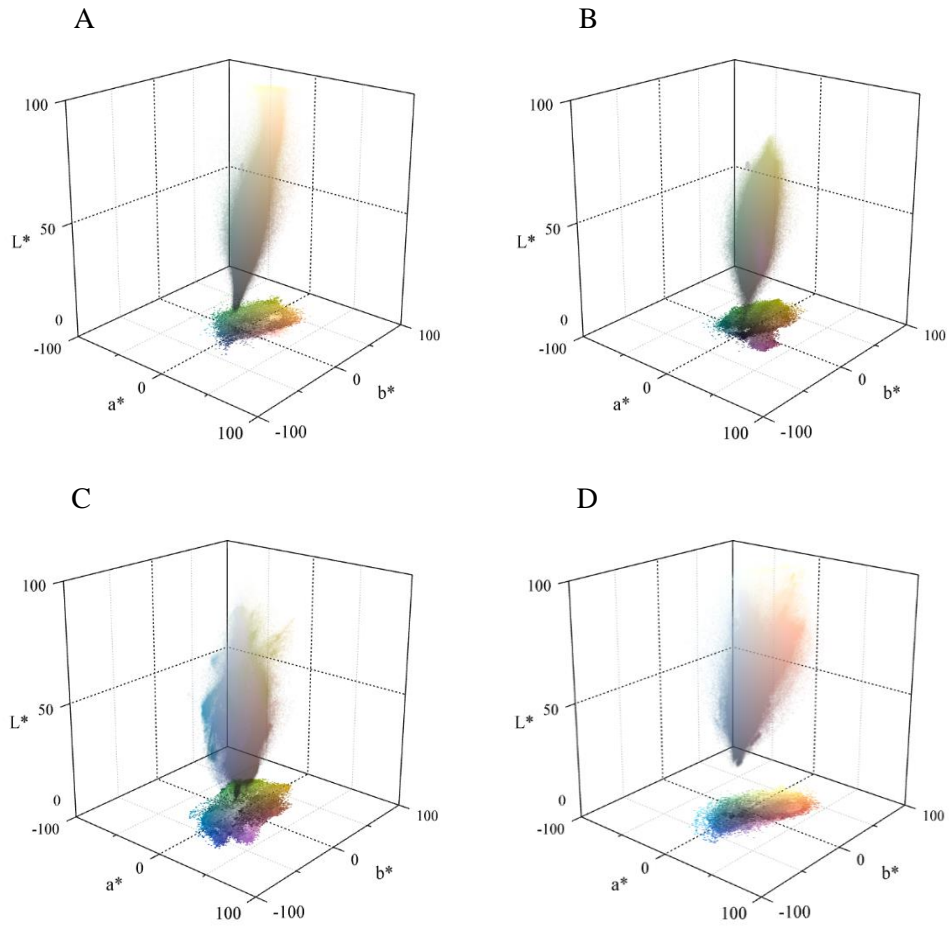


Figure 3.3. Color volume of each natural scene represented in Figure 3.2. The illumination was the adapting illuminant with a CCT of 5200 K and the colors are represented in the CIELAB color space for the CIE 1964 standard observer.

### 3.2.3. Procedure

Each trial consisted of a sequence of three time intervals where the scene could be seen, separated by dark interstimulus interval (ISI) of 0.5 s. Figure 3.4 illustrates the sequence. In the first interval it was shown the adapting illuminant, i.e., the same as the light reflected from the Styrofoam mask, for 1.5 s. Then, spectrum 1 and spectrum 2 illuminated the scene with spectra drawn from random pixels of one of the four scenes tested, lasting 0.5 s each, and separated by an ISI of 0.5 s. In each session, only one natural scene was tested. The 4 scenes were tested 3 times each in separate sessions in a counterbalanced design. Each observer carried out 12

sessions of 220 trials each, in a total of 2640 test trials plus 240 control trials were spectrum 1 and spectrum 2 were made deliberately equal to estimate false alarm rates.

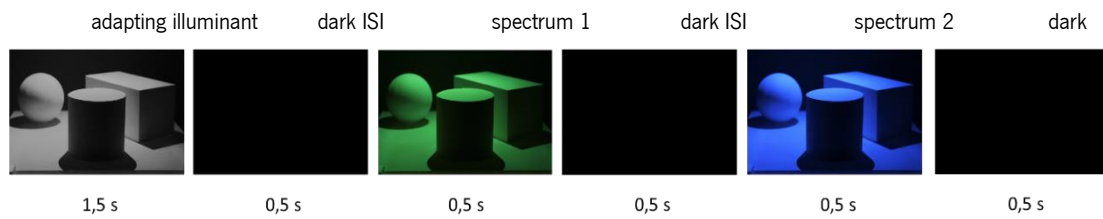


Figure 3.4. Stimuli sequence of each trial. The experiment was a 1AFC single alternative same-different test. The adapting illuminant was kept on for the first 1.5 s of the trial. The two test spectra and the three dark ISI lasted 0.5 s each. The adapting illuminant was the same in all trials but spectrum 1 and spectrum 2 varied between trials.

Thus, the design corresponds to a one-alternative forced choice (1AFC) version of a same-different task [150]. The task of the observers was to indicate whether the color of the objects was the same or different. No indication was given to the observers about which type of scene was being tested.

### 3.2.4. Observers

Four normal trichromats and four dichromats carried out the experiment. The normal trichromats were students of 20, 22, 23, and 23 YO (1 male and 3 females). The dichromats were 2 protanopes and 2 deuteranopes of 26, 41, 42, and 49 YO (3 males and 1 female), respectively. Each had normal or corrected-to-normal visual acuity. Their color vision was tested with Rayleigh anomaloscope (Oculus Heidelberg Multi Color), Cambridge Colour Test [151], Ishihara plates and the Color Assessment and Diagnosis (CAD) Test [152]. The experiments were performed in accordance with the tenets of the Declaration of Helsinki and informed consent (see Appendix I) was obtained from all observers.

### 3.3. Results

Figure 3.5 shows the results of the experiment for normal observers (N) and dichromats, protanopes (P) and deuteranopes (D). Figure 3.5 A represents the average across observers of pairs of spectra identified as different. Data was based on 2640 trials for each observer. Error bars represent the standard deviation across observers. Average performance is about 80% for normal observers and protanopes and about 10% lower for deuteranopes. As these results are affected by observers' criterion the discrimination index  $d'$  [153] was computed for each observer. The computation was based on the assumption of a 1AFC, same-different task by the differencing mode [150]. Figure 3.5 B shows the average  $d'$  values across observers. For normal observers  $d'$  was about 4 and for dichromats about 3, expressing quite high discrimination performance. To express this discrimination performance in a more familiar way the percentages of pairs of spectra discriminated were computed as if the all observers had the same criterion. This was done by inverting the  $d'$  computations [150]. These data are represented in Figure 3.5 C. For normal observers the discrimination was 67%, for protanopes 45% and for deuteranopes 46%. Thus, performance of dichromats was about 67% of that of normal observers.

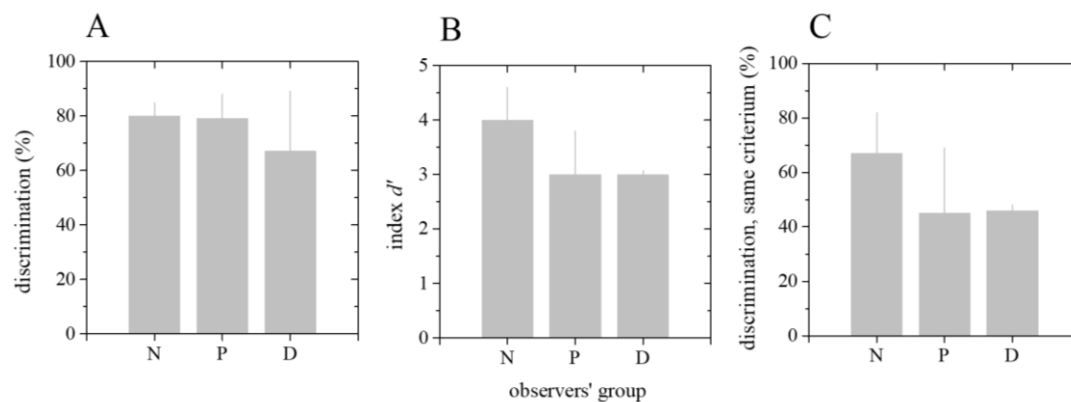


Figure 3.5. Results from the experiment for normal observers (N) and dichromats, protanopes (P) and deuteranopes (D). (A) Average pairs of colors identified as different. (B) Average discrimination index  $d'$  computed for an 1AFC, same-different task by the differencing mode [150]. (C) Average pairs of colors identified as different derived by the discrimination index  $d'$  assuming that all observers have the same criterion. Data based on 2640 trials for each observer. Error bars represent standard error across observers.

### 3.4. Discussion

The color discrimination for dichromats in natural environments was found to be about 45%, only 22% less than the performance of normal trichromats. This result translates into an impairment of 33% on dichromats discrimination relatively to normal discrimination. Dichromats in natural environments are therefore much better than anticipated by models that do not take into account the frequency distributions of natural colors.

Dichromats had a performance almost as good as trichromats distinguishing colors of natural scenes in general, but for discriminating specifically between fruits and foliage the trichromats may have the advantage [4] making frugivory the main reason for trichromacy development in pre-historic primates [3]. The satisfactory results of dichromats found in this work could help explain why dichromacy was kept in some individuals until the current human population, and why dichromacy is the most common form of color vision in mammals [2]. Dichromacy must allow satisfactory discrimination in natural scenes, otherwise trichromacy would probably be more frequent among species of mammals. This idea is consistent with a spectral analysis suggesting that the receptors of dichromatic mammals coincide with the optimal spectral tuning predicted for discrimination in natural scenes [154].

The illumination simulated in the tested natural scenes was the same as that used for the adapting field, produced by the discharge lamp shining on the Styrofoam mask. Although this light source is different from daylight the distributions of color difference it produces are very similar, thus the discrimination levels inferred here are very similar to those expected in natural conditions.

The discrimination measured here assumes uniform colors across object surfaces. Real objects are not uniform and thresholds for natural textures are known to differ from those for uniform surfaces [155,156]. However, the relative discrimination between normal trichromats and dichromats in real conditions is not expected to change much as the individual chromatic diversity of objects is likely to favor an impaired visual system.

In summary, although dichromats perceive much less colors than normal trichromats the color diversity of natural environments matches their vision and the colors they confound may not frequent and overall, they have a discrimination close to normal trichromats.



## **Chapter 4. Data base of spectral data from normal and abnormal skin of hospital patients.**

## 4.1. Introduction

The color of normal skin has already been the object of study of several research groups that presented databases for populations like United States [157], United Kingdom [158–160], Finland [161], China [158–160], South Korea [162], Philippines [161], Iran [158] and Thailand [158]. These studies focus on characterizing the color of human skin in different countries with the main objective of making colorimetric comparison between the various races and ethnicities. But it was not found in literature any databases of the skin color of Portuguese population.

Skin color changes occur due to anatomic or physiologic skin alterations that affect significantly the skin spectrum [163]. The color of skin disorders can be uniform or variegated and can assume colors like pink, red, purple, white, tan, brown, black, blue, gray, and yellow [164]. The color and spectral changes that skin can present on an extended range of pathological situations are not yet properly described in the literature. Studies on the colorimetry of dermatological pathology are scarce and each study focus only on specific anomalies, mostly erythema [165–170], cyanosis [171,172], and pigmented lesions [163,173]. In addition, mostly of these studies only provide chromaticity data, but the data needed for the computation of Chapter 5 should be spectral reflectance. Therefore, there is an interest to collect a set of spectral data for a wide range of skin abnormalities.

The purpose of this work was to construct a data base of spectral reflectance of normal and abnormal skin of hospital patients to be implemented on the computations at Chapter 5 of a colored filter for a medical practitioner with protanopia.

## 4.2. Methods

A partnership was established with the dermatology service of the Coimbra Hospital and University Centre (CHUC) to implement a protocol that aimed to measure *in vivo* samples of the skin variety that a physician could encounter in hospital patients. A research protocol to be held in hospital environment was devised (see Appendix I) and approved by the Subcommission of Ethics for Life and Health Sciences (SECVS) of the University of Minho (see Appendix III).

### 4.2.1. Participants

The participants were recruited from the user population of the dermatology service of CHUC, which were approached on dermatological consultations, hospitalization rooms, or in the emergency department. Demographic data (age, gender, and race) was recorded on the acquisition record sheet (see Appendix IV). Only patients and possible companions over the age of 18 presenting one or more types of skin disorders could participate. 91 patients participated on the study but the data of 7 participants was rejected due to dubious measuring, light contaminations or incomplete demographic data. The remaining participants were 1 African female 46 years old, and 83 Caucasians from which 52 were women and 31 were men. The ages of the Caucasian participants ranged from 19 to 93 and its distribution is shown on Figure 4.1.

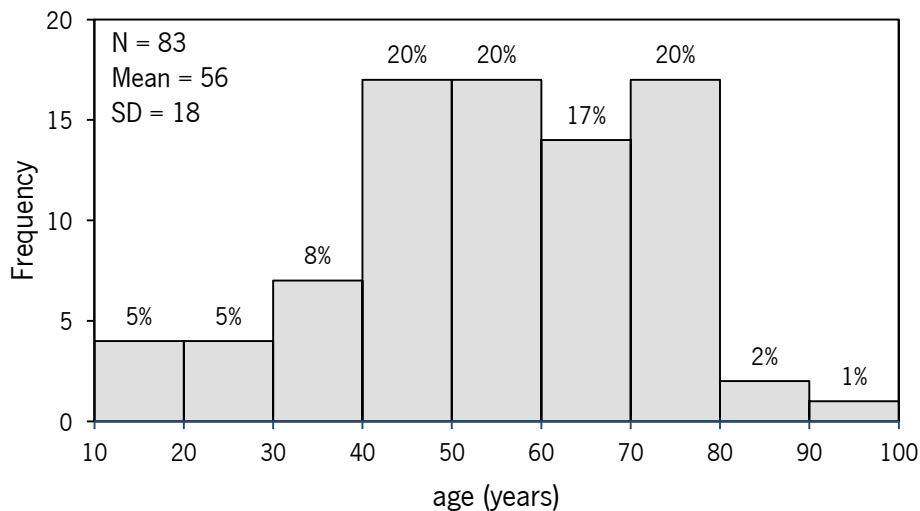


Figure 4.1. Age distribution of the participants recruit at the hospital.

### 4.2.2. Skin measuring

The patients selected during medical consultation were led to a separated office to undergo skin measurement. The patients who were in the hospitalization and emergency rooms were measured at the site. The measurement sessions had an average period of approximately 5 minutes per patient.

The skin measurements of patients were done using a contact spectrophotometer (CM-2600D, Konica Minolta, Japan) that was packed with a transparent plastic protector (see Figure 4.2) conveniently discarded between uses on different participants as a measure against

transmission of contaminants. For that reason, the recurrent white calibration of the spectrophotometer had to be done with the plastic protector placed on the sensor. The obtained data was spectral reflectance with specular component excluded from 400 nm to 700 nm in spectral steps of 10 nm.



Figure 4.2. Contact spectrophotometer (CM-2600D, Konica Minolta, Japan) used for measuring dermatological patients. For biological protection it was repacked with a new plastic protector for every new patient. The transparent plastic covered the measure sensor at the bottom of the instrument and therefore its calibration had to be made having the plastic in account.

It was done a minimum of 3 measurements for each type of the anomalies detected on a patient and 7 measurements of healthy skin done in body locations typically analyzed in similar studies [158–160,162] on normal skin: forehead, right cheek, left cheek, back of right hand, back of left hand, right inner forearm, and left inner forearm (see Figure 4.3). When one or more of these 7 sites were affected by anomalies, alternative body areas seemingly unaffected were measured. This study took preference on dermal anomalies with potential to be hard to see by a dichromat like very subtle erythema and for cases of special interest like this, it was also measured the normal skin around the sample of abnormal skin. Thus, cases of very accentuated hyperpigmentation like nevus were more overlooked.

A photographic record of the site of the abnormal skin measurements was also maintained and accompanied by the annotation of the clinical signal type and medical etiology. The investigators involved in the acquisition and processing of these data were required by term of confidentiality to maintain the privacy of the participants, ensuring that neither the recorded data nor the photographs would allow any patient to be identified. The measurements were performed in accordance with the tenets of the Declaration of Helsinki and informed consent was obtained from all observers (see Appendix V).

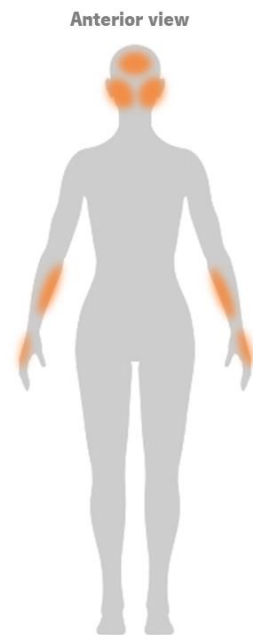


Figure 4.3. The 7 body locations of the normal skin measures (forehead, right cheek, left cheek, back of right hand, back of left hand, right inner forearm, and left inner forearm).

### 4.3. Results

The only African participant presented hyperpigmentation (see Figure 4.5 (a) due to scars from pityriasis rosea. The list of clinical signs encountered on Caucasian participants is presented at Table 4.1. It describes the Caucasian data sets by number of cases, number of measurements and lists at the Records of etiology column the causes and pathologies recorded, when possible, as being associated with the different types of abnormal skin.

Figure 4.4 shows the mean spectra of normal skin for the different body areas measured. The spectra of the different areas have similar shape but the forehead presents relatively larger values for long wavelengths and the inner forearms have larger values for almost all wavelengths giving a brighter color its skin.

Table 4.1. Data base of Caucasian skin samples organized by type of clinical sign.

<b>Clinical sign</b>	<b>Number of participants</b>	<b>Number of measurements</b>	<b>Records of etiology</b>
Normal skin	82*	614	—————
Crust	1	5	—————
Cyanosis	8	95	Poor circulation; unknown.
Erythema	57	670	Acne; actinic keratosis; angioma; allergies; burn; dermatomyositis; eczema; erysipelas; granuloma; hives; lupus; medical intervention; perniosis; psoriasis; rosacea; scab; telangiectasia; trauma; unknown.
Hyperkeratosis	1	5	—————
Hyperpigmentation	17	177	Dermatofibroma; keratosis seborrheic; melasma; notalgia; old scar; solar lentigo; unknown.
Hypopigmentation	10	133	Burn scar; congenital; hypomelanosis; lupus; pityriasis alba; vitiligo, unknown.
Scale	1	3	Pityriasis rubra pilar
Scar tissue	9	68	Accidental trauma; medical intervention; trauma.
Yellowing	1	9	Callus.

\* One of the 83 participants did not have any normal skin available for measure.

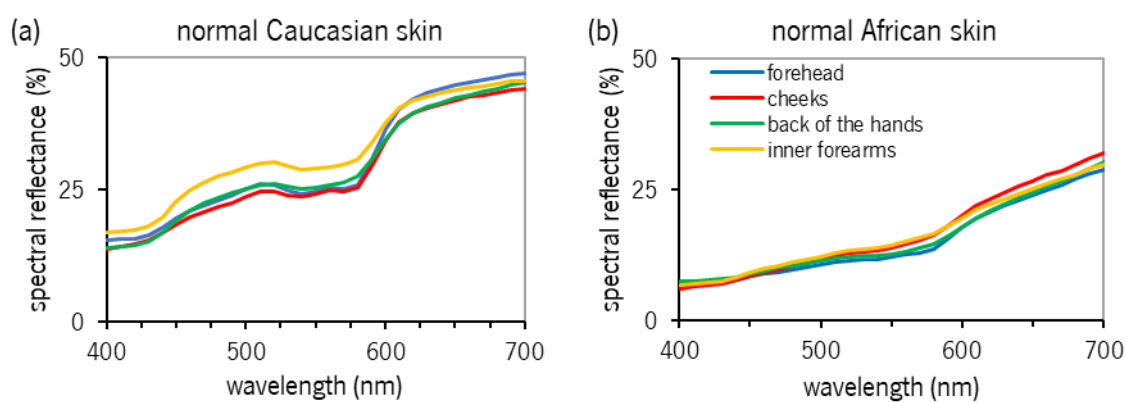
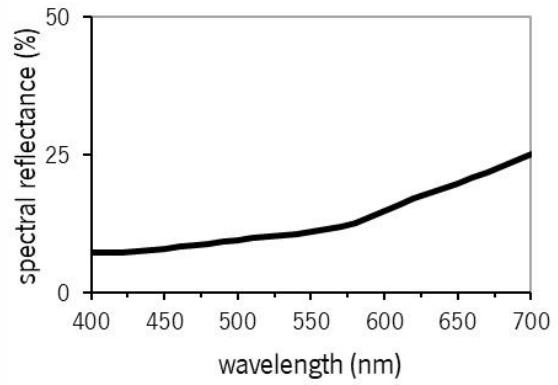
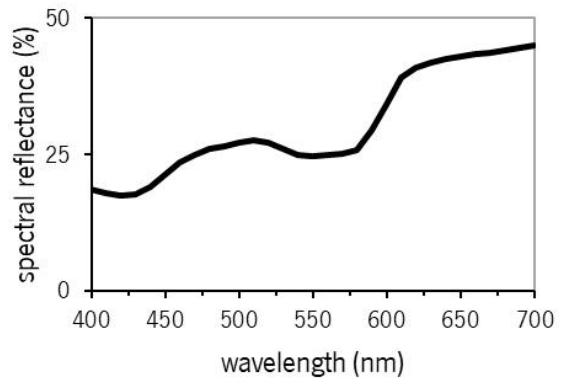


Figure 4.4. Mean reflectance spectra of the normal skin on forehead, cheeks, back of hands, and inner forearms. The data of the 83 Caucasian are presented on (a) and (b) shows the same data for the only African participant.

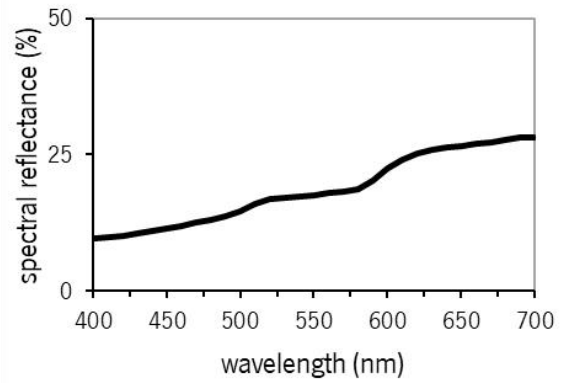
(a) **hyperpigmentation of African skin**



(b) **cyanosis**



(c) **yellowing of a callus**



(d) **erythema**

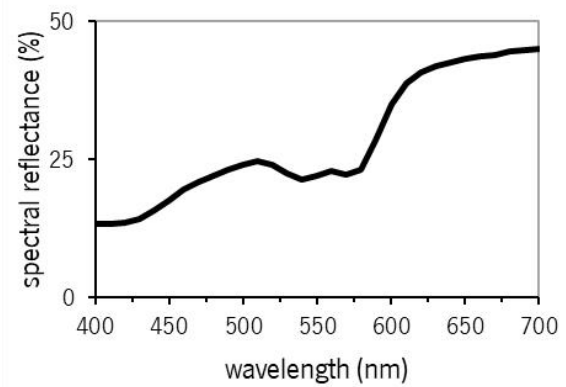


Figure 4.5. Pictures and mean reflectance spectra of examples of abnormal skin cases.

## 4.4. Discussion

A data base with a with range of abnormal skin types was achieved. But no cases of pallor were found which was one of the clinical signs of major interest for the protanope of Chapter 5. The other clinical signs of interest were erythema, cyanosis and yellowing. The Caucasian data sets of normal skin and of erythema are the two larger sets contain more than 600 samples each. Since the erythema is data set of abnormal skin with satisfactory number of cases, it was decided to apply it as input for the computations of Chapter 5.

**Chapter 5. Computation of a colored filter to improve erythema detection on the skin of patients for a medical practitioner with protanopia – a case report.**

## 5.1. Introduction

All mentions of CVD filters found in literature refer only to filters intended to improve the colors of all objects in general [15–18]. The findings in Chapter 3 suggest that even individuals with severe impairments in color vision like dichromats can distinguish colors of general environments almost as well as normal trichromats. In addition, a specific filter may improve the discrimination of some objects but have the opposite effect on others. Because of these reasons, filters that take a generalized approach may not get as efficient or useful as expected [15]. A better way to maximize efficiency could be to specialize the filter to a specific task with specific objects that a color vision defective is required to do professionally on a daily-basis.

Medical professionals and medical students with color vision deficiencies report some difficulties with tasks involving color discrimination, like recognition of color variations in the body (pallor, cyanosis, jaundice, rash, and dermal erythema), tissue distinction in surgery, observation of oral and pharyngeal lesions, observation of biological samples (blood, urine, bile in urine, feces, sputum, and vomiting), microscopy, ophthalmoscopy, and otoscopy [174,175]. During an enquiry, a protanope working in the medical field reported many of these profession-related problems and manifested major interest in using some form of visual aids specific for improving detection of areas of erythema, cyanosis, pallor or yellowing, among the normal skin of his patients. It was found one commercial company that sells colored lenses intended to enhance bruises and other forms of blood concentration under the skin [176]. With the available information is not possible to tell if those lenses were developed to also include color vision defective users.

Changes on normal skin color may indicate significant clinical changes and are often considered in the process of diagnosing dermal pathologies [164]. In the literature is possible to find several studies that describe cases of clinical professionals with color vision deficiencies that similarly to the protanope previously mentioned reported difficulties detecting skin color variations on their patients that could signal dermatological disorders [171,172,177,178]. Therefore, there is an interest to exploit the possibility of visual aids to help in this kind of cases.

The goal of the present work was to compute the best filter transmittance spectrum that optimize for the protanope the chromatic difference between normal skin and erythema. We propose a method to design specialized CVD filters that take into account the type of color vision

of the user, the spectral composition of the objects which he works with, and the light of its work place.

## 5.2. Methods

To compute filters specialized for the protanope physician it was used as input the illuminant of its work place and samples of normal skin and abnormal skin from hospital patients. For more details on the skin data base see Chapter 4.

### 5.2.1. Appointed illuminant

The ambient light of a hospital office indicated by the protanope as the best example of its work place was measured. He works under window light with the office lights turned off and the measurements were done in these conditions. Figure 5.1 shows the mean spectrum of the this illuminant.

The measurement procedure consisted on measuring a reference white ( $BaSO_4$ ) three times in 12 different places throughout the room with a telespectroradiometer (PR-650 SpectraScan Colorimeter; Photo Research, Chatsworth, CA) with wavelength range from 380 nm to 780 nm with a 4 nm step. The mean spectrum was normalized and interpolated to a spectral step of 10 nm from 400 nm to 700 nm to fit the spectral profile of the rest of the data used in the filter computations. The resulting data is the appointed illuminant to be use later in the filter computations.

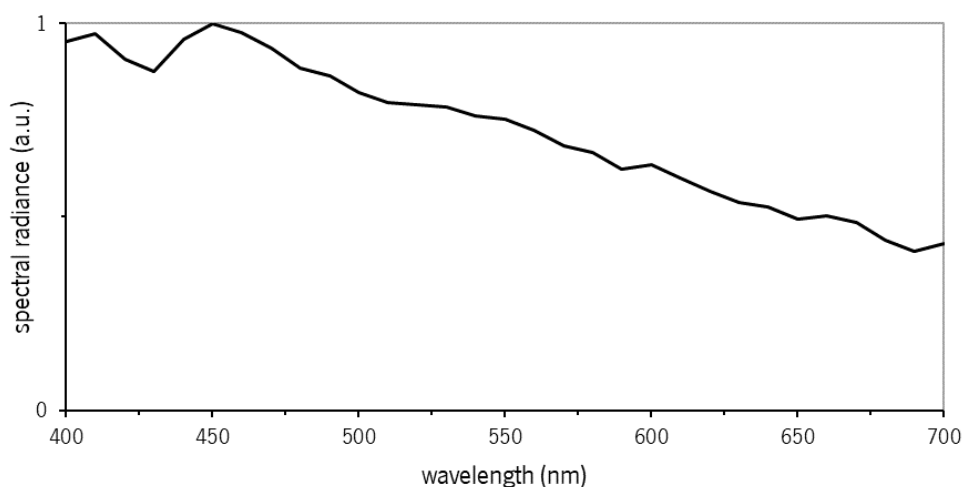


Figure 5.1. Mean radiance spectrum of the work place illuminant indicated by the protanope medical practitioner to be used in the filter computations.

## 5.2.2. Filter computation

An in-house software was developed on matlab (MathWorks, Inc., Natick, MA, United States of America) to find the transmittance spectrum for a filter that optimize the color difference between the data sets of normal skin and erythema. The colors of those data sets as seen by a protanope are represented at Figure 5.2 (a) and (b) respectively. The colors see by the protanope were simulated using the computational model of Brettel et al. (Brettel, Viénot, and Mollon 1997). To server as reference the colors as seen by a normal observer are also represented in Figure 5.2 at (c) and (d). The main difference between the skin colors seen by protanopes and normal observers is the  $a^*$  component which assumes negative values for the protanope giving to the skin a more greenish coloration in comparison to the perception of normal observers.

Figure 5.2 (c) and (d) represent for the normal observer the chromaticities of the data sets of normal skin and erythema, respectively. The data set of erythema samples is slightly shifted towards more saturated red colors and darker colors due to larger positive  $a^*$  values and lower  $L^*$  values, respectively. Either for normal observer or for protanope, there is some overlap between the gamuts of the two sets of skin. This means that the normal skin of some people can have the same coloration as erythema of others, and vice-versa.

The filter parameter which is optimized corresponds to the set of 31 values from 0 to 1 that make the transmittance spectrum of 400 nm to 700 nm in spectral steps of 10 nm. The software runs an existing optimization algorithm [179] that varies each of the 31 spectral transmittance values in order to find the best possible combination of those values. The best possible combination was considered to be the one that results in the global maximum of the mean  $\Delta E_{L^*a^*b^*}$  estimated between normal skin data and erythema data. The  $\Delta E_{L^*a^*b^*}$  values were estimated by the Euclidian distance between all points of the two data sets, in a pairwise manner on the CIELAB color space.

The filter effect was accounted on the tristimulus calculations by replacing the relative spectral radiance  $\phi(\lambda)$  on equations (1.1),(1.2), and (1.3), by the relative spectral radiance transmitted by the filter  $\phi(\lambda)_t$ . The  $\phi(\lambda)_t$  was determined by the following equation [180]:

$$\phi(\lambda)_t = \phi(\lambda)_i \times T(\lambda) \quad (5.1)$$

Where  $T(\lambda)$  is the spectral transmittance of the filter and  $\phi(\lambda)_i$  is the spectral radiance incident on the filter which is the same as the relative spectral radiance that leaves the observed

object  $\phi(\lambda)$ . This method of computing the filter effect assumes that the reflectance of the filter is null.

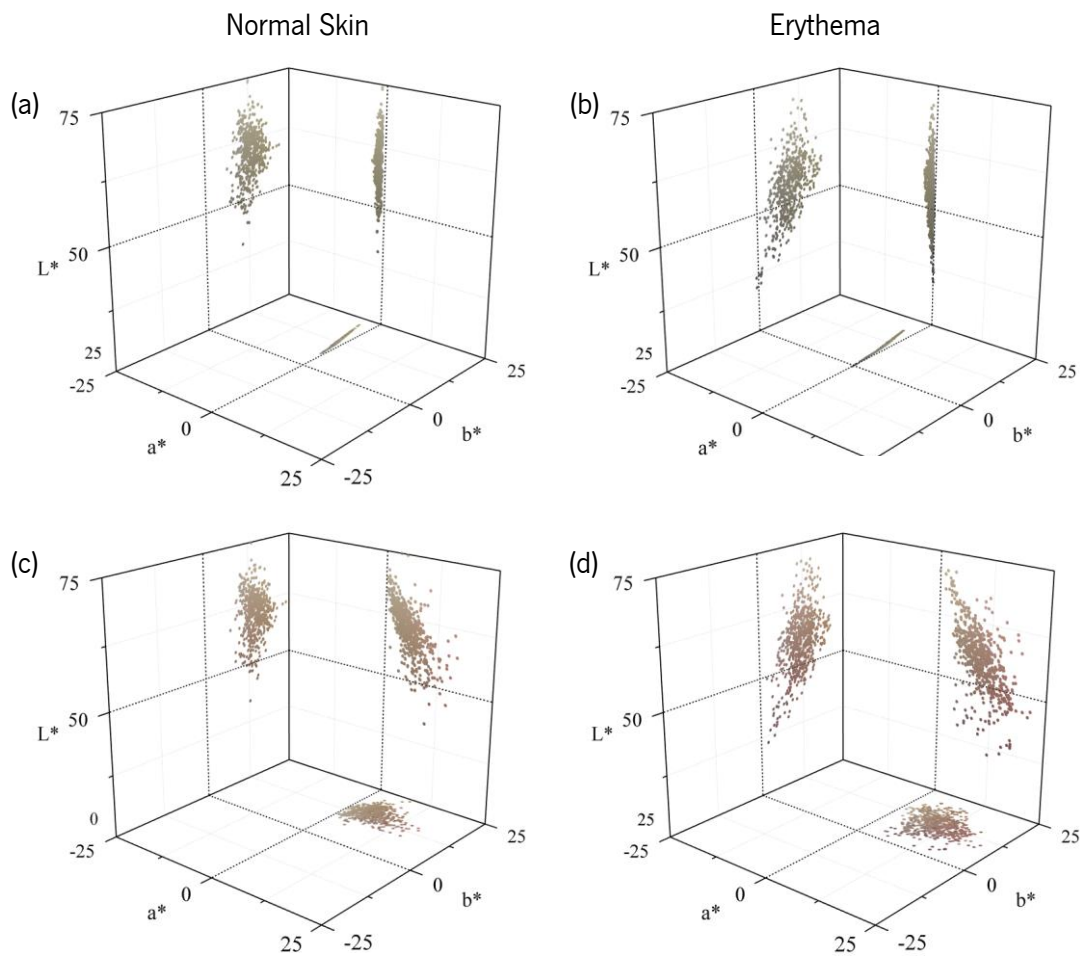


Figure 5.2. Representation in projections of the CIELAB color space planes of the colors perceived by a protanope, for the data sets of normal skin (a) and erythema (b). Similar data is also shown for the CIE 1931 standard observer in (c) and (d), respectively. It is assumed the appointed illuminant.

The CIELAB color coordinates were then calculated from tristimulus by using equations (1.5), (1.6), (1.7), and assuming the illuminant appointed by the protanope. For the normal observer the tristimulus calculations were computed using the CIE 1931 standard colorimetric observer [113]. To model the CIELAB colors for dichromats another in-house software was used in parallel, (for more details on this software computations see [12]). It applies a computational algorithm [10,70] based on sets of color stimuli that give the same perception on dichromats and normal trichromats, inferred from reports on unilateral inherited color vision deficiencies [71–73]. This algorithm models the colors perceived by a given dichromat, in the LMS color space. Therefore

it is required to use Vos conversion [181] and Smith and Pokorny's fundamentals [182] to convert between LMS chromaticities and XYZ tristimulus values. These transformations included the necessary assumption that Judd's modified photopic luminous efficiency function  $Y_{Judd}$  coincide with the CIE nonmodified function  $Y$ , i.e.  $Y = Y_{Judd}$ .

The optimized filter transmittance computations were executed for both protanope and normal observer.

## 5.3. Results

### 5.3.1. Filter optimization

The filter transmittance spectrum optimized for erythema detection by a protanope is represented in Figure 5.3 by the red line, and the equivalent result for the normal observed is represented by the blue line. In both cases the spectral transmittance values have large amplitude, varying from near zero values to about 1. For the protanope filter the spectrum presents only one peak that starts at 520 nm and ends at 600 nm. The normal observer filter has two peaks. The peak at medium wavelengths is similar to the one of the protanope case but is slightly shifted for small wavelengths, and the second peak lets pass all light with wavelengths larger than 610 nm.

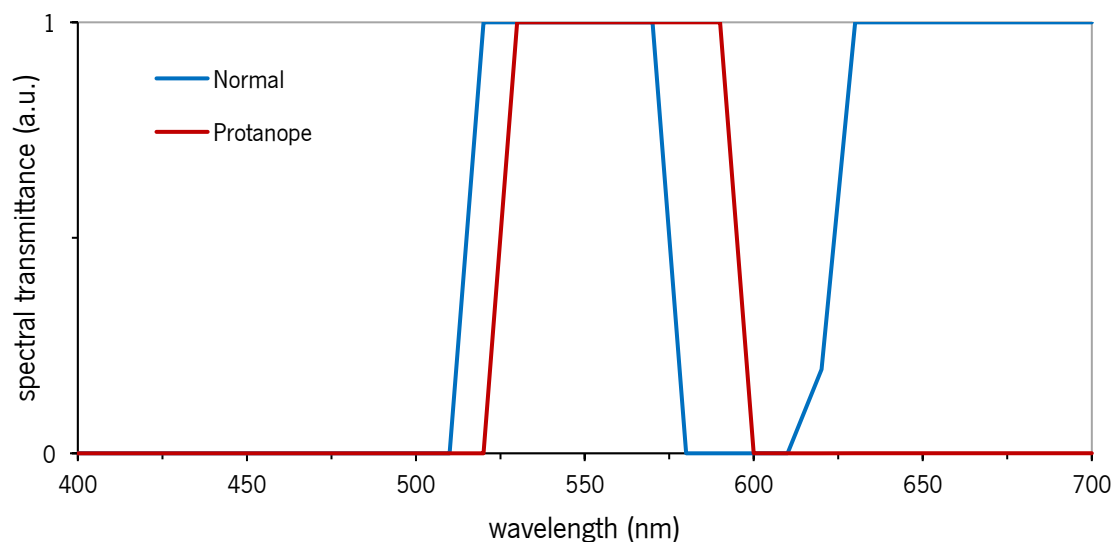


Figure 5.3. Filter transmittance spectrum optimized for erythema detection, for protanope (red line) and for normal CIE 1931 standard observer (blue line).

### 5.3.2. Filter assessment

Figure 5.4 shows the effect that the filters of Figure 5.3 have on the mean spectra of normal skin and erythema. Either with or without filter, the erythema spectra present a very similar shape to the normal skin spectra but with slightly lower radiance values. For the protanope using its filter only the medium wavelengths of skin will reach the eye. Whereas, for the normal observer besides a small band of medium wavelengths its filter will also pass long wavelengths to the eye.

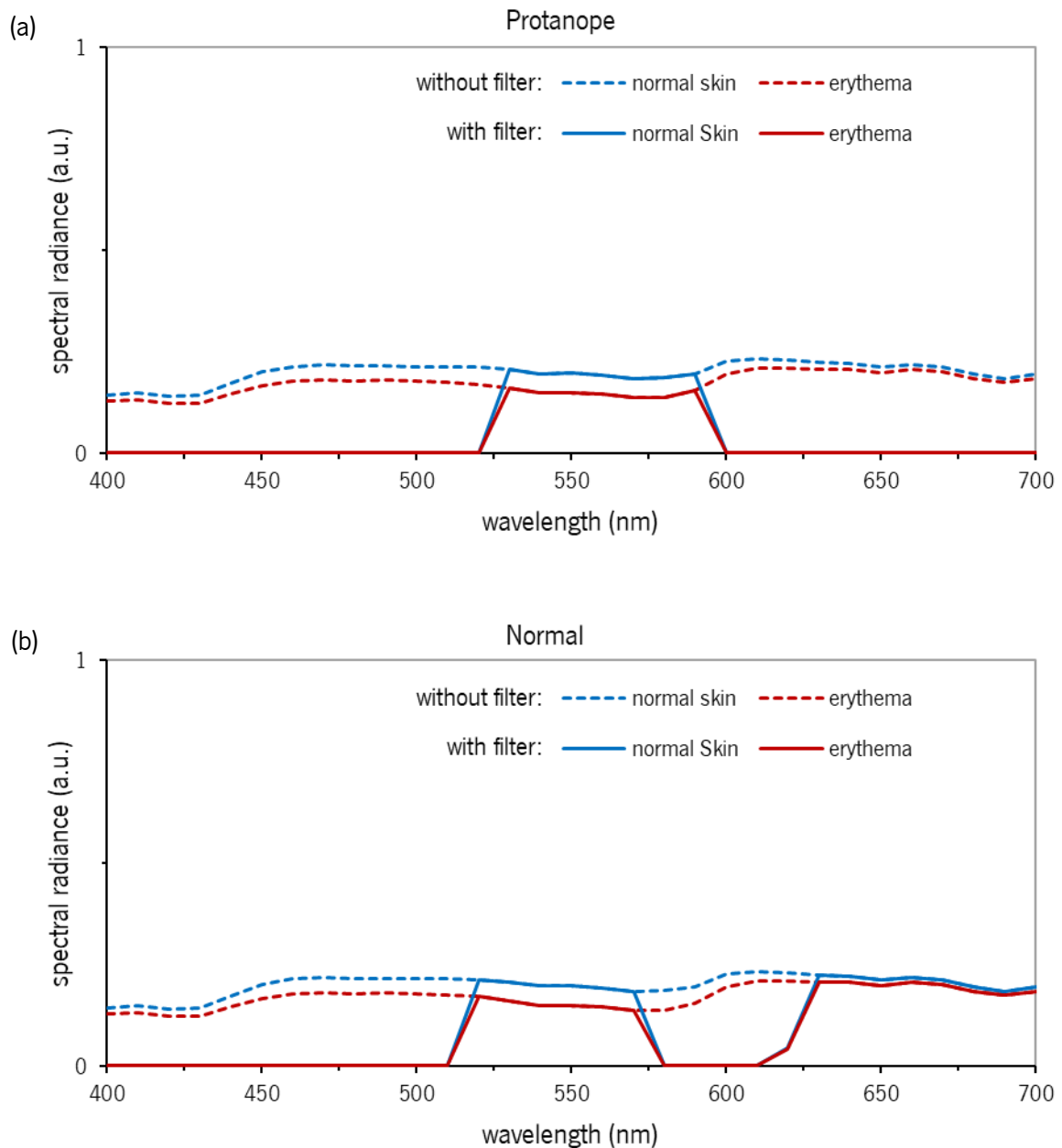


Figure 5.4. Spectral effect of the computed filters on the radiance spectra of normal skin (blue lines) and erythema (red lines). Comparison between the radiance spectra of skin seen through the filters (solid lines) and the original spectra (dashed lines), for the protanope filter (a) and the filter computed for the CIE 1931 standard observer (b).

The spectra of skin with filter represented by the solid colored lines at Figure 5.4, produces the set of colors represented at the Figure 5.5 as 2-D projections of the gamut in CIELAB space. The colors seen by the protanope with and without filter are represented in Figure 5.5 (b) and (a) respectively. For the normal observer the same data is shown in (d) and (c). The protanope filter induces a chromatic shift towards more saturated protanope colors and the filter for the normal observer shifts the normal skin colors to green saturated colors. The filter for the normal observer produces a diagonal flattening on the cluster of points that is revealed on the  $L^*b^*$  plane of figure (d). The cluster of points shown in (b) is oval and vertical but in (d) it is shaped almost into a plane due to the filter flattening effect. The same effect occurs on the protanope case but because the protanope gamut already is plane shaped, as suggested by the  $L^*a^*$  results in (a), it becomes line shaped when the filter effect is added.

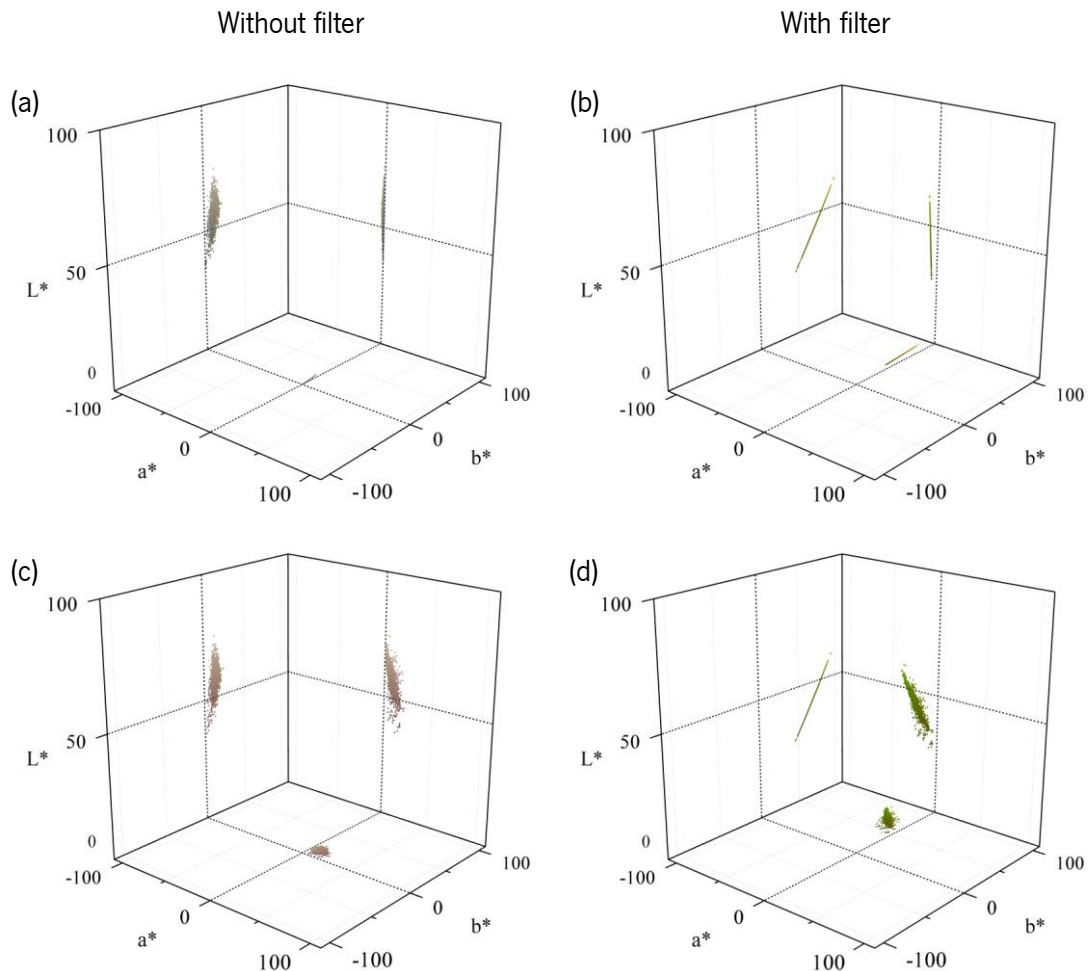


Figure 5.5. Chromatic effect of the computed filters. Representation of skin colors (normal skin and erythema) by its 2-D projections on planes of the CIELAB color space, as seen by the protanope observer, without filter (a) and with filter (b). Similar data is also shown for the CIE 1931 standard observer in (c) and (d), respectively. It is assumed the illuminant of Figure 5.1.

Thus, the filters alter the shape of the chromatic volume of skin by flattening it in one orientation but also stretching it in the perpendicular orientation. This stretching effect improves mostly the separation of colors through saturation level, as suggested by the length increment of the  $a^*b^*$  gamut. In the protanope case  $a^*b^*$  gamut with filter has a length of about 3 times the length without filter.

Figure 5.6 analyses the color differences ( $\Delta E_{L^*a^*b^*}$ ) between the colors of the data sets of normal skin and erythema, and compares the results with (solid lines) and without filter (dashed lines) for the cases of protanope and normal observer.

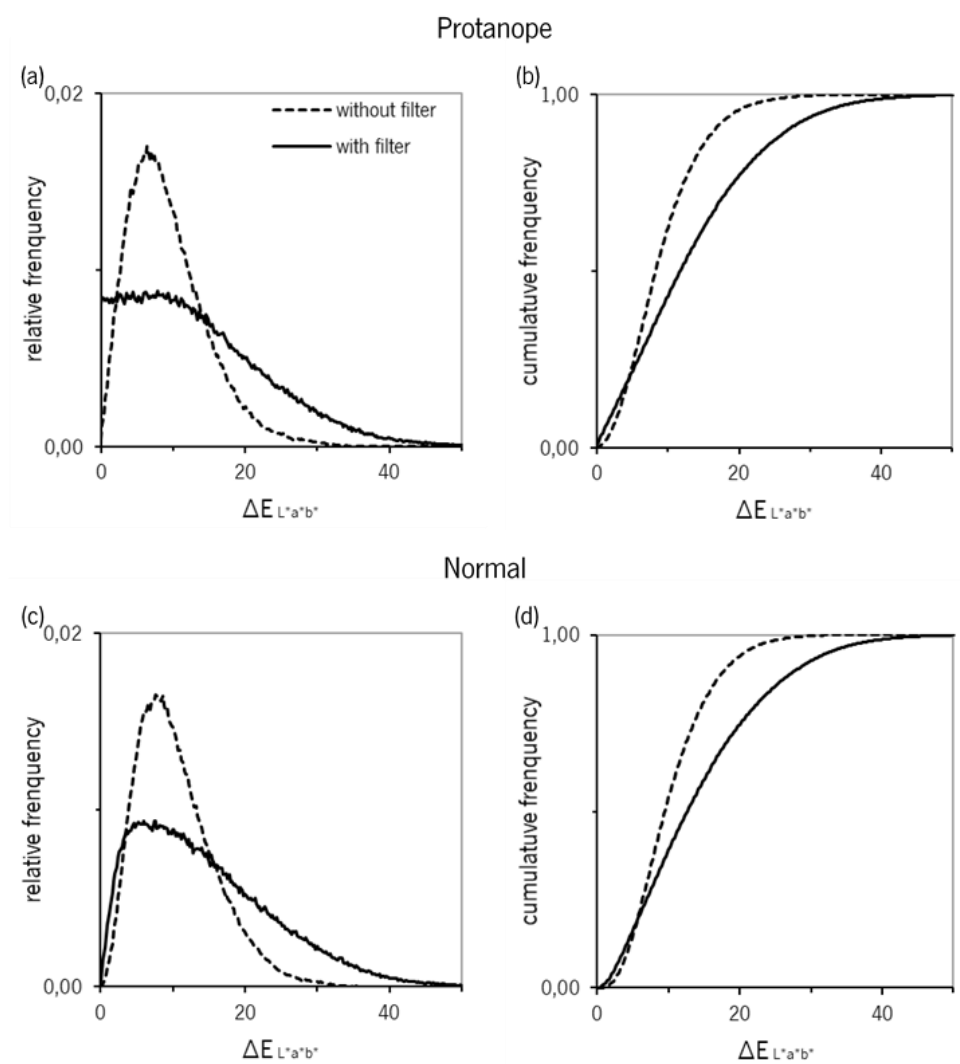


Figure 5.6. Comparison of color difference results for skin observation without filter (dashed lines) and with filter (solid lines). (a) and (b) Represent the relative frequency and cumulative frequency, respectively, of the color differences expressed in CIELAB between the data sets of normal skin and erythema when viewed by a protanope. (c) and (d) Represent similar data but assuming the normal CIE 1931 standard observer.

The protanope filter increased the mean  $\Delta E_{L^*a^*b^*}$  from about 9.4 ( $\pm 5.4$ ) to 13,6 ( $\pm 9.6$ ) CIELAB units. The filter of the normal observer increased the its mean  $\Delta E_{L^*a^*b^*}$  from about 10.6 ( $\pm 5.4$ ) to 14.6 ( $\pm 9.5$ ) CIELAB units. The color difference distributions of protanope and normal observer with filter are represented by solid lines at Figure 5.6 (a) and (c), respectively. The cumulative distributions of color differences for protanope and normal observer are represented at Figure 5.6 (b) and (d), respectively. It is revealed at (a) and (c) that the filter increased the frequency of large color differences (at about  $\Delta E_{L^*a^*b^*} > 14$  for protanope and about  $\Delta E_{L^*a^*b^*} > 16$  for normal observer). In both cases there is also some frequency increment of low color differences (at about  $\Delta E_{L^*a^*b^*} < 2$  for protanope and about  $\Delta E_{L^*a^*b^*} < 3$  for normal observer). According to the cumulative functions of Figure 5.6 (b) and (d) those low color differences represent about 9% and 8% of the total of color differences between the two sets of skin color.

## 5.4. Discussion

Figure 5.4 (a) reveals that the portion of skin spectrum that the filter lets to pass corresponds to the band of wavelengths on which the difference between skin spectrum and normal skin spectrum is larger. The fact that erythema spectra has lower radiance values than normal skin is related to existence of larger quantities of hemoglobin in the skin. In comparison, the filter of the normal observer has an extra peak at long wavelengths, probably making advantage of the L cone sensitivity.

According to the results of Figure 5.5, in both observers the filters shift the clusters of skin colors to larger  $b^*$  positive values, i.e. to more saturated greens, while also flattening the chromatic volume into an almost plane shape. In order for the filters to stretch the chromatic volume in a beneficial orientation it also must induce a flattening effect on a perpendicular orientation. Therefore, it was possible to increase the mean color difference perceived by the protanope between normal skin and erythema by about 44% of the original value, but at the expenses of the chromatic volume which decreased to 0.04% of the original volume. This suggests that increasing color differences do not necessary mean to have to increase the chromatic volume, at least, not for spectra of normal skin and erythema. For the normal observer the mean color difference increased about 38% and the chromatic volume decreased to 5.08%. Therefore, in regard to mean color difference the protanope filter performed better than the filter for the normal observers.

In regard to the distribution of color differences, the protanope filter decreases almost in half the amount of medium color difference to increase the amount of large color difference (above 14 CIELAB units). This means that almost half of the skin samples were shifted in color in a way that increased their color difference with all the other samples. This is increasing of the amount of large color difference is desired. But the protanope filter also increase the frequency some small color difference (less than 2 CIELAB units), probably due to the flattening effect of the chromatic volume. These color differences represent 9% of the total color differences.



## **Chapter 6. Conclusion and future work**

## 6.1. Main conclusions

The assessment of the Munsell and NCS color order systems done in Chapter 2 suggests that they are both good representing natural colors, except for very dark colors of about  $L^* < 20$ . During the analysis of this chapter it was found that the most frequent colors of Minho's environments are desaturated dark colors.

From Chapter 3 it is concluded that dichromats can distinguish pairs of natural spectra of real objects almost as much as normal observers, at least for the test conditions: monocular comparison of different spectra showed at different intervals, from a tridimensional scene seen through an aperture on a white adapting field. The performance of the dichromats was about 70% of performance of the normal observers. This fraction much higher than what would be expected when only considering the total number of object-colors that a dichromat can perceive. This difference may be due to the statistics of natural spectra, that may benefit the dichromats because the colors they confound maybe rare in the urban and rural environments.

The acquisition protocol of Chapter 4 allowed to obtain data sets of spectral reflectance of erythema and normal skin of the population of interest (hospital patients) for the case of the protanope medical practitioner of Chapter 5. This skin data was used on Chapter 5 to compute a specialized filter to improve erythema detection on the skin of the protanope's patients. It was achieved a filter design method that for the case of the protanope medical practitioner resulted on an improvement of 44% on the mean color difference between normal skin and erythema. The same method applied for normal vision also reveal improvements in the chromatic discriminability. There may be an interest for the industry and clinicians to apply the filter optimization method developed on Chapter 5.

## 6.2. Future work

The next step on the research line addressed on Chapter 5 would be to implement the same process on other color-detection tasks and other observers.

A discrimination experiment like the one described in Chapter 3 could be used to test the protanope's performance on distinguishing erythema from normal skin spectra. Such experiment could be also using to test a real filter based on the filter computed for the protanope.

## References

1. S. G. Solomon and P. Lennie, "The machinery of colour vision," *Nat. Rev. Neurosci.* **8**, 276–286 (2007).
2. G. H. Jacobs, "Evolution of colour vision in mammals," *Philos. Trans. R. Soc. B Biol. Sci.* **364**, 2957–2967 (2009).
3. J. D. Mollon, "'Tho'she kneel'd in that place where they grew..." The uses and origins of primate colour vision," *J. Exp. Biol.* **146**, 21–38 (1989).
4. D. Osorio and M. Vorobyev, "Colour Vision as an Adaptation to Frugivory in Primates," *Proc. R. Soc. B Biol. Sci.* **263**, 593–599 (1996).
5. J. M. M. Linhares, P. D. Pinto, and S. M. C. Nascimento, "The number of discernible colors in natural scenes," *J. Opt. Soc. Am. A* **25**, 2918 (2008).
6. M. R. Pointer and G. G. Attridge, "The number of discernible colours," *Color Res. Appl.* **23**, 52–54 (1998).
7. G. Jordan, N. Atkinson, and J. D. Mollon, "Do tetrachromatic women exist?," *Percept. ECVF Abstr.* **35**, 0 (2006).
8. J. Neitz and M. Neitz, "The genetics of normal and defective color vision," *Vision Res.* **51**, 633–651 (2011).
9. L. T. Sharpe, A. Stockman, H. Jägle, and J. Nathans, "Opsin genes, cone photopigments, color vision, and color blindness," in *Color Vision: From Genes to Perception* (Cambridge University Press, 1999), pp. 3–52.
10. H. Brettel, F. Viénot, and J. D. Mollon, "Computerized simulation of color appearance for dichromats," *J. Opt. Soc. Am. A* **14**, 2647 (1997).
11. G. Wyszecki and W. S. Stiles, *Color Science* (Wiley New York, 1982), Vol. 8.
12. E. Perales, F. M. Martínez-Verdú, J. M. M. Linhares, and S. M. C. Nascimento, "Number of discernible colors for color-deficient observers estimated from the MacAdam limits," *J. Opt. Soc. Am. A* **27**, 2106 (2010).
13. J. M. M. Linhares, P. D. Pinto, K. Amano, D. H. Foster, C. De Gualtar, C. N. Group, and M.

- Building, "Enhancing the chromatic diversity of natural scenes with optimized coloured filters," in *AIC Colour*. (2005).
14. J. M. M. Linhares, P. D. Pinto, and S. M. C. Nascimento, "The number of discernible colors perceived by dichromats in natural scenes and the effects of colored lenses," *Vis. Neurosci.* **25**, 493–499 (2008).
  15. J. D. Moreland, S. Westland, V. Cheung, and S. J. Dain, "Quantitative assessment of commercial filter 'aids' for red-green colour defectives," *Ophthalmic Physiol. Opt.* **30**, 685–692 (2010).
  16. O. M. Oriowo and A. Z. Alotaibi, "Chromagen lenses and abnormal colour perception," *African Vis. Eye Heal.* **70**, 69–74 (2011).
  17. M. A. D. D. E. Fez, M. A. J. Luque, and V. Viqueira, "Enhancement of Contrast Sensitivity and Losses," **79**, 590–597 (2002).
  18. S. Wolffsohn, James S.; Cochrane, Anthea L.; Khoo, Hana; Yoshimitsu, Yota; Wu, "Contrast Is Enhanced by Yellow Lenses Because of Selective R... : Optometry and Vision Science," **77**, 73–81 (2000).
  19. S. E. Palmer, "An Introduction to Vision Science," in *Vision Science: Photons to Phenomenology* (MIT Press, 1999).
  20. E. B. Goldstein, "Introduction to Vision," in *Sensation and Perception*, 8th ed. (Wadsworth, 2010), pp. 43–71.
  21. C. A. Curcio, K. R. Sloan, R. E. Kalina, and A. E. Hendrickson, "Human photoreceptor topography.," *J. Comp. Neurol.* **292**, 497–523 (1990).
  22. S. Hattar, "Melanopsin-Containing Retinal Ganglion Cells: Architecture, Projections, and Intrinsic Photosensitivity," *Science (80- )*. **295**, 1065–1070 (2002).
  23. M. W. Hankins, S. N. Peirson, and R. G. Foster, "Melanopsin: an exciting photopigment," *Trends Neurosci.* **31**, 27–36 (2008).
  24. A. J. Zele, P. Adhikari, B. Feigl, and D. Cao, "Cone and melanopsin contributions to human brightness estimation," *JOSA A* **35**, B19–B25 (2018).
  25. T. M. Brown, S. Tsujimura, A. E. Allen, J. Wynne, R. Bedford, G. Vickery, A. Vugler, and R.

- J. Lucas, "Melanopsin-based brightness discrimination in mice and humans," *Curr. Biol.* **22**, 1134–1141 (2012).
26. P. A. Barrionuevo and D. Cao, "Contributions of rhodopsin, cone opsins, and melanopsin to postreceptoral pathways inferred from natural image statistics," *JOSA A* **31**, A131–A139 (2014).
  27. H. Horiguchi, J. Winawer, R. F. Dougherty, and B. A. Wandell, "Human trichromacy revisited," *Proc. Natl. Acad. Sci.* **110**, E260–E269 (2013).
  28. D. M. Dacey, H.-W. Liao, B. B. Peterson, F. R. Robinson, V. C. Smith, J. Pokorny, K.-W. Yau, and P. D. Gamlin, "Melanopsin-expressing ganglion cells in primate retina signal colour and irradiance and project to the LGN," *Nature* **433**, 749 (2005).
  29. A. Stockman and L. T. Sharpe, "The spectral sensitivities of the middle-and long-wavelength-sensitive cones derived from measurements in observers of known genotype," *Vision Res.* **40**, 1711–1737 (2000).
  30. D. L. Sparks and I. S. Nelson, "Sensory and motor maps in the mammalian superior colliculus," *Trends Neurosci.* **10**, 312–317 (1987).
  31. E. B. Goldstein, "The Visual Cortex and Beyond," in *Sensation and Perception*, 8th ed. (Wadsworth, 2010), pp. 73–97.
  32. V. A. Casagrande and T. T. Norton, "Lateral geniculate nucleus: a review of its physiology and function," *neural basis Vis. Funct.* **4**, 41–84 (1991).
  33. A. L. Humphrey and A. B. Saul, "The temporal transformation of retinal signals in the lateral geniculate nucleus of the cat: Implications for cortical function," in *Thalamic Networks for Relay and Modulation* (Elsevier, 1993), pp. 81–89.
  34. R. Ramanath, *Color: An Introduction to Practice and Principles* (Wiley Online Library, 2005).
  35. P. Lennie, "The physiology of color vision," *Sci. Color* **2**, 217–242 (2003).
  36. J. Martinovic, "Magno-, Parvo-, Koniocellular Pathways," in *Encyclopedia of Color Science and Technology* (Springer Berlin Heidelberg, 2015), pp. 1–5.
  37. S. Chatterjee and E. M. Callaway, "Parallel colour-opponent pathways to primary visual cortex," *Nature* **426**, 668 (2003).

38. S. H. C. Hendry and R. C. Reid, "The koniocellular pathway in primate vision," *Annu. Rev. Neurosci.* **23**, 127–153 (2000).
39. F. Tong, "Cognitive neuroscience: primary visual cortex and visual awareness," *Nat. Rev. Neurosci.* **4**, 219 (2003).
40. J. C. Meadows, "Disturbed perception of colours associated with localized cerebral lesions," *Brain* **97**, 615–632 (1974).
41. S. Zeki, "A century of cerebral achromatopsia," *Brain* **113**, 1721–1777 (1990).
42. C. Heywood and A. Cowey, "With color in mind," *Nat. Neurosci.* **1**, 171 (1998).
43. N. Hadjikhani, A. K. Liu, A. M. Dale, P. Cavanagh, and R. B. H. Tootell, "Retinotopy and color sensitivity in human visual cortical area V8," *Nat. Neurosci.* **1**, 235 (1998).
44. K. S. Dulai, M. von Dornum, J. D. Mollon, and D. M. Hunt, "The evolution of trichromatic color vision by opsin gene duplication in New World and Old World primates," *Genome Res.* **9**, 629–638 (1999).
45. B. C. Regan, C. Julliot, B. Simmen, F. Vienot, P. Charles-Dominique, and J. D. Mollon, "Fruits, foliage and the evolution of primate colour vision," *Philos. Trans. R. Soc. B Biol. Sci.* **356**, 229–283 (2001).
46. K. R. Gegenfurtner and D. C. Kiper, "Color vision," *Annu. Rev. Neurosci.* **26**, 181–206 (2003).
47. M. A. Changizi, Q. Zhang, and S. Shimojo, "Bare skin, blood and the evolution of primate colour vision," *Biol. Lett.* **2**, 217–221 (2006).
48. C. F. Benitez-Quiroz, R. Srinivasan, and A. M. Martinez, "Facial color is an efficient mechanism to visually transmit emotion," *Proc. Natl. Acad. Sci.* 201716084 (2018).
49. André A. Fernandez and Morris, "Sexual Selection and Trichromatic Color Vision in Primates: Statistical Support for the Preexisting-Bias Hypothesis," *Am. Nat.* **170**, 10 (2007).
50. J. M. Steward and B. L. Cole, "What do color vision defectives say about everyday tasks?," *Optom. Vis. Sci.* **66**, 288–95 (1989).

51. J. A. B. Spalding, "Confessions of a colour blind physician," *Clin. Exp. Optom.* **87**, 344–349 (2004).
52. B. L. Cole, "The handicap of abnormal colour vision," *Clin. Exp. Optom.* **87**, 258–275 (2004).
53. D. M. Cockburn, "Confession of a colour blind optometrist," <http://doi.wiley.com/10.1111/j.1444-0938.2004.tb05066.x>.
54. J. L. Campbell, J. Spalding, F. a Mir, and J. Birch, "Doctors and the assessment of clinical photographs—does colour blindness matter?," *Br. J. Gen. Pract.* **49**, 459–61 (1999).
55. M. J. Reiss, D. a Labowitz, S. Forman, and G. P. Wormser, "Impact of Color Blindness on Recognition of Blood in Body Fluids," *Arch. Intern. Med.* **161**, 461 (2001).
56. E. Hering, "Outlines of a theory of the light sense.," (1964).
57. S. K. Shevell, "Color appearance," *Sci. Color* 149–190 (2003).
58. E. B. Goldstein, "Perceiving Color," in *Sensation and Perception*, 8th ed. (Wadsworth, 2010), pp. 201–227.
59. F. Martínez-Verdú, E. Perales, E. Chorro, D. de Fez, V. Viqueira, and E. Gilabert, "Computation and visualization of the MacAdam limits for any lightness, hue angle, and light source," *J. Opt. Soc. Am. A* **24**, 1501 (2007).
60. G. Jordan and J. D. Mollon, "A study of women heterozygous for colour deficiencies," *Vision Res.* **33**, 1495–1508 (1993).
61. E. Konstantakopoulou, M. Rodriguez-Carmona, and J. L. Barbur, "Processing of color signals in female carriers of color vision deficiency," *J. Vis.* **12**, 11–11 (2012).
62. G. Verriest, "Further studies on acquired deficiency of color discrimination," *JOSA* **53**, 185–195 (1963).
63. J. D. Mollon, "The origins of modern color science," *Sci. Color* **2**, 1–39 (2003).
64. T. M. P. Fernandes, S. M. Andrade, M. J. O. de Andrade, R. M. T. B. L. Nogueira, and N. A. Santos, "Colour discrimination thresholds in type 1 Bipolar Disorder: a pilot study," *Sci. Rep.* **7**, 16405 (2017).

65. A. Stockman and L. T. Sharpe, "Human cone spectral sensitivities and color vision deficiencies," in *Visual Transduction and Non-Visual Light Perception* (Springer, 2008), pp. 307–327.
66. J. Carroll, M. Neitz, H. Hofer, J. Neitz, and D. R. Williams, "Functional photoreceptor loss revealed with adaptive optics: An alternate cause of color blindness," *Proc. Natl. Acad. Sci. U. S. A.* **101**, 8461–8466 (2004).
67. D. H. Brainard, "Color appearance and color difference specification," in *The Science of Color*, 2nd ed. (Elsevier, 2003), pp. 191–216.
68. M. McClements, W. I. L. Davies, M. Michaelides, J. Carroll, J. Rha, J. D. Mollon, M. Neitz, R. E. MacLaren, A. T. Moore, and D. M. Hunt, "X-linked cone dystrophy and colour vision deficiency arising from a missense mutation in a hybrid L/M cone opsin gene," *Vision Res.* **80**, 41–50 (2013).
69. V. C. Smith and J. Pokorny, "Color matching and color discrimination," *Sci. Color* **2**, 103–148 (2003).
70. F. Viénot, H. Brettet, L. Ott, A. Ben M' Barek, and J. D. Mollon, "What do colour-blind people see?," *Nature* **376**, 127–128 (1995).
71. D. B. Judd, "Color perceptions of deuteranopic and protanopic observers," *J. Res. Natl. Bur. Stand* **41**, 247–271 (1948).
72. K. H. Ruddock, "Psychophysics of inherited colour vision deficiencies," *Inherit. Acquir. colour Vis. Defic. Fundam. Asp. Clin. Stud.* **7**, 4–37 (1991).
73. M. Alpern, K. Kitahara, and D. H. Krantz, "Perception of colour in unilateral tritanopia.," *J. Physiol.* **335**, 683–697 (1983).
74. T. Wachtler, U. Dohrmann, and R. Hertel, "Modeling color percepts of dichromats," *Vision Res.* **44**, 2843–2855 (2004).
75. G. M. MacHado, M. M. Oliveira, and L. A. F. Fernandes, "A physiologically-based model for simulation of color vision deficiency," *IEEE Trans. Vis. Comput. Graph.* **15**, 1291–1298 (2009).
76. S. Nascimento, J. Linhares, C. João, J. Santos, and V. de Almeida, "Testing perceptual

- models of dichromacy and anomalous trichromacy with a computer-based color-vision test," *J. Vis.* **15**, 1313 (2015).
77. S. J. Dain, "Clinical colour vision tests," *Clin. Exp. Optom.* **87**, 276–293 (2004).
  78. K. Mancuso, W. W. Hauswirth, Q. Li, T. B. Connor, J. A. Kuchenbecker, M. C. Mauck, J. Neitz, and M. Neitz, "Gene therapy for red-green colour blindness in adult primates," *Nature* **461**, 784–787 (2009).
  79. T. Waggoner, "Free Color Coding System to aid the colorblind.," <http://www.colorvisiontesting.com/color8>.
  80. Feelipa Color Code, "Feelipa Color Code," <http://www.feelipa.com/>.
  81. M. Neiva, "CODE ColorADD," <http://www.coloradd.net/code.asp>.
  82. A. S. Manaf and R. F. Sari, "Color recognition system with augmented reality concept and finger interaction: Case study for color blind aid system," *Int. Conf. ICT Knowl. Eng.* 118–123 (2011).
  83. L. Troiano, C. Birtolo, and M. Miranda, "Adapting palettes to color vision deficiencies by genetic algorithm," *GECCO'08 Proc. 10th Annu. Conf. Genet. Evol. Comput.* 2008 1065–1072 (2008).
  84. K. Wakita and K. Shimamura, "SmartColor," *Proc. 7th Int. ACM SIGACCESS Conf. Comput. Access. - Assets '05* 158 (2005).
  85. A. Dobie, "Android L includes new display modes for color blind users | Android Central," <https://www.androidcentral.com/android-l-includes-new-display-modes-color-blind-users>.
  86. G. Iaccarino, D. Malandrino, M. Del Percio, and V. Scarano, "Efficient edge-services for colorblind users," *Proc. 15th Int. Conf. World Wide Web - WWW '06* 919 (2006).
  87. G. Lausegger, M. Spitzer, and M. Ebner, "OmniColor – A Smart Glasses App to Support Colorblind People," **11**, 161–177 (n.d.).
  88. B. S. Ananto, R. F. Sari, and R. Harwahyu, "Color transformation for color blind compensation on augmented reality system," *Proc. - 2011 Int. Conf. User Sci. Eng. i-USER* 2011 129–134 (2011).

89. C. Lau, N. Perdu, C. E. Rodr, and S. Sabine, "An Interactive App for Color Deficient Viewers," **9395**, 1–9 (2015).
90. E. Tanuwidjaja, D. Huynh, K. Koa, C. Nguyen, C. Shao, P. Torbett, C. Emmenegger, and N. Weibel, "Chroma: AWearable Augmented-Reality Solution for Color Blindness," Proc. 2014 ACM Int. Jt. Conf. Pervasive Ubiquitous Comput. - UbiComp '14 Adjun. 799–810 (2014).
91. P. Melillo, D. Riccio, L. Di Perna, G. Sanniti Di Baja, M. De Nino, S. Rossi, F. Testa, F. Simonelli, and M. Frucci, "Wearable Improved Vision System for Color Vision Deficiency Correction," IEEE J. Transl. Eng. Heal. Med. **5**, (2017).
92. T. Ohkubo and K. Kobayashi, "A color compensation vision system for color-blind people," Proc. SICE Annu. Conf. 1286–1289 (2008).
93. E. Perales, J. M. M. Linhares, O. Masuda, F. M. Martínez-Verdú, and S. M. C. Nascimento, "Effects of high-color-discrimination capability spectra on color-deficient vision.," J. Opt. Soc. Am. A. Opt. Image Sci. Vis. **30**, 1780–6 (2013).
94. J. M. M. Linhares, P. E. R. Felgueiras, P. D. Pinto, and S. M. C. Nascimento, "Colour rendering of indoor lighting with CIE illuminants and white LEDs for normal and colour deficient observers," Ophthalmic Physiol. Opt. **30**, 618–625 (2010).
95. H. I. Zeltzer, "Method of improving color discrimination," (October 31, 1972).
96. I. M. Siegil, "The X-Chrom lens. On seeing red," Surv. Ophthalmol. **25**, 312–324 (1981).
97. H. I. Zeltzer, "Contact lens for correction of color blindness," (March 12, 1991).
98. J. K. Hovis, "Long wavelength pass filters designed for management of color vision deficiencies," Optom. Vis. Sci. **74**, 222–230 (1997).
99. G. Abraham, G. Wenzel, and J. Szappanos, "Method and optical means for improving or modifying color vision and method for making said optical means," (June 30, 1998).
100. H. A. Swarbrick, P. Nguyen, T. Nguyen, and P. Pham, "The ChromaGen contact lens system: colour vision test results and subjective responses.," Ophthalmic Physiol. Opt. **21**, 182–96 (2001).
101. A. W. Schmeder and D. M. McPherson, "Multi-band color vision filters and method by Ip-optimization," (August 21, 2014).

102. VINO, "Color Blind Glasses," <https://www.vino.vi/collections/color-blind-glasses>.
103. B. Drum, "FDA regulation of labeling and promotional claims in therapeutic color vision devices: A tutorial," *Vis. Neurosci.* **21**, 461–463 (2004).
104. L. T. Sharpe and H. Jagle, "I used to be color blind," *Color Res. Appl.* **26**, S269–S272 (2001).
105. O. Masuda, J. M. M. Linhares, P. E. R. Felgueiras, and S. M. C. Nascimento, "Lighting spectra for the maximum colorfulness," *Proc. SPIE - Int. Soc. Opt. Eng.* **8001**, (2011).
106. P. D. Pinto, J. M. M. Linhares, J. A. Carvalhal, and S. M. C. Nascimento, "Psychophysical estimation of the best illumination for appreciation of Renaissance paintings," *Vis. Neurosci.* **23**, 669–674 (2006).
107. O. Masuda and S. M. C. Nascimento, "Best lighting for naturalness and preference," *J. Vis.* **13**, 4–4 (2013).
108. Y. Kohmura, S. Murakami, and K. Aoki, "Effect of yellow-tinted lenses on visual attributes related to sports activities," *J. Hum. Kinet.* **36**, 27–36 (2013).
109. A. Cerviño, J. M. Gonzalez-Meijome, J. M. M. Linhares, S. L. Hosking, and R. Montes-Mico, "Effect of sport-tinted contact lenses for contrast enhancement on retinal straylight measurements," *Ophthalmic Physiol. Opt.* **28**, 151–156 (2008).
110. E. Porisch, "Football players' contrast sensitivity comparison when wearing amber sport-tinted or clear contact lenses," *Optometry* **78**, 232–235 (2007).
111. G. B. Erickson, F. C. Horn, T. Barney, B. Pexton, and R. Y. Baird, "Visual performance with sport-tinted contact lenses in natural sunlight," *Optom. Vis. Sci.* **86**, 509–516 (2009).
112. D. H. Brainard and A. Stockman, "Colorimetry," in (McGraw Hill, 2010).
113. CIE, *CIE 015:2004: Colorimetry*, Third Edit (CIE, 2004), Vol. 15.
114. M. D. Fairchild, *Color Appearance Models*, Second Ed. (John Wiley & Sons, 2005).
115. AZO Materials, "How to Measure Solid Colors Using 45/0 and Sphere Geometry," <https://www.azom.com/article.aspx?ArticleID=10627>.
116. A. R. Robertson, "Colour order systems: An introductory review," *Color Res. Appl.* **9**, 234–

- 240 (1984).
117. S. Hesselgren, "Why colour order systems?," *Color Res. Appl.* **9**, 220–228 (1984).
  118. R. W. G. Hunt and M. R. Pointer, *Measuring Colour*, The Wiley-IS&T Series in Imaging Science and Technology (John Wiley & Sons, 2011).
  119. F. W. Billmeyer, "Survey of color order systems," *Color Res. Appl.* **12**, 173–186 (1987).
  120. M. E. Bond and D. Nickerson, "Color-Order Systems, Munsell and Ostwald," *J. Opt. Soc. Am.* **32**, 709 (1942).
  121. A. H. Munsell, "A Color Notation, 1905; 1907; with new preface, 1913; 1916, Geo. H. Ellis Co., Boston, Mass.,," (1919).
  122. D. Nickerson, "History of the Munsell Color System, Company, and Foundation. II. Its Scientific Application," in *Color Research & Application* (1976), Vol. 1, pp. 69–77.
  123. R. G. Kuehni, "The Early Development of the Munsell System," *Color Res. Appl.* (2001).
  124. W. D. Wright, "The basic concepts and attributes of colour order systems," *Color Res. Appl.* **9**, 229–233 (1984).
  125. R. S. Berns and F. W. Billmeyer, "Development of the 1929 munsell book of color: A historical review," *Color Res. Appl.* **10**, 246–250 (1985).
  126. M. Newhall, "Preliminary Report of the O.S.A. Subcommittee on the Spacing of the Munsell Colors," (1940).
  127. S. M. Newhall, D. Nickerson, and D. B. Judd, "Final Report of the OSA Subcommittee on the Spacing of the Munsell Colors\*," *J. Opt. Soc. Am.* **33**, 385 (1943).
  128. A. Hård and L. Sivik, "NCS—Natural Color System: A Swedish Standard for Color Notation," *Color Res. Appl.* **6**, 129–138 (1981).
  129. K. Nassau, "The physics and chemistry of color: The 15 mechanisms," in *The Science of Color* (Elsevier, 2003), pp. 247–280.
  130. D. H. Foster, K. Amano, S. M. C. Nascimento, and M. J. Foster, "Frequency of metamerism in natural scenes," *J. Opt. Soc. Am. A* **23**, 2359 (2006).
  131. D. H. Foster, S. M. C. Nascimento, and K. Amano, "Information limits on neural

- identification of colored surfaces in natural scenes.," *Vis. Neurosci.* **21**, 331–336 (2004).
132. J. Hiltunen, "Munsell colors matt (Spectrofotometer measured)," <https://www.uef.fi/web/spectral/munsell-colors-matt-spectrofotometer-measured>.
  133. C. B. Barber, D. P. Dobkin, and H. Huhdanpaa, "The quickhull algorithm for convex hulls," *ACM Trans. Math. Softw.* **22**, 469–483 (1996).
  134. S. Lloyd, "Least squares quantization in PCM," *IEEE Trans. Inf. Theory* **28**, 129–137 (1982).
  135. D. Arthur and S. Vassilvitskii, "k-means++: The advantages of careful seeding," in *Proceedings of the Eighteenth Annual ACM-SIAM Symposium on Discrete Algorithms* (Society for Industrial and Applied Mathematics, 2007), pp. 1027–1035.
  136. J. M. Quintero, A. Sudrià, C. E. Hunt, and J. Carreras, "Color rendering map: a graphical metric for assessment of illumination," *Opt. Express* **20**, 4939 (2012).
  137. S. M. C. Nascimento, K. Amano, and D. H. Foster, "Spatial distributions of local illumination color in natural scenes," *Vision Res.* **120**, 39–44 (2016).
  138. C. D. Hendley and S. Hecht, "The Colors of Natural Objects and Terrains, and Their Relation to Visual Color Deficiency\*," *J. Opt. Soc. Am.* **39**, 870 (1949).
  139. L. Álvaro, J. Lillo, H. Moreira, J. Linhares, and S. Nascimento, "Robust color constancy with natural scenes in red-green dichromacy," *J. Vis.* **15**, 406 (2015).
  140. R. C. Baraas, D. H. Foster, K. Amano, and S. M. C. Nascimento, "Protanopic observers show nearly normal color constancy with natural reflectance spectra," *Vis. Neurosci.* **21**, 347–351 (2004).
  141. R. C. Baraas, D. H. Foster, K. Amano, and S. M. C. Nascimento, "Color Constancy of Red-Green Dichromats and Anomalous Trichromats," *Investig. Ophthalmology Vis. Sci.* **51**, 2286 (2010).
  142. L. Rüttiger, H. Mayser, L. Sérey, and L. T. Sharpe, "The color constancy of the red-green color blind," *Color Res. Appl.* **26**, (2001).
  143. L. T. Sharpe, E. de Luca, T. Hansen, H. Jägle, and K. R. Gegenfurtner, "Advantages and disadvantages of human dichromacy," *J. Vis.* **6**, 3 (2006).

144. M. J. Morgan, A. Adam, and J. D. Mollon, "Dichromats Detect Colour-Camouflaged Objects that are not Detected by Trichromats," *Proc. R. Soc. B Biol. Sci.* **248**, 291–295 (1992).
145. A. Saito, A. Mikami, T. Hosokawa, and T. Hasegawa, "Advantage of Dichromats over Trichromats in Discrimination of Color-Camouflaged Stimuli in Humans," *Percept. Mot. Skills* **102**, 3–12 (2006).
146. E. D. Montag, "Surface color naming in dichromats," *Vision Res.* **34**, 2137–2151 (1994).
147. E. D. Montag and R. M. Boynton, "Rod influence in dichromatic surface color perception," *Vision Res.* **27**, 2153–2162 (1987).
148. T. Pramanik, B. Khatiwada, and R. Pandit, "Color vision deficiency among a group of students of health sciences," *Nepal Med. Coll. J.* **14**, 334–336 (2012).
149. P. Lanthony, "Daltonism in painting," *Color Res. Appl.* **26**, (2001).
150. N. Prins, *Psychophysics: A Practical Introduction* (Academic Press, 2009).
151. B. C. Regan, J. P. Reffin, and J. D. Mollon, "Luminance noise and the rapid determination of discrimination ellipses in colour deficiency," *Vision Res.* **34**, 1279–1299 (1994).
152. M. L. R. Carmona, "Variability of chromatic sensitivity: fundamental studies and clinical applications," (2006).
153. J. A. Swets, W. P. Tanner, and T. G. Birdsall, "Decision processes in perception.," *Psychol. Rev.* **68**, 301–340 (1961).
154. C.-C. Chiao, M. Vorobyev, T. W. Cronin, and D. Osorio, "Spectral tuning of dichromats to natural scenes," *Vision Res.* **40**, 3257–3271 (2000).
155. M. Giesel, T. Hansen, and K. R. Gegenfurtner, "The discrimination of chromatic textures," *J. Vis.* **9**, 11–11 (2009).
156. T. Hansen, M. Giesel, and K. R. Gegenfurtner, "Chromatic discrimination of natural objects," *J. Vis.* **8**, 2 (2008).
157. J. L. Sandell and T. C. Zhu, "A review of in-vivo optical properties of human tissues and its impact on PDT," *J. Biophotonics* **4**, 773–787 (2011).
158. K. Xiao, J. M. Yates, F. Zardawi, S. Sueeprasan, N. Liao, L. Gill, C. Li, and S. Wuerger,

- "Characterising the variations in ethnic skin colours: a new calibrated data base for human skin," *Ski. Res. Technol.* **23**, 21–29 (2017).
159. K. Xiao, Y. Zhu, C. Li, D. Connah, J. M. Yates, and S. Wuerger, "Improved method for skin reflectance reconstruction from camera images," *Opt. Express* **24**, 14934 (2016).
  160. Y. Wang, M. R. Luo, M. Wang, K. Xiao, and M. Pointer, "Spectrophotometric measurement of human skin colour," *Color Res. Appl.* **42**, 764–774 (2017).
  161. J. B. Martinkauppi, "Basis Functions of the Color Signal of Skin under Different Illuminants," 3–6 (n.d.).
  162. I. S. Yun, W. J. Lee, D. K. Rah, Y. O. Kim, and B. Y. Park, "Skin color analysis using a spectrophotometer in Asians," *Ski. Res. Technol.* **16**, 311–315 (2010).
  163. G. N. Stamatias, B. Z. Zmudzka, N. Kollias, and J. Z. Beer, "Non-Invasive Measurements of Skin Pigmentation *\textit{in situ}*," *Pigment Cell Res.* **17**, 618–626 (2004).
  164. K. Wolff and R. A. Johnson, *Fitzpatrick's Color Atlas and Synopsis of Clinical Dermatology* (McGraw Hill, 2009).
  165. A. Anders, H. J. Altheide, and H. Tronnier, *Action Spectroscopy of Skin with Tunable Lasers* (Commission internationale de l'éclairage, 2002).
  166. N. Kollias, A. Baqer, and I. Sadiq, "Minimum erythema dose determination in individuals of skin type V and VI with diffuse reflectance spectroscopy.," *Photodermatol. Photoimmunol. Photomed.* **10**, 249–254 (1994).
  167. A. Fullerton, T. Fischer, A. Lahti, K. P. Wilhelm, H. Takiwaki, and J. Serup, "Guidelines for measurement of skin colour and erythema. A report from the Standardization Group of the European Society of Contact Dermatitis.," *Contact Dermatitis* **35**, 1–10 (1996).
  168. J. K. Wagner, C. Jovel, H. L. Norton, E. J. Parra, and M. D. Shriver, "Comparing quantitative measures of erythema, pigmentation and skin response using reflectometry.," *Pigment Cell Res.* **15**, 379–384 (2002).
  169. T. Ha, H. Javedan, K. Waterston, L. Naysmith, and J. L. Rees, "The relationship between constitutive pigmentation and sensitivity to ultraviolet radiation induced erythema is dose-dependent," *Pigment Cell Res* **16**, 477–479 (2003).

170. S. Y. Jeon, C. Y. Lee, K. H. Song, and K. H. Kim, "Spectrophotometric measurement of minimal erythema dose sites after narrowband ultraviolet b phototesting: Clinical implication of spetrophotometric values in phototherapy," *Ann. Dermatol.* **26**, 17–25 (2014).
171. S. Dain, "Color changes in cyanosis and the significance of congenital dichromasy and lighting," *Color Res. Appl.* **32**, 428–432 (2007).
172. S. J. Dain, "Recognition of simulated cyanosis by color-vision-normal and color-vision-deficient subjects," *J. Opt. Soc. Am. A* **31**, A303 (2014).
173. M. Maeda, H. Kachi, K. Matubara, S. Mori, and Y. Kitajima, "Pigmentation abnormalities in systemic scleroderma examined by using a colorimeter (Choromo Meter CR-200)," *J. Dermatol. Sci.* **11**, 228–233 (1996).
174. J. A. B. Spalding, "Colour vision deficiency in the medical profession," *Br. J. Gen. Pract.* **49**, 469–475 (1999).
175. J. A. B. Spalding, "Medical students and congenital colour vision deficiency: Unnoticed problems and the case for screening," *Occup. Med. (Chic. Ill)*. **49**, 247–252 (1999).
176. VINO Optics, "Bruise Glasses," <https://www.vino.vi/collections/bruise-glasses>.
177. T. Pramanik, B. Khatiwada, and R. Pandit, "Color vision deficiency among a group of students of health sciences.," *Nepal Med. Coll. J.* **14**, 334–336 (2012).
178. T. Pramanik, M. T. Sherpa, and R. Shrestha, "Color vison deficiency among medical students: an unnoticed problem.," *Nepal Med. Coll. J.* **12**, 81–83 (2010).
179. Z. Ugray, L. Lasdon, J. Plummer, F. Glover, J. Kelly, and R. Marti, "Scatter Search and Local NLP Solvers: A Multistart Framework for Global Optimization," *INFORMS J. Comput.* **19**, 328–340 (2007).
180. M. Bass, C. DeCusatis, J. Enoch, V. Lakshminarayanan, G. Li, C. MacDonald, V. Mahajan, and E. Van Stryland, "Handbook of Optics. Vol. II. Design, Fabrication and Testing; Sources and Detectors; Radiometry and Photometry," (2010).
181. J. J. Vos, "Colorimetric and photometric properties of a 2° fundamental observer," *Color Res. Appl.* **3**, 125–128 (1978).

182. V. C. Smith and J. Pokorny, "Spectral sensitivity of color-blind observers and the cone photopigments," *Vision Res.* **12**, 2059–2071 (1972).



## **Appendices**

Appendix I: Model of informed consent for the experiment of Chapter 3

Appendix II: Research protocol submitted to the SECVS ethics committee of the University of Minho.

Appendix III: Copy of the approval given by the SECVS ethics committee of the University of Minho.

Appendix IV: Acquisition record sheet

Appendix V: Model of informed consent for the experiment of



## Appendix I. Model of informed consent for the experiment of Chapter 3



Campus de Guaitar  
4710-057 Braga - P  
Portugal

**Universidade do Minho**  
Escola de Ciências

### **INFORMAÇÃO AOS VOLUNTÁRIOS E CONSENTIMENTO INFORMADO**

*Estudo: Discriminação Cromática em Cenários Naturais.*

*Responsável: Sérgio Nascimento, Departamento de Física, [smcn@fisica.uminho.pt](mailto:smcn@fisica.uminho.pt), 253604328/20*

Este documento tem como objectivo informar sobre as experiências psicofísicas que vai realizar no âmbito do projecto acima indicado e obter o seu consentimento informado de acordo com a Declaração de Helsínquia.

Este estudo pretende estudar de forma comparativa a visão das cores dos daltónicos com a visão dos observadores normais. As experiências enquadram-se num projecto que tem como objetivo quantificar o nível de discriminação das cores em cenários naturais. Este projeto tem apenas objetivos científicos e não comerciais.

As experiências serão realizadas através da visualização de estímulos numa caixa de luzes standard. Dada a sua natureza não constituem qualquer risco para a saúde.

Eu, \_\_\_\_\_ declaro:

- Que me foram explicados todos os aspectos relevantes sobre as experiências a serem realizadas;
- Tive oportunidade questionar o investigador, tendo sido respondida de modo satisfatório;
- Posso recusar a qualquer momento a participação ou continuidade no estudo sem quaisquer consequências;
- Autorizo a que os dados sejam publicados de forma anónima com os fins científicos.

Braga, \_\_\_\_\_ de \_\_\_\_\_ de 2016

Assinatura: \_\_\_\_\_

Appendix II. Research protocol submitted to the SECVS ethics committee of the University of Minho.

---

# PROTOCOLO DE INVESTIGAÇÃO

---

## TÍTULO DO PROJETO: **CARACTERIZAÇÃO ESPECTRAL DO CORPO HUMANO E ESTUDO DAS SUAS APLICAÇÕES**

---

### INTRODUÇÃO

---

As propriedades óticas do tecido dérmico podem permitir a detecção e diagnóstico de anomalias da pele. Quando a luz incide na pele, penetra-a e sofre interação com os componentes presentes no tecido e a componente refletida é detetada pelo olho do observador. A forma como essa interação ocorre irá influenciar a luz refletida e consequentemente o aspeto visual que esse a área em análise terá para observador. Portanto, propriedades como a cor e brilho podem evidenciar o estado e a composição da pele.

A detecção de sinais clínicos de relevância na pele está muitas vezes dependente da aptidão visual do profissional clínico que a analisa. É possível a existência de alterações subtis na cor da pele que não sejam detetadas pela observação visual do profissional clínico. Neste estudo pretende-se verificar se existem alterações não detetáveis ao olho humano mas que podem ser exploradas com o auxílio de lentes coloridas ou iluminação específica que permitam detetar alterações dérmicas num estado mais precoce ou facilitar a análise da evolução da condição. A medição, análise e caracterização da cor associada às diferentes condições dérmicas pode ter aplicações no desenvolvimento de tecnologias que permitem potenciar a detecção de sinais clínicos, quer para o profissional clínico experiente, quer para clínicos com menor experiência ou com algum nível de deficiência na visão das cores, permitindo a quantificação independente do utilizador/clínico.

## OBJETIVOS

---

Este projeto tem como objetivo principal caracterizar ao nível espectral a interação entre a luz visível e os vários elementos dérmicos da anatomia externa do corpo humano saudável e não saudável, utilizando técnicas de espectrometria como a espectrometria pontual de contacto, espectrometria pontual à distancia e imagiologia hiper-espectral. As estruturas que serão estudadas são: a pele, o cabelo, as unhas, a face, a boca e os olhos e os seus anexos oculares. Os resultados encontrados no estudo dos tecidos saudáveis serão comparados com versões com achados clínicos significativos das mesmas estruturas e tecidos.

A caracterização da cor da pele, no formato de refletância espectral, que apresente alterações dérmicas permitirá formar uma base de dados anónima e classificativa de cada uma das condições analisada, atualmente inexistente e de utilidade para as comunidades científicas de colorimetria e dermatologia.

O conhecimento obtido a partir da análise dos resultados obtidos ao construir a base de dados referida no objetivo anterior permitirá, ainda, o desenvolvimento de tecnologia que potencie a deteção de sinais clínicos e sub-clínicos na pele ao propor iluminação ou filtros coloridos específicos que auxiliem à visão humana e/ou software para equipamentos eletrónicos, assim como o desenvolvimento de software que realize análises automatizadas, tornando a avaliação e análise independente do observador.

## INVESTIGADORES PRINCIPAIS

---

### **Ciências da Visão e Luz:**

Sérgio Miguel Cardoso Nascimento, Professor Associado com Agregação do Departamento de Física da Escola de Ciências da Universidade do Minho.

### **Dermatologia:**

José Carlos Cardoso, Departamento de dermatologia dos Hospitais da Universidade de Coimbra.

Alterações à cor normal da pele podem indicar alterações clínicas significativas e são um fator frequentemente considerado no processo de diagnóstico de alterações dérmicas. A alteração de cor dá-se devido a modificações da pele por influencia da condição clínica na anatomia e fisiologia da pele [1], correspondendo a alterações do espectro de luz refletida. As alterações de cor e da luz refletida que a pele sofre para uma gama alargada de situações patológicas ainda não estão devidamente descritas na bibliografia.

A cor da pele saudável foi já alvo de estudo de vários grupos de investigação que apresentaram bases de dados para populações como: Estados Unidos [2], Reino Unido [3][4][5], Finlândia [6], China [3][5][4], Coreia do Sul [7], Filipinas [6], Irão [3] e Tailândia [3]. Esses estudos centram-se em caracterizar a cor da pele em diferentes países com o principal objetivo de fazer comparação colorimétrica entre as varias raças e etnias. Não se encontra na literatura bases de dados sobre a cor da pele da população portuguesa, estando assim aberta a necessidade da caracterização da população portuguesa.

Os estudos no âmbito da colorimetria de patologia dermatológica são escassos e relacionam-se com anomalias específicas, como o eritema [8][9][10][11][12][13] cianose[14][15] e lesões pigmentadas [1][16]. Alguns dos dados apresentados não produzem dados no formato de refletância espectral, informação esta que é necessária para o calculo de ajudas visuais à discriminação cromática e para a correta classificação cromática das condições clínicas. No desenvolvimento de lentes ou filtros para otimização da distinção entre pele anormal e pele saudável são necessários dados de refletância espectral. Não existe, no entanto, uma base de dados colorimétrica no formato de refletância espectral, para uma gama alargada de condições clínicas dermatológicas e na qual também se incluem medidas de pele normal do próprio paciente para comparação. Este dados colorimétricos são obtido através de técnicas de espectrometria de contacto ou não contacto como foi feito, por exemplo, pelo Laboratório da Cor do Centro de Física da Universidade do Minho para idealizar lentes otimizadas que permitiam incrementar o numero de cores distinguidas por observadores com a visão das cores normais e observadores com deficiência na visão das cores [17]. Não está documentado na literatura casos em que se aplique este tipo de abordagem à discriminação das cores da pele.

Os profissionais e alunos de medicina reportam algumas dificuldades com a discriminação da cor, principalmente relacionadas com realização de microscopia, distinção de tecidos em cirurgia, observação de lesões orais e faríngeas, observação de

amostras biológicas (sangue, urina, bñlis na urina, fezes, expetoração, vomito), e reconhecimento de variações de cor no corpo (palidez, cianose, icterícia, erupção cutânea, e eritema dérmico) [18]. Há vários casos descritos na literatura de profissionais clínicos com deficiências na visão das cores que apresentam dificuldade na deteção de alterações de cor na pele dos seus pacientes e que correspondem a patologias dermatológicas [14][15][18][19]. Assim, lentes otimizadas que aumentam o numero de cores percebidas e facilitem a distinção cromática podem ser um beneficio importante não só para profissionais clínicos com deficiências na visão das cores, mas também para profissionais clínicos com a visão das cores normal.

#### METODOLOGIA

---

De modo a facilitar a descrição metodológica do projeto, este será dividido em várias tarefas. Em cada uma delas serão descritas as técnicas a utilizar e os métodos a seguir.

Cada uma delas pode ser realizada individualmente em pequenos projetos individualizados (como no caso de uma tese de mestrado, por exemplo) ou em conjunto com outras.

---

TAREFA 1. COMPARAÇÃO DO ESPECTRO DE REFLETÂNCIA DE PELE NORMAL E PELE ANORMAL.

---

Esta tarefa avaliará a alteração cromática presente em anomalias dérmicas.

Será medida a refletância sob a luz visível de intensidade controlada de pele normal e pele com alterações patológicas de um mesmo paciente utilizando um espectrómetro portátil (ver descrição abaixo). Este aparelho permite utilizar a luz visível para medir a refletância de uma pequena área em análise. Esta refletância será posteriormente comparada para analisar e caracterizar achados com significado clínico e lesões dérmicas. A população estudada será obtida a partir de uma rede de comunicação baseada em rede hospitalar de consultórios de clínica geral e dermatologia, por forma a encontrar uma gama alargada de achados clínicos dérmicos de interesse. Para a realização desta tarefa será necessário contar com a colaboração de médicos clínicos de Medicina Geral e Dermatologia para se poderem realizar as medidas com o mínimo de alteração do estado do paciente e nas zonas pretendidas, afetadas e normais.

Sempre que possível e com a devida autorização por escrito do paciente, a lesão dermatológica será ainda fotografada com uma câmara fotográfica digital tradicional. Para respeitar a identidade do paciente é garantido que nem os dados registados nem as fotografias permitirão reconhecer o paciente diretamente. Existirá uma chave alfanumérica impessoal e única que ligará os dados pessoais do paciente à recolha de refletâncias, a área de amostragem e respetiva fotografia.

Assim, durante o procedimento de recolha de dados é de esperar a presença do médico identificador da condição clínica para além do responsável pela medição e respetivo paciente. Cada participante será avaliado apenas uma vez e o exame deverá ter a duração máxima de 5 a 10 minutos.

#### **AMOSTRA**

Os participantes numa primeira fase do estudo serão selecionados a partir da população utente dos *Hospitais da Universidade de Coimbra* que se voluntariem após indicação e encaminhamento durante o procedimento de uma consulta de clínica geral ou de dermatologia. Farão parte do estudo apenas pacientes maiores de 18 anos que apresentem sinais clínicos correspondentes a uma ou mais classes de alterações dérmicas, devidamente identificadas pelo médico que encaminha o paciente. Esta seleção para encaminhamento será efetuada pelos clínicos e apenas nos pacientes que aceitem participar no estudo após este lhe ser devidamente explicado e assinarem o respetivo consentimento informado.

O número de participantes deverá situar-se entre os 50 e os 100 pacientes.

### **LOCAL**

Os serviços de medicina geral e de dermatologia dos *Hospitais da Universidade de Coimbra* servirão como a principal fonte de participantes do estudo. Outras instituições, como hospitais e clínicas, poderão vir a ser consideradas para trabalhar em rede ou em alternativa aos *Hospitais da Universidade de Coimbra*, sempre que a totalidade das partes esteja de acordo, transferindo-se os termos deste protocolo de investigação para a relação com novos parceiros.

A recolha de dados decorrerá no ambiente clínico da instituição onde o paciente solicitou consulta. Apenas em casos especiais e do interesse e com o acordo do paciente este se deslocará ao laboratório de Ciências da Cor do Centro de Física da Universidade do Minho para uma análise mais aprofundada.

### **TÉCNICAS A UTILIZAR**

Todas as técnicas a utilizar nesta tarefa são não-invasivas e não representam um risco para a pessoa que está a ser avaliada nem para o avaliador. A espectrometria pontual de contacto será considerada a técnica principal. A espectrometria pontual à distância e a espectrometria hiper-espectral serão usadas em associação caso seja necessário medir áreas extensas, como por exemplo, uma anomalia dermatológica que ocupe toda a área facial. Em todos os casos o procedimento é não invasivo, pois são técnicas de medição à distância ou apenas toque superficial.

#### **ESPECTROMETRIA PONTUAL DE CONTACTO**

A técnica de espectrometria pontual de contacto a utilizar usará o espectrómetro de contacto CM-2600D (Konica Minolta, Japan). O aparelho de medição é portátil e será usado para medir o espectro luminoso refletido em pontos específicos ou pequenas áreas da pele. É um pequeno aparelho portátil que, em contacto com a pele, emitirá um pequeno feixe de luz visível de baixa intensidade não prejudicial à pele, nem em intensidade nem em comprimento de onda, e analisará a luz refletida. A aquisição é rápida, demorando entre 1 a 2 segundos. O procedimento é não invasivo, havendo apenas um pequeno contacto entre o aparelho e a pele. E para garantir a segurança do paciente e do investigador serão tomadas medidas protetoras e sanitárias contra o risco de exposição a agentes contaminantes: o espectrómetro será embalado em protetor plástico esterilizado,

que será convenientemente descartado entre utilizações para diferentes pacientes.

#### ESPECTROMETRIA PONTUAL À DISTÂNCIA

A espectrometria pontual à distancia será realizada usando o espectrometro PR-650 SpectraScan Colorimeter (Photo Research, Chatsworth CA), por exemplo. É um espectrómetro com tripé acoplado que será usado para obter dados de cor da iluminação ambiente ou de uma área de interesse na pele do paciente. Este equipamento utiliza uma lente telescópica para efetuar a medição. Assim, não há qualquer contacto com o paciente durante este processo.

#### ESPECTROMETRIA HÍPER-ESPECTRAL

A espectrometria híper-espectral consiste na aquisição espectral de múltiplos pontos em simultâneo. Este sistema pode ser descrito como a cooperação entre uma camara e um filtro de cores sintonizável que permite adquirir imagem em diferentes comprimentos de onda. O resultado final é uma imagem digital especial em que cada pixel contem a informação do seu espectro de refletância. Para produzir espectros de refletância é necessário definir a iluminação ambiente e para isso usa-se a técnica de espectrometria pontual à distancia. A câmara é uma câmara digital monocromática. A imagem produzida nunca irá ser usada para identificar o paciente. Será garantido o mascaramento facial caso necessário. Esta é também uma técnica de não contacto que vai permitir a aquisição de elevadas áreas de interesse em simultâneo, sendo necessária a exposição da área de interesse a luz visível durante um período estimado de 10 minutos.

#### **PROTOCOLO**

1. Preenchimento e assinatura do consentimento informado pelo paciente.
2. Embalar o espectrómetro em protetor plástico descartável esterelizado.
  - O protetor plástico descartável esterilizado será trocado por um novo entre cada paciente.
  - Garantir que o plástico fica esticado e não enrugado na abertura do espectrómetro, que entrara em contacto com a pele e permitirá a medição da refletância.

- A calibração do espectrómetro deverá ser efetuada previamente utilizando um branco de referência (pequeno objecto plástico de cor cinza), e com o protetor plástico descartável colocado, antes de entrar em contacto com o paciente.
3. Medição de pele anormal.
- Realizar 3 medidas por cada local de interesse na pele do paciente.
  - Se devido à natureza da lesão não for aconselhável fazer pressão sobre a pele com o espectrómetro é sempre possível recorrer à técnica de medição sem contacto desde que se refaça a calibração do aparelho tendo em conta a distancia de medida a usar (idealmente o mais próximo possível sem tocar).
  - Registrar a área e localização da amostra numa folha separada do registo de amostragem e dos dados do paciente.
4. Registo fotográfico da lesão.
- Tirar uma fotografia a cada local de interesse em que se fez 3 medidas.
  - A fotografia deverá permitir identificar lesão e a parte do corpo a que pertence, mas não o paciente.
5. Medição de pele normal para referencia.
- 7 locais (fronte, bochecha direita e esquerda, dorso da mão direita e esquerda, lado interno do antebraço direito e esquerdo).
  - Caso um ou mais destes locais apresentem anomalia deverá se utilizar zonas alternativas se possível e anotar a alteração na “Ficha da Aquisição de Dados”.
6. Preenchimento da “Ficha da Aquisição de Dados”.
- Garantir o registo dos seguintes dados: idade, género, raça, nome da anomalia dermatológica medida após diagnóstico confirmado pelo dermatologista, código identificador da fotografia de cada medida, numero de medida dado pelo espectrómetro.
  - Para respeitar a identidade do paciente é garantido que nem os dados registados nem as fotografias permitirão reconhecer o paciente diretamente. Existirá uma chave alfanumérica impessoal e única que ligará os dados pessoais do paciente à recolha de dados efetuada.

---

## TAREFA 2. DESENVOLVER E TESTAR TECNOLOGIAS PARA DETEÇÃO DE ANOMALIAS DÉRMICAS.

---

O objetivo geral deste trabalho é montar e validar técnicas para o auxílio da detecção e identificação profissionais de alterações dérmicas através da cor. Mais especificamente:

1. Desenvolver e testar ajudas visuais no formato de lentes coloridas especializadas para profissionais de visão das cores normal e profissionais daltônicos que potencie a discriminação de cores;

2. Desenvolver e testar ajudas visuais no formato de iluminação especializada para profissionais de visão das cores normal e profissionais daltônicos que potencie a discriminação de cores;

3. Desenvolver e testar ajudas eletrônicas no formato de uma aplicação para smartphones e equipamentos clínicos especializados para profissionais de visão das cores normal e profissionais daltônicos que potencie a discriminação de cores;

O desenvolvimento destes três tipos de ajuda é permitido através dos conhecimentos obtidos na Tarefa 1. O funcionamento destas tecnologias baseia-se na seleção especializada das componentes da luz que são enviadas ao olho a partir da pele. Essa seleção dá-se ao nível dos comprimentos de onda da luz visível e é feita de tal forma que anomalias dérmicas subtis ou normalmente não detetáveis ao olho humano sejam vistas com uma cor diferente da pele envolvente, permitindo ao profissional melhor eficiência na tarefa de detecção e identificação de achados clínicos de interesse, preferencialmente sub-clínicos.

### **VALIDAÇÃO DE TECNOLOGIA**

A validação das tecnologias propostas será realizada com participantes voluntários em ambiente controlado. A validação é compreendida por 3 fases:

1. Simular o efeito das lentes coloridas e iluminantes especializados em ambiente controlado com monitor calibrado. Usando para isso as imagens híper-espectrais de pele recolhidas na Tarefa 1.
2. Testar as lentes coloridas em ambiente controlado com testes psicofísicos, para comparar a visão das cores e capacidade de detecção de anomalias dérmicas, com e sem lentes.
3. Testar as lentes coloridas, iluminantes especializados de variação espectral e

ajudas eletrônicas no contexto clínico ao qual se destina a aplicação da tecnologia.

### ***AMOSTRA***

Serão avaliados daltônicos e sujeitos com visão das cores normal.

Os observadores serão recrutados ou através de anúncios (email, por exemplo) publicidade ou a partir de um banco de dados já existente.

Deverão fazer parte do estudo cerca de 50 observadores.

Os participantes da Tarefa 2 nunca poderão ser pacientes da Tarefa 1.

### ***LOCAL***

As experiências aqui propostas serão realizadas no laboratório da Ciência da Cor do Centro de Física da Universidade do Minho.

### ***TÉCNICAS A UTILIZAR***

Cada participante será avaliado apenas uma vez e cada exame deverá ter a duração máxima de 20 minutos. Todas estas técnicas são não invasivas e utilizam equipamentos comerciais para utilização visual, estando salvaguardada a integridade física dos participantes.

Testes de visão das cores em monitor.

Neste tipo de testes de avaliação da visão das cores, são apresentados objetos de diferentes cores num monitor de computador que devem ser identificados pelo observador. Os testes disponíveis para aplicação no estudo correspondem a um exame desenvolvido na Universidade do Minho (CVA by UMinho) e 2 exames de referencia na área (o teste Colour Assessment & Diagnosis e o Cambridge Colour Test). O exame será realizado com e sem as ajudas visuais, permitindo comparar as discriminações cromáticas com e sem as ajudas.

Teste de simulação da pele, em monitor.

Neste teste de avaliação das ajudas visuais simuladas, são apresentadas imagens de

pele com e sem anomalias. As cores apresentadas simulam o efeito das ajudas visuais testadas. O teste será realizado com e sem o efeito simulado das ajudas visuais para determinar a taxa de eficácia.

#### Teste de comparação de espectros

Neste teste de avaliação das ajudas visuais desenvolvidas, são apresentados em sequencia espectros de pele normal e pele anormal que o observador deve tentar distinguir. O teste usa uma lâmpada especial cujo o espectro da sua luz é altamente ajustável (OL 490 Agile Light Source, Gooch & Housego). Portanto, o seu estímulo luminoso terá a vantagem de ser mais realista que a imagem de um monitor. No entanto, o campo de estímulo só pode apresentar uma cor de cada vez, o que não permite a apresentação de imagens complexas e torna necessário o teste de simulação de pele com monitor sempre que se queira uma comparação lado a lado do estímulo e não sequencial como aqui descrito. O teste será realizado com e sem o uso das ajudas visuais para determinar a taxa de eficácia.

## Referências

- [1] G. N. Stamatias, B. Z. Zmudzka, N. Kollias, and J. Z. Beer, "Non-Invasive Measurements of Skin Pigmentation \textit{in situ}," *Pigment Cell Res.*, vol. 17, no. 6, pp. 618–626, 2004.
- [2] J. L. Sandell and T. C. Zhu, "A review of in-vivo optical properties of human tissues and its impact on PDT," *J. Biophotonics*, vol. 4, no. 11–12, pp. 773–787, 2011.
- [3] K. Xiao *et al.*, "Characterising the variations in ethnic skin colours: a new calibrated data base for human skin," *Ski. Res. Technol.*, vol. 23, no. 1, pp. 21–29, 2017.
- [4] K. Xiao, Y. Zhu, C. Li, D. Connah, J. M. Yates, and S. Wuerger, "Improved method for skin reflectance reconstruction from camera images," *Opt. Express*, vol. 24, no. 13, p. 14934, 2016.
- [5] Y. Wang, M. R. Luo, M. Wang, K. Xiao, and M. Pointer, "Spectrophotometric measurement of human skin colour," *Color Res. Appl.*, no. March, p. n/a-n/a, 2017.
- [6] J. B. Martinkauppi, "Basis Functions of the Color Signal of Skin under Different Illuminants," pp. 3–6.
- [7] I. S. Yun, W. J. Lee, D. K. Rah, Y. O. Kim, and B. young Y. Park, "Skin color analysis using a spectrophotometer in Asians," *Ski. Res. Technol.*, vol. 16, no. 3, pp. 311–315, 2010.
- [8] A. Anders, H. J. Altheide, and H. Tronnier, *Action spectroscopy of skin with tunable lasers*. Commission internationale de l'éclairage, 2002.
- [9] N. Kollias, A. Baqer, and I. Sadiq, "Minimum erythema dose determination in individuals of skin type V and VI with diffuse reflectance spectroscopy," *Photodermatol. Photoimmunol. Photomed.*, vol. 10, no. 6, pp. 249–254, 1994.
- [10] A. Fullerton, T. Fischer, A. Lahti, K. P. Wilhelm, H. Takiwaki, and J. Serup, "Guidelines for measurement of skin colour and erythema. A report from the Standardization Group of the European Society of Contact Dermatitis," *Contact Dermatitis*, vol. 35, no. 1, pp. 1–10, 1996.
- [11] J. K. Wagner, C. Jovel, H. L. Norton, E. J. Parra, and M. D. Shriver, "Comparing quantitative measures of erythema, pigmentation and skin response using reflectometry," *Pigment Cell Res.*, vol. 15, no. 5, pp. 379–384, 2002.
- [12] T. Ha, H. Javedan, K. Waterston, L. Naysmith, and J. L. Rees, "The relationship between constitutive pigmentation and sensitivity to ultraviolet radiation induced erythema is dose-dependent," *Pigment Cell Res.*, vol. 16, no. 5, pp. 477–479, 2003.
- [13] S. Y. Jeon, C. Y. Lee, K. H. Song, and K. H. Kim, "Spectrophotometric measurement of minimal erythema dose sites after narrowband ultraviolet b phototesting: Clinical implication of spectrophotometric values in phototherapy," *Ann. Dermatol.*, vol. 26, no. 1, pp. 17–25, 2014.
- [14] S. Dain, "Color changes in cyanosis and the significance of congenital dichromasy and lighting," *Color Res. Appl.*, vol. 32, no. 6, pp. 428–432, 2007.
- [15] S. J. Dain, "Recognition of simulated cyanosis by color-vision-normal and color-vision-deficient subjects," *J. Opt. Soc. Am. A*, vol. 31, no. 4, p. A303, 2014.
- [16] M. Maeda, H. Kachi, K. Matubara, S. Mori, and Y. Kitajima, "Pigmentation abnormalities in systemic scleroderma examined by using a colorimeter (Choromo Meter CR-200)," *J. Dermatol. Sci.*, vol. 11, no. 3, pp. 228–233, 1996.
- [17] J. M. M. Linhares *et al.*, "Enhancing the chromatic diversity of natural scenes with optimized coloured filters," in *AIC Colour.*, 2005.
- [18] T. Pramanik, B. Khatiwada, and R. Pandit, "Color vision deficiency among a group of students of health sciences," vol. 14, no. 4, pp. 334–336, 2012.
- [19] T. Pramanik, M. T. Sherpa, and R. Shrestha, "Color vision deficiency among medical students: an unnoticed problem," *Nepal Med. Coll. J.*, vol. 12, no. 2, pp. 81–83, 2010.

---

## CONSIDERAÇÕES ÉTICAS

---

Serão acauteladas as Regras de Conduta Ética e de Boas Práticas para que serão cumpridos os preceitos da Declaração de Helsínquia [1], a Convenção sobre os Direitos do Homem e da Biomedicina [2], as orientações do Council for International Organizations of Medical Sciences [3] e o Guia das Boas Práticas Clínicas (ICH, GCP) [4].

1. World Medical Association. Ethical principles for medical research involving human subjects. Helsinki 1964 (revisão 2008). Disponível em: <http://www.wma.net/en/30publications/10policies/b3/17c.pdf>.
2. Convenção para a Protecção dos Direitos do Homem e da Dignidade do Ser Humano Face às Aplicações da Biologia e da Medicina: Convenção sobre os Direitos do Homem e da Biomedicina (Conselho da Europa 1997). Resolução da Assembleia da República n.º 1/2001, Diário da República – I Série A, nº 2, 3 de Janeiro de 2001. Disponível em: <http://dre.pt/util/getpdf.asp?s=dip&serie=1&iddr=2001.2A&iddip=20010014>
3. Council for International Organizations of Medical Sciences. International Ethical Guidelines for Biomedical Research Involving Human Subjects. Geneva, Switzerland: CIOMS, 1993.
4. Good Clinical Practice, European Medicines Agency, 2000. Disponível em: [http://www.ema.europa.eu/docs/en\\_GB/document\\_library/Scientific\\_guideline/2009/10/WC500004343.pdf](http://www.ema.europa.eu/docs/en_GB/document_library/Scientific_guideline/2009/10/WC500004343.pdf)

---

## C R O N O G R A M A

---

Este projeto terá início a 1 de Dezembro de 2017 e uma duração de 5 anos.

Tarefa	Início	Duração	Observações
1	A determinar	5 anos	
2	A determinar	5 anos	Dará inicio após a realização da Tarefa 1.

## CONFIDENCIALIDADE E ANONIMATO

---

Serão garantidos o anonimato e a confidencialidade dos participantes assim como o uso exclusivo dos dados recolhidos para o presente estudo. Para respeitar a identidade do paciente é garantido que nem os dados registados nem as fotografias permitirão reconhecer o paciente diretamente. Os sociodemográficos recolhidos correspondem à Idade, Género e Raça/Etnia. Os dados pessoais serão mantidos em separado dos resultados recolhidos e guardados em armários fechados com chave. Existirá uma chave alfanumérica impessoal e única que ligará os dados pessoais do paciente à recolha de dados efetuada.

## CONDIÇÕES E FINANCIAMENTO

---

Os instrumentos/técnicas que serão utilizadas neste projeto já existem no Centro de Física da Universidade do Minho. Poderá ter que ser adquirido algum material ao longo da sua execução e serão usadas verbas de projetos de investigação sob a responsabilidade dos cientistas responsáveis, quando acordado mutuamente.

A participação será de carácter voluntário podendo os participantes desistir a qualquer momento, sem que essa decisão tenha qualquer tipo de consequência. Não haverá qualquer pagamento de deslocações ou outras contrapartidas financeiras.

Não estão previstos outros custos, ou abuso de recursos institucionais, hospitalares e/ou outros para a realização do projeto.

Os investigadores principais deste projeto não têm qualquer afiliação ou envolvimento com qualquer empresa ou entidade com interesse financeiro direto ou equipamento utilizados neste projeto. Sempre que necessário, os membros da equipa de investigação deverão assinar uma Declaração de Interesses e Incompatibilidades de acordo com o Decreto Lei 14/2014 de 22 de janeiro.



Appendix III. Copy of the approval given by the SECVS ethics committee of the University of Minho.



Universidade do Minho

SECVS

### **Subcomissão de Ética para as Ciências da Vida e da Saúde**

Identificação do documento: SECVS 175/2017

Título do projeto: *Caracterização espectral do corpo humano e estudo das suas aplicações*

Investigador(a) responsável: Sérgio Miguel Cardoso Nascimento, Departamento de Física da Escola de Ciências da Universidade do Minho; José Carlos Cardoso, Departamento de Dermatologia dos Hospitais da Universidade de Coimbra.

Subunidade orgânica: Laboratório de Ciências da Cor, Centro de Física, Escola de Ciências, Universidade do Minho

Outras Unidades: Serviços de Medicina Geral e de Dermatologia dos Hospitais da Universidade de Coimbra que serão a principal fonte de participantes do estudo. Outras instituições, como hospitais e clínicas, poderão vir a ser consideradas para trabalhar em rede ou em alternativa aos Hospitais da Universidade de Coimbra, sempre que a totalidade das partes esteja de acordo, transferindo-se os termos deste protocolo de investigação para a relação com novos parceiros.

### **PARECER**

A Subcomissão de Ética para as Ciências da Vida e da Saúde (SECVS) analisou o processo relativo ao projeto intitulado *Caracterização espectral do corpo humano e estudo das suas aplicações*.

Os documentos apresentados revelam que o projeto obedece aos requisitos exigidos para as boas práticas na experimentação com humanos, em conformidade com o Guião para submissão de processos a apreciar pela Subcomissão de Ética para as Ciências da Vida e da Saúde.

Face ao exposto, a SECVS nada tem a opor à realização do projeto.

Braga, 30 de janeiro de 2018.

A Presidente

**MARIA CECÍLIA DE  
LEMONS PINTO  
ESTRELA LEÃO** Assinado de forma digital por  
MARIA CECÍLIA DE LEMOS  
PINTO ESTRELA LEÃO  
Dados: 2018.02.01 12:09:04 Z

Maria Cecilia de Lemos Pinto Estrela Leão

Appendix IV. Acquisition record sheet



## Appendix V. Model of informed consent for the experiment of Chapter 4

**CONSENTIMENTO INFORMADO, LIVRE E ESCLARECIDO PARA PARTICIPAÇÃO EM  
INVESTIGAÇÃO**

*Este documento tem como objetivo informar sobre o estudo em que vai participar e obter o seu consentimento informado de acordo com a Declaração de Helsínquia. Por favor, leia com atenção a seguinte informação. Se achar que algo está incorreto ou que não está claro, não hesite em solicitar mais informações. Se concorda com a proposta que lhe foi feita, queira assinar este documento.*

**Título do estudo:** Caracterização espectral do corpo humano e estudo das suas aplicações.

**Enquadramento:** O estudo será realizado no âmbito de um projeto de investigação em desenvolvimento no Centro de Física da Universidade do Minho sob a orientação do Doutor Sérgio Nascimento.

**Explicação do estudo:** Este estudo, resultante da colaboração entre a Universidade do Minho e o Centro Hospitalar e Universitário de Coimbra, pretende estudar as mudanças de cor que a pele sofre com o surgimento de patologias dérmicas. Este estudo ajudará a entender melhor as doenças dermatológicas e a forma como a pele interage com a luz visível. Pretende desenvolver tecnologias auxiliares à deteção clínica de alterações da pele no formato de lentes coloridas e software para equipamentos eletrónicos como smartphones.

**Descrição do exame a realizar:** Um espectrómetro, pequeno aparelho portátil não invasivo, irá ser usado para medir o espectro luminoso refletido por pontos específicos da sua pele. A medição de cada ponto demora apenas alguns segundos, mas deverá manter-se o mais imóvel possível. Um espectrómetro é um pequeno aparelho que, em contacto com a pele, emitirá um pequeno feixe de luz e analisará a luz refletida. O procedimento é não invasivo, à exceção do contacto do aparelho com a pele. Serão tomadas medidas protetoras e sanitárias contra o risco de exposição a agentes contaminantes para garantir a segurança do paciente e do investigador. O espectrómetro será embalado em protetor plástico descartável esterilizado, que será descartado entre utilizações entre diferentes pacientes. Não estão previstas consequências na realização deste exame.

**Condições e financiamento:** A participação será de carácter voluntário podendo desistir a qualquer momento, sem que essa decisão tenha qualquer tipo de consequência. Não haverá qualquer pagamento de deslocações ou outras contrapartidas financeiras. Este projeto tem apenas objetivos de carácter científico e não comercial.

**Confidencialidade e anonimato:** Se possível, a lesão dermatológica será fotografada com uma câmara fotográfica digital tradicional. Para respeitar a identidade do paciente é garantido

que nem os dados registados nem as fotografias permitirão reconhecer o paciente diretamente. Existirá uma chave alfanumérica impessoal e única que ligará os dados pessoais do paciente à recolha de dados efetuada.

Eu, \_\_\_\_\_ declaro que:

- *Foram me explicados todos os aspetos relevantes sobre a medição de dados para o estudo citado acima;*
- *Tive oportunidade de questionar pessoalmente e presencialmente o investigador responsável pela recolha dos dados, tendo sido respondido de modo satisfatório;*
- *Posso recusar a qualquer momento a participação ou continuidade no estudo sem quaisquer consequências;*
- *Autorizo a que os dados sejam publicados de forma anónima para fins científicos;*
- *Autorizo a recolha dos dados espectrais e de fotografias de áreas de interesse, sem que haja identificação do paciente.*

Data: \_\_\_\_ / \_\_\_\_ / \_\_\_\_\_

Assinatura: \_\_\_\_\_

**ESTE DOCUMENTO É COMPOSTO POR 2 PÁGINAS E FEITO EM DUPLICADO: UMA VIA PARA O/A INVESTIGADOR/A, OUTRA PARA A PESSOA QUE CONSENTE.**